Karl-Franzens Universität Graz

Institut für Physik
Abteilung Oberflächen und Grenzflächenphysik

High Resolution Electron Energy Loss Spectroscopy on V_2O_3 (0001) thin films: the adsorption of water and the metal-insulator phase transition

Diplomarbeit
an der naturwissenschaftlichen Fakultät

eingereicht von Florian Pfuner

vorgelegt bei o. Univ. Prof. Dr. Falko P. Netzer

im Februar 2005

Contents

1. Introduction

Studying metal oxides and the adsorption of water is from great interest, the knowledge about their structure, electronic properties and the interaction with the environment is important for the development of novel applications, such as sensors, coatings, electronic devices and in catalysis. Additionally, water is probably the most important and interesting molecule, it is necessary in all kinds of biochemical, chemical and physical reactions and occurs in the bio- and geosphere. The understanding of water adsorption and its interaction with solids is therefore fundamental. It depends on the adsorption site whether water coordinates as a molecule or dissociate on the surface. Its interaction with the substrate, for example with the before mentioned metal oxide, influences the behaviour of the interface. The goal is to get more information about the processes on the surface.
In particular thin films have been investigated by scientists all over the world, because the properties of a thin film can be completely different to the one know from the bulk structure. For a deeper understanding single crystal surfaces with low indices are used as model systems. Moreover, ultrahigh vacuum in combination with surface science techniques is a perfect way to improve the understanding of the growth and the behaviour on such thin films, because it allows experiments with well-defined and controllable parameters. Often a change in the substrate orientation or the surface termination is enough to induce also changes in the prepared films.

A range of vanadium oxides exist in different oxidation states, which are used in different scientific research areas, e.g. VO and V_2O_3 are known for their metal-to-insulator transition, whereas V_2O and V_2O_5 are used in catalysis.

In this work the main interest is focused on thin films of V_2O_3, which were characterised before with STM, LEED, HREELS and XPS by F.P. Netzer, S. Surnev, J. Schoiswohl and M. Sock. Three surface terminations were found, namely the vanadyl termination (1x1) V=O, the O-rich termination (√3x√3)R30° and the V-rich (1x1) termination.

Studying the adsorption behaviour of water was the main purpose for all three surface terminations. The question of how the water molecules are adsorbing and if there are differences between the different surface terminations is the topic of Chapter 4. A part in this chapter addresses the vibration modes of adsorbed water on clean Rh(111), because Rh(111) is the substrate for the V_2O_3 films and because metal substrates show a different adsorption behaviour of water than oxide surfaces.

In Chapter 5 the metal-to-insulator phase transition of the V_2O_3 films as observed with HREELS is reported. The surface termination plays also here a important role, the O-rich termination (√3x√3)R30° seems to have the phase transition quenched. But small amounts of water adsorbed on this termination can restore the typical HREEL spectrum for V_2O_3, which has changed from the metallic to the insulating state.
In Chapter 2 and 3 the experimental preparations are described, like film growth or dosing of water. The UHV system and the measurement methods used are presented.

2. Techniques

2.1 HREELS – spectroscopy with electrons

2.1.1 Scattering of electrons

To excite vibrations on a sample a highly monochromatic beam of electrons is targeted towards the surface. The electrons are scattered on the surface due to the interaction with the atoms sitting at the interface. By using electrons with a low primary energy (E_p = 1-10 eV) and obtaining a high energetic resolution due to an arrangement of electrostatic lenses in combination with energy dispersive elements allows to do HREELS – high-resolution electron energy spectroscopy – studies.

The so produced monochromatic electron beam possesses a FWHM of 3-4 meV, which is poor in terms of optical spectroscopy. Nevertheless HREELS has its advantages in the surface sensitivity, the incident electrons do not penetrate the sample very deeply, only several monolayers. In optical spectroscopy gracing incidence of the incoming light is needed to reach the same surface sensitivity. Another important factor is that the electrons can excite atoms and molecules in different ways and they are not limited to the dipole interaction.

Most electrons scatter elastically at the surface without any energy loss, but a small fraction of them are losing energy during the interaction with the surface. These inelastic scattered electrons correspond to the excitations and their amount of loss energy is used for a vibrational mode.

The spectrometer detects the scattered electrons as a function of energy loss; the resulting spectrum starts at the initial energy with the primary peak of all elastically scattered electrons and goes further on to higher loss energies. A high loss energy means that the electron gives a large amount of its kinetic energy to an excitation of a vibration.
Typically, the spectrum of an HREEL spectrometer is in the range of 0-550 meV, which corresponds to 0 – 4500 cm^{-1} in wave numbers.

The resulting energy spectrum brings information about the vibration modes of surfaces. It can be used to characterise the adsorption sites on the surface. The frequency of the vibration reflects the bond strength to the substrate or a neighbouring atom, in a very simplified model the vibration of an atom can be interpreted like for a oscillating mass on a spring. The bond strength represents the force constant of the spring and the mass of the atom is the mounted mass on the spring. For example, higher coordination of a molecule leads to a stronger bonding, therefore a higher force constant, and a shift for this mode to higher frequencies. As mentioned before, the neighbourhood can influence the vibration too, a coupling of the modes is possible and introduce a shift.
But beside the vibrational information of adsorbed atoms or molecules, also the lattice of the substrate can be excited. The lattice vibrations are called phonons and their energy ranges from zero to several hundreds of meV. The phonons are separated into two types: the acoustic phonons with long wave length, which represent in-phase vibrations of the atoms within one unit cell, and the optical phonons with a short wavelength, where the atoms within one unit cell move in opposite directions. In case of a metal oxide the optical phonons generate also electrical dipole fields and therefore are able to interact with charged particles like the probing electrons in HREELS.

2.1.2 Excitation mechanisms

Dipole scattering

The incident electron scatters at a “large” distance from the surface, around 70 Å, due to dipole interaction between the electron and the adsorbed molecule on the surface. For an atom or molecule on the surface the approaching electron induces a time-varying dipole field. If the substrate is a metal the dipole field is generated between the electron and the image charge on the surface. An excitation takes place if the dipole of the incoming electron interacts with the dipole of the adsorbed molecule (Fig. 2.1)
Not every mode can be excited in a dipole interaction. A dipole-excitable mode leads to an effective dipole moment in the investigated molecule and a break in the symmetry

of the molecule. (This is the reason why isolated homodiatomic molecules can not be dipole-excited. Because the only possible vibration, the stretch vibration, maintains the symmetry of the molecule.)
For adsorbed molecules the surface selection rule gives an additional restriction: Only vibrational modes can be activated, which have a dipole moment perpendicular to the surface plane. If the dipole moment lies parallel to the surface it will be cancelled by its image charge in the substrate, therefore these modes are not excited by dipole scattering (Fig. 2.2).

However, reality is not obeying the strict theoretical prediction and "forbidden" modes are often detected very weak. The reason is that the surface is not perfect and so the screening of the parallel dipole is not completely cancelled.

The momentum transfer during the interaction is small, thus the scattering occurs in forward direction. The electrons after the dipole interaction are found in a small angular distribution, close to the specular geometry (Fig. 2.3).

Impact scattering

In the regime of impact scattering the interaction of the electron with the adsorbed molecule happens in the distance of atomic dimensions. Short-range potentials are important, because the electron directly scatter at the ion cores of the molecule combined with a huge change of momentum. Therefore the angular distribution is broad for the emerging electron from the sample, no narrow lobes will form like for the dipole scattering.

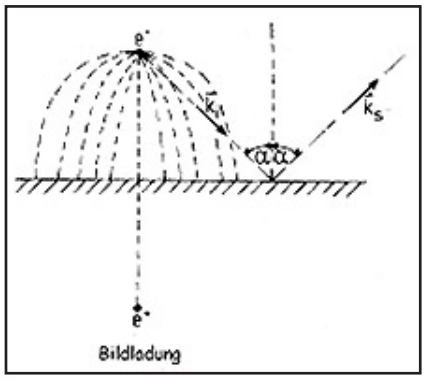

Fig. 2.1: The approaching electron generates an image charge in the substrate and the dipole field interacts with the molecule on the surface [4]

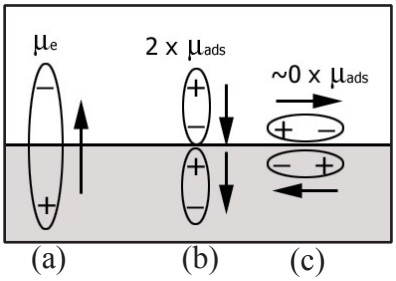

Fig. 2.2: Scheme of the surface selection rule, the dipole moment of the electron (a) interacts with the not vanishing dipole (b), a parallel dipole will be cancelled (c)

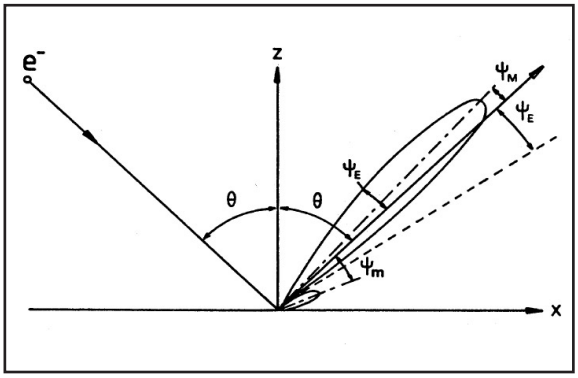

Fig. 2.3: Picture of the dominant dipole lobe near specular geometry [7]

The incident electron approaches so close to the molecule (or atom) that it cannot be distinguished from the electron in the molecules orbital. In the quantum mechanical description an exchange interaction has to be added [9].

In principle, every vibration mode can be excited with the impact scattering, the cross section depends on the primary energy E_p and the angle of incidence. For well ordered molecules on the surface a selection rule can be postulated: The incoming and the outgoing electron has nearly the same kinetic energy and the scattering symmetry has to be reversal in time. Further on vibrations perpendicular to the plane containing the path of incoming electrons and the surface normal can not be detected, when the detector is moved into this plane.

The intensity of the impact mode is much weaker than the ones from dipole scattering. Moving towards off-specular geometry, and thus attenuating the strong dipole modes in this way, it is possible to see the impact excitations.

Negative Ion Resonance scattering

Here, the probe electrons may be captured in an empty electronic energy level of the molecule on the surface. The additional electron transforms the molecule or atom to a temporary negative ion with a lifetime in the range of femto to nanoseconds.

A square-well potential is a good model for this: the incident electron tunnels through the energy barrier and occupies an empty energy level in the well. After the lifetime the trapped electron leaves the molecule in an excited state, which in turn may result in the excitation of a vibrational or rotational mode.

The resonance scattering can be classified by three types, mainly:

- the shape-resonance, when an electron goes to an unoccupied orbital of the

molecule, which is in the ground state, also called “single-particle shape resonance”;
- the core-excited-shape-resonance, when the electron excites the molecule before it gets trapped;
- the Feshback-resonance, where electron tunnels into an already excited molecule or atom.

The first two cases have their name (“shape”) because of the special form of the potential which forms between the electron and the molecule. On the one hand, an attractive polarisation potential exists and on the other hand a repulsive centrifuged barrier coming from the electron. The superposition of both results in a quasibound level, where the electron can be captured.

2.2 LEED - electron diffraction on surfaces

Low **e**nergy **e**lectron **d**iffraction is the standard method to determine the ordered structure of a surface. Whereas HREELS gives answers about how the atoms or molecules are bound to the surface, LEED tells how they arrange on the surface. In principle electrons with a primary energy in the range of 20-500 eV are targeted to the surface of the sample. There they are elastically backscattered and go to an hemispherical fluorescent screen. (Fig. 2.4)

Before the electrons reach the screen they have to pass in general two grids, the potential difference between G_1 and G_2 allows only the elastically backscattered electrons to go further on. (Note: electrons which are not elastically scattered have a kinetic energy lower than before the scattering process, they are not able to pass the electrical potential between the grids G_1 and G_2). The screen is held at a large positive potential to accelerate the electrons before they hit the screen and excite the phosphor coating their. Constructions with more than two grids are able to narrow the energy range of the passing electrons to the screen more precisely.

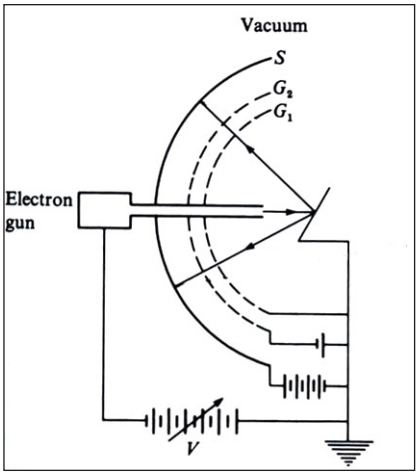

Fig 2.4: Sketch of a LEED, electrons are backscattered to the screen S, the two grids G_1, G_2 acting like a filter, only elastically scattered electrons can pass the potential barrier [2]

The LEED screen shows an image of the surface in the reciprocal space. Under ideal experimental conditions the resulting spots are infinitely sharp and the diffraction pattern is the Fourier transformed of the real space structure. (Abbe theory). In real experiments the pattern is of finite size due to instrumental distortions and surface imperfections, the Fourier transformation is not that straightforward any more.
The LEED pattern shows only the intensities but the phase is lost and therefore a reconstruction of the structure is not unambiguous. The exact positions cannot be derived, only the periodicity/ordering of the atoms. The distances in the reciprocal lattice are inversely proportional to the distances between points of the direct lattice.
For diffraction the incident electrons have to satisfy the Laue condition in reciprocal space:

$$\vec{G} = \vec{k}_f - \vec{k}_i \qquad \text{(eq. 2.1)}$$

$\vec{G}$ the reciprocal lattice vector has to be equal to the difference of the two wave vectors of the scattered ($\vec{k}_f$) and the incident ($\vec{k}_i$) electron.
In the Ewald construction this can be understood as follows: every electron leaving the surface in the direction where the sphere intersects a reciprocal lattice rod produces a diffraction spot on the screen (see Fig 2.5). The radius of the Ewald sphere is determined by the value of the wave vector of the incoming electron (by its primary energy). For smaller energies the sphere shrinks and less reciprocal lattice rods intersect the sphere.
Because of the hemispherical LEED screen the displayed pattern is not distorted compared to the intersection points of the Ewald sphere.

The 2D reciprocal lattice vector $\vec{G}$ is a linear combination of the two unit cell vectors $\vec{a}_1^*$, $\vec{a}_2^*$ of the reciprocal lattice (h and k are the Miller indices)

$$\vec{G} = h\,\vec{a}_1^* + k\,\vec{a}_2^* \qquad \text{(eq. 2.2)}$$

The relation between the reciprocal lattice and the real lattice is given by

$$\vec{a}_1^* = 2\pi\left(\frac{\vec{a}_2 \times \vec{n}}{\vec{a}_1(\vec{a}_2 \times \vec{n})}\right) \qquad \vec{a}_2^* = 2\pi\left(\frac{n \times \vec{a}_1}{\vec{a}_2(n \times \vec{a}_1)}\right) \qquad \text{(eq. 2.3)}$$

In this way it is possible to calculate the unit cell vectors for the real space lattice and vice versa. If an overlayer is formed on the surface, e.g. adsorption of atoms on the surface, the LEED pattern will get additional spots, when the new atoms form an ordered structure. This order can be expressed in terms of the so called Matrix notation, which links both lattices and unit cell vectors via a transformation matrix.

$$\vec{b} = \overleftrightarrow{M}\ \vec{a}$$
$$\vec{b} = \begin{pmatrix} b_1 \\ b_2 \end{pmatrix} = \begin{pmatrix} m_{11} & m_{12} \\ m_{21} & m_{22} \end{pmatrix} \begin{pmatrix} a_1 \\ a_2 \end{pmatrix} \qquad \text{(eq. 2.4)}$$

The same can be expressed very similar for the reciprocal lattice.

$$\overrightarrow{b^*} = \overleftrightarrow{M^*}\ \overrightarrow{a^*}$$
$$\overrightarrow{b^*} = \begin{pmatrix} b^*_1 \\ b^*_2 \end{pmatrix} = \begin{pmatrix} m^*_{11} & m^*_{12} \\ m^*_{21} & m^*_{22} \end{pmatrix} \begin{pmatrix} a^*_1 \\ a^*_2 \end{pmatrix} \qquad \text{(eq. 2.5)}$$

A (√3x√3)R30° structure, one of the structures of the presented vanadium film (see Chapter 3.3.2 O-rich termination (√3x√3)R30°), has the following relation

$$\begin{pmatrix} b_1 \\ b_2 \end{pmatrix} = \begin{pmatrix} 2 & 1 \\ -1 & 1 \end{pmatrix} \begin{pmatrix} a_1 \\ a_2 \end{pmatrix} \qquad \text{(eq. 2.6)}$$

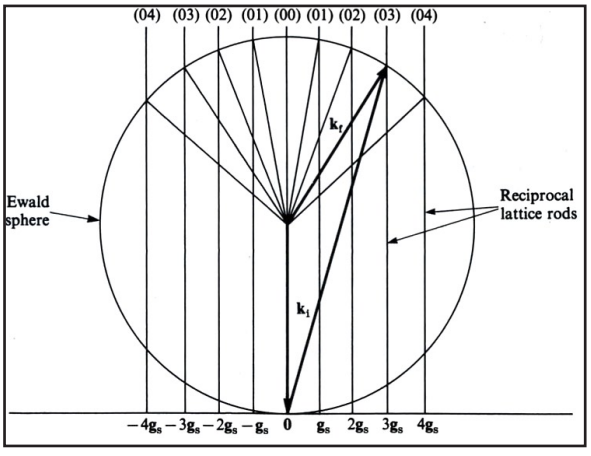

Fig 2.5: Construction of the Ewald sphere and the lattice rods on the surface in reciprocal space. The wave vector of the electron determine the radius of the sphere [2]

2.3 Photoelectron Spectroscopy

The basic concept of this method is known since a long time, it is the “photoelectric effect”: if light with the frequency ν hits a metal sample, electrons with a certain energy are ejected from the sample. The resulting kinetic energy contains three terms

$$E_{kin} = h\nu - E_B - \phi \qquad \text{(eq. 2.6)}$$

where hν represents the energy of the incident photon, E_B the binding energy and ϕ is the work function. To free an electron from its state, hν has to be higher than the binding energy and the work function together to lift the excited electron into vacuum. Depending on the energy of the photons a distinction is made in the naming : XPS (X-ray Photoelectron Spectroscopy) has a photon energy $E_P > 100eV$ and UPS (Ultraviolet Photoelectron Spectroscopy) has $E_P < 100eV$.
XPS is used to excite the core level electrons, whereas UPS investigates the valence electrons. The emitted electrons are detected by an electron analyser. For a fixed photon energy hν one gets an energy spectrum showing the occupied states in the sample. Electrons will be emitted into the vacuum, as long as the photon energy hν is larger than the binding energy and the work function. This is shown in Fig. 2.6, for a certain hν electrons from different levels excited having the same distance in kinetic energy as in the atom. Thus XPS/UPS brings information about the binding energies and the structure of the occupied levels. This is useful for the characterisation of atoms, moreover they can be identified by their core level structures. Additionally, the bonding changes the electronic environment of the electrons in the valence band. Exactly this change can be resolved in UPS and leads to the knowledge of bonding types and even bonding partners, by comparing the results to other references.

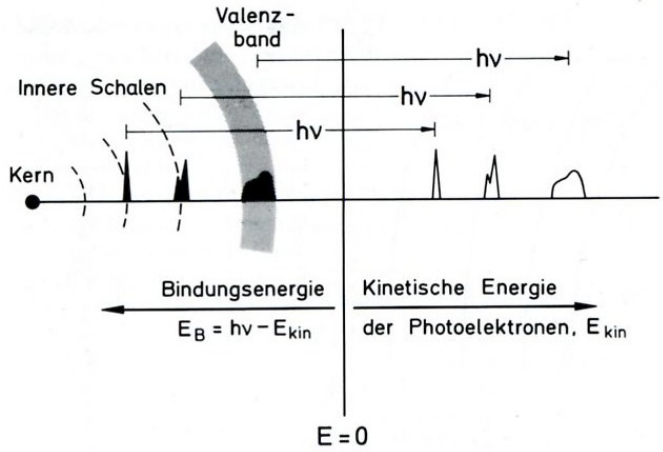

Fig 2.6: Probing an atom with constant energy hν, the occupied levels are detected in the XPS spectrum, in the way they are arranged in the atom [6, p. 329]

Later in this thesis resonant photoemission is used to determine the changes in the V3d level of the V_2O_3 film upon cooling to 100K. The incident photon with an energy of hν=517eV excites the electron of the V3d state. Moreover in a coherent process electrons from the V3p level get excited and are pumped to higher states little bit above the valence band. When they relax back to the V3p state they emit an photon, which can excite another V3d electron and thus increase the count rate. It is additionally an example, where different initial states leading to the same final state V3d.

3. Experimental Setup

3.1 UHV System

3.1.1 General

The main purpose of the ultra high vacuum system (UHV system) used for the here presented work is the vibrational spectroscopy done with electrons.
The system is separated into two chambers with different tasks: the “preparation chamber” (PC), mainly used for sample cleaning and film preparation and the “measurement chamber” (MC), where the high-resolution electron energy loss spectroscope is built in. A gatevalve separates the two chambers, this is necessary to reach pressures close to $9x10^{-11}$mbar in the “measurement chamber”, which is essential when one is studying interfaces from solid to gas phase.
Surfaces will be covered with the rest gas atoms in the chamber in 1 second, if the pressure is in the range of ~10^{-6}mbar (high vacuum). Pumping down to the region of ultra high vacuum (10^{-10}mbar) prolongs the lifetime of a clean prepared surface by a factor of 10^4, which is a reasonable time period to do proper experiments.
To attain the latter mentioned pressure range, a combination of various pumps is necessary and have to work in series to hold the pressure at this range.
At the HREELS system a roughing-pump (not visible in Fig. 3.1) works as backing pump for an oil diffusion pump (Fig. 3.1, D) and a turbo molecular pump (Fig. 3.1, T), sitting directly underneath the PC and generating a pressure of ~$5x10^{-10}$mbar in the chamber. After problems with hydrogen in the past and in consequence complications during surface preparations the oil diffusion pump was added between the turbo molecular pump and

the roughing-pump. It has the ability to pump especially light atoms/molecules, whereas the turbo pump is much better for heavier atoms/molecules. Hidden by the metal covers on the frame of the system, in the bottom part sits an “ion getter pump” and a “titanium sublimation pump” (TSP) (Fig. 3.1, Ps), which pump the measurement chamber.
This arrangement allows a separate pumping of the two chambers, which is indeed necessary during surface cleaning cycles, where the pressure in the “prep-chamber” (PC) goes up to $2x10^{-4}$mbar (sputtering with argon needs such high pressures and is a completely unacceptable high value for the spectrometer in the MC).

For measuring the pressure in the chambers, both are equipped with ion gauges. These hot filament gauges are suitable for UHV, they use the principle that electrons leaving the hot filament ionise residual gas atoms/molecules during collision. The so produced ions generating a measurable current on a grid close to the filament. This current is direct proportional to the gas density and the pressure in the chamber.
The samples can be transported from one chamber to the other with the transfer rod (Fig. 3.1, TR). The crystals themselves are mounted on sample plates (Fig. 3.2, Sa), which are fitted to the mountings on the manipulators. The sample plates are fixed with two springs (Fig. 3.2, S), pressing the plate to the mounting. The transfer rod head works with a “push & turn” lock. The tip of the rod has a slit-opening, which fits to the nipple of the sample

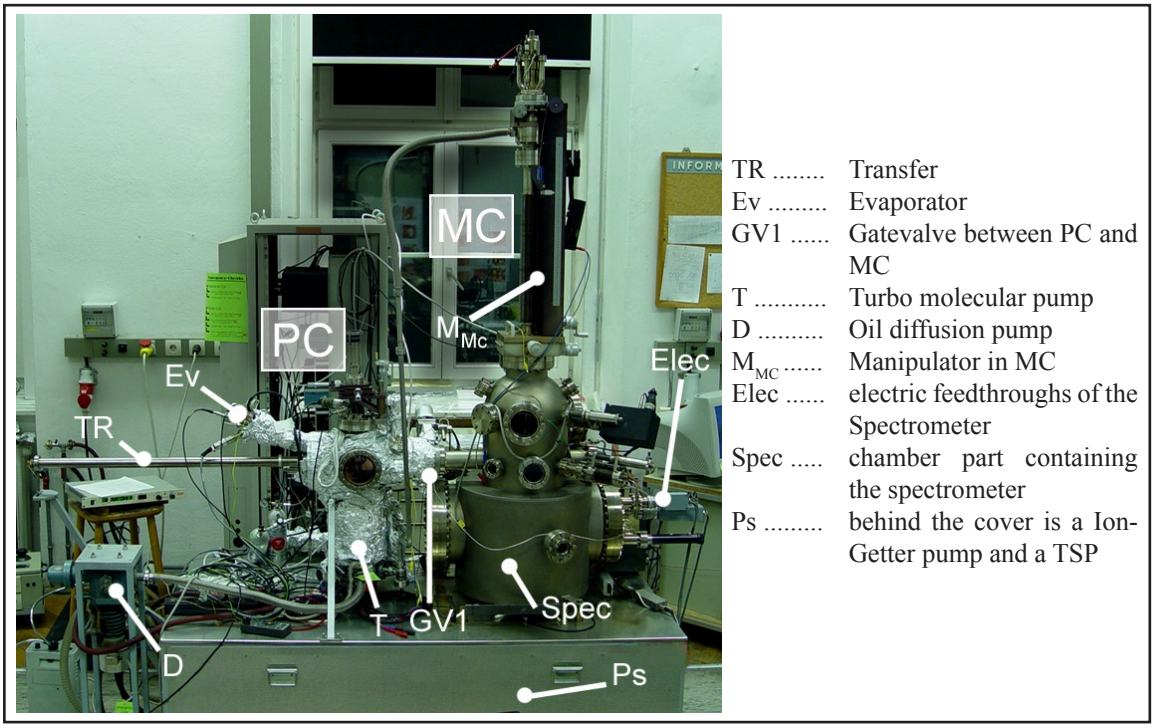

Fig 3.1: Sideview of the HREELS system, on the left side is the preparation chamber (PC) and on the right side is the measurement chamber (MC). Both chambers have windows installed on this side, so the user can see directly to the manipulators when a sample-transfer from one chamber to the other is done.

plate (left part of Sa in Fig. 3.2). This slit is slipped over the plate nipple, from inside the transfer rod head a spring pushes against it. Now turning the transfer rod by 90°, from vertical to horizontal orientation, locks the sample plate to the transfer rod. The plate can be pulled out of the manipulator mounting and moved to the other chamber, where it can be put to manipulator and freed from the transfer lock.

3.1.2 Preparation Chamber (PC)

In this UHV chamber the sample is prepared for measurements, this includes "sputtering" of the surface and evaporation of other materials onto the surface under controlled temperature, background gas conditions and evaporation rate.
Therefore the preparation chamber manipulator is able to heat the sample from the backside. Moreover high voltage (~1kV) can be applied to the sample plate (which is isolated from the manipulator), creating a potential difference between the outgoing electrons of the heating filament and the sample. The so emitted electrons are accelerated towards the sample and heat it up ("electron-beam heating"); temperature values up to 1000°C on the sample can be easily reached in this mode.

The temperature is supervised with the thermocouple, mounted at the springs of the manipulator (Fig. 3.2, TC). The thermocouple cannot be put on the crystal itself, because the sample plate has to be transferred to the measurement chamber. The permanent thermocouple at the springs is far away from the actual heating spot, which is at the centre of the sample plate. A controlled heating of the sample is impossible in this way.
Thus a temperature calibration is necessary for every new sample once, to find for each temperature value at the sample the respective temperature on the spring. A second thermocouple on the crystal side is temporally attached for this. Now the filament is set to a constant heating power. The temperature values measured by the two thermocouples (spring and sample) are recorded with a xt-plotter (Fig. 3.4 (a)). One will see that the temperature on the sample rises exponential with time till the maximum is reached. In the

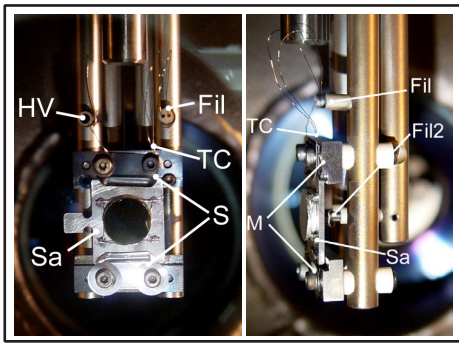

HV ..... High voltage wire
Fil ..... Filament wires
Fil2 ..... Heating coil, sitting behind sample
TC ..... Thermocouple wires
M ..... Mounting for sample plate, with the springs
S ..... Springs, holding sample plate
Sa ..... Sample plate & crystal

Fig. 3.2: Front- and sideview of the sample plate on the manipulator head in the preparation chamber.

xt-diagram the temperature, as a function of time, forms a plateau. The thermocouple at the spring displays a temperature development, which is reduced because of the temperature gradient. Thermal equilibrium is reached after 24 min. for a filament current of I_{Fil}= 2.0A. At this point the final sample temperature can be set in relation to the final temperature measured at the spring. If this is done for several different filament currents (= heating powers) a linear relation gives for each temperature value on the sample a corresponding one for the thermocouple mounted at the spring (Fig. 3.4 (b)). In a second step a diagram can be build up, which gives for each required sample temperature the necessary filament current (Fig. 3.4 (c)).

Two high precision valves are mounted to the preparation chamber to adjust well-defined background pressures of oxygen and argon (Fig. 3.3 V_O, V_{Ar}).

The metal electron-beam evaporator (Fig. 3.3, Ev) targets to the centre of the chamber. By rotating and adjusting the position of the manipulator (Fig. 3.3, M_{PC}) the sample can

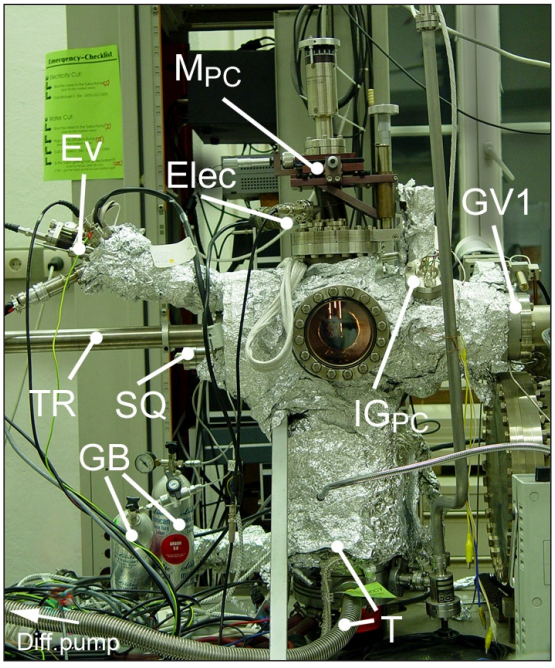

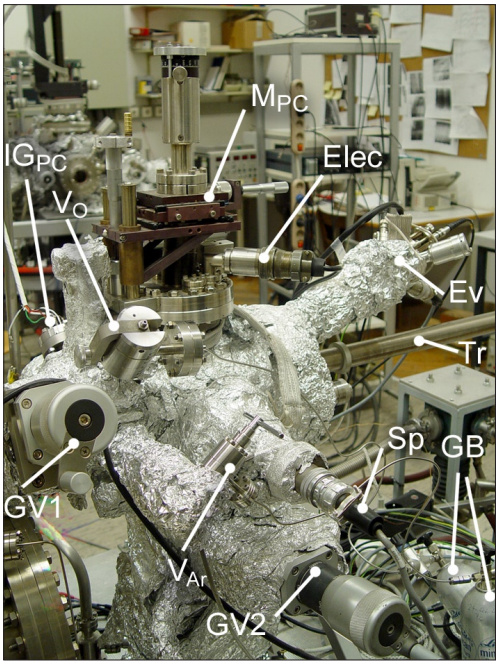

M_{PC}	Manipulator	TR	Transfer rod
Elec	Connectors/feedthroughs for sample heating, filament & HV	Ev	Evaporator, charged with a vanadium rod
GV1	Gatevalve between PC and MC	V_O	high precision valve, for oxygen
IG_{PC}	Ion gauge	V_{Ar}	high precision valve, for argon
T	Turbo molecular pump with exhaust to diffusion pump	GV2	Gatevalve between trubo pump (T) and the prepararion chamber
GB	Gas bottles, argon & oxygen	Sp	Connector/feedthrough for the sputter gun
SQ	Handle for rotating the microbalance		

Fig 3.3: The preparation chamber (PC), front (left picture). and back (right picture); this chamber is used for surface cleaning and film evaporations under controlled temperature, background pressure conditions

be brought into the beam of the evaporator. The evaporation rate is adjusted and stabilised with the proper setting of high voltage and filament current (see Chapter 3.2 and Chapter 3.3 for a detailed introduction to the film growth and the necessary settings). The rate itself is verified with a micro balance before the evaporation. If the desired rate is stable the arm with the micro balance is turned away and the sample is brought into the beam.

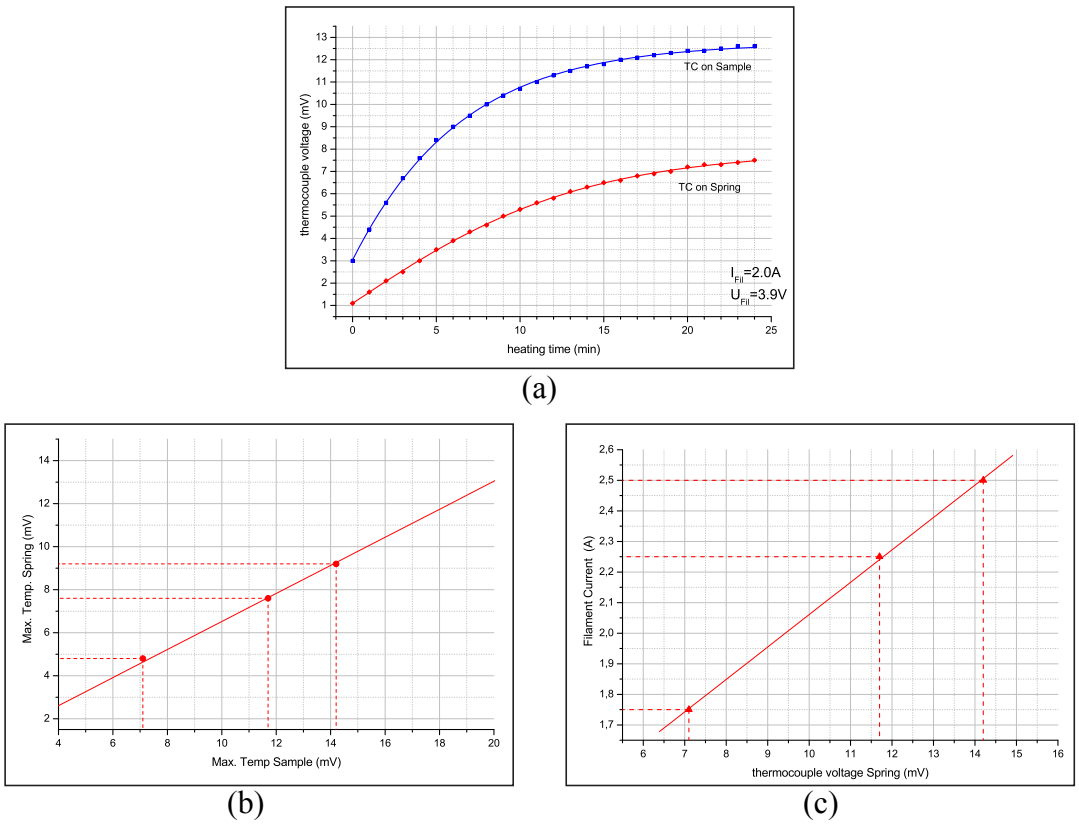

Fig. 3.4: The temperature calibration of the spring thermocouple
(a) example for the temperature on both thermocouples as function of heating time
(b) linear relation for the final thermocouple voltage (≡ temperature) pairs, each value on the spring has a corresponding one on the sample
(c) the temperature on the spring as a function of the applied filament current

3.1.3 Measurement chamber (MC)

The measurement chamber comprise the high-resolution energy loss spectrometer (ErEELS 31) (Fig. 3.5, Spec). All electrical connections to the lens system of the spectrometer go through two multi-pin connectors, which are linked with the control-computer of the HREELS (Fig. 3.5, CE). The two pumps in the measurement chamber, an ion getter pump in combination with a TSP, are directly connected to the scattering chamber of the spectrometer (see Fig. 3.1, Ps).

Moreover the measurement chamber is equipped with a mass spectrometer to determine the composition of the residual gas in the measurement chamber (Fig. 3.5, M_{Spec}). For structural analyses the chamber possesses a LEED screen (Fig. 3.5, L).

Via a high precision valve or a pin-hole doser the sample can be exposured to various gases, (Fig. 3.5, V, PD), supplied by the "gas handing line" of the UHV-system. The pin-hole doser is mounted on a linear motion to approach it to the sample for dosing. The manipulator in the chamber can be moved in x,y,z direction and rotated 360°: On top are feedthroughs for two thermocouple connectors and the sample heating (high voltage and filament current) for electron-beam heating, like in the preparation chamber. Moreover

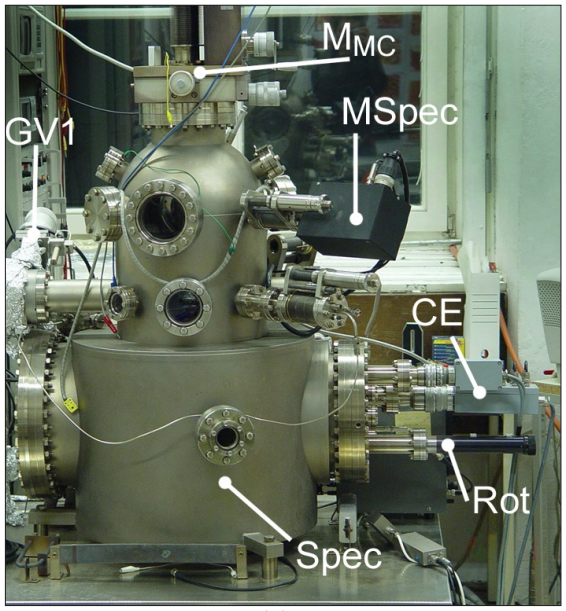

(a)

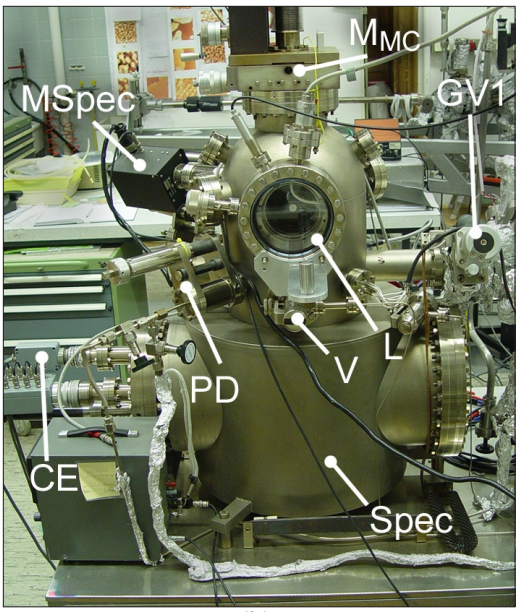

(b)

M_{MC}	Manipulator	Spec	Chamber part hosting the HREELS inside
MSpec	Mass-spectrometer		
CE	Connectors/feedsthroughs for the HREELS	GV1	Gatevalve between PC and MC
		L	LEED screen
Rot	Bar to rotate the analysator in the HREEL spectrometer	V	high precision valve
		PD	Pin-hole doser with linear motion

Fig 3.5: The measurement chamber (MC), front (left picture) and back (right picture); this chamber contains the HREEL spectrometer, heart of the UHV-system, for vibrational studies on the here presented surfaces

it is build in the way that it can be filled with liquid nitrogen or helium to enable sample cooling. It takes about 40min to bring a sample from room temperature (300K) to 100K.

The manipulator head has, like the manipulator head in the “prep-chamber”, two springs where the sample plate can be pushed in or pulled out with the transfer rod. (Additionally the head where the sample sits can be rotated for azimuthal resolved studies, but this option was not used in this work; see Fig. 3.6, the close up shows the rotatable head with the sample)

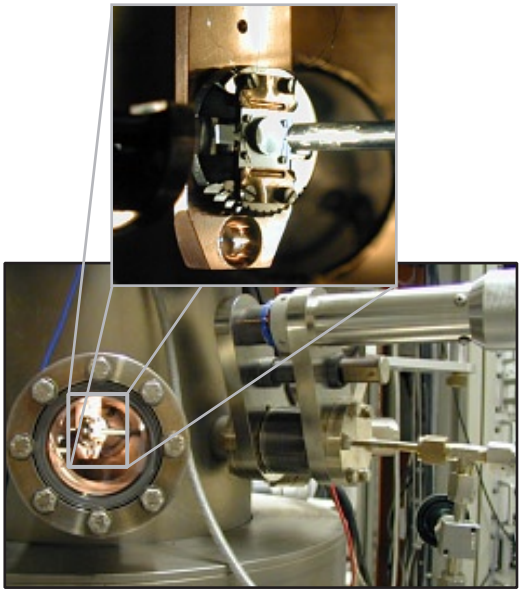

Fig. 3.6: The pin-hole doser in action, brought closer to the sample via the linar motion.

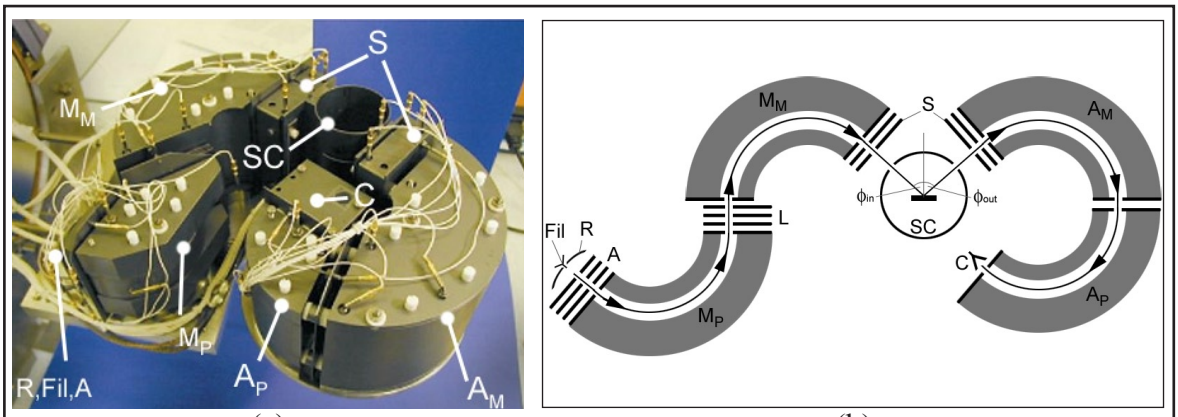

(a) (b)

Fil	Hair-pin filament, tungsten wire
R	Repeller
A	set of three lenses, focus the electrons in M_P
M_P	Premonochromator, narrows the energy window of the electrons inside
L	three lenses to refocus electron beam
M_M	Mainmonochromator
SC	Scatter chamber
S	Scatter lenses, two focusing to the sample, other two are refocusing the scattered electrons
ϕ_{in},ϕ_{out} ...	angle of incoming & scattered electrons
A_M	Mainanalysator
A_P	Postanalysator, fades out reflected electrons
C	Channeltron

Fig 3.7: Picture of the HREEL spectrometer (a) and the sketch of the lenses and monochromators inside (b)

HREEL spectrometer

The spectrometer ErEELS31 has been designed at the University of Nürnberg-Erlangen by Dr. Gossman and Prof. Froitzheim. As written in the techniques (see Chapter 2 "Techniques", p. 3) about energy loss spectroscopy, it is possible to detect vibration modes on a surface by measuring the kinetic energy of the electrons after a scattering process. With the additional knowledge of the energy before the interaction, one can calculate the energy difference and thus determine the value of energy loss energy, which was given to the other interaction partner.

$$E_{in} - E_{out} = \Delta E \qquad \text{(eq. 3.1)}$$

The construction of the spectrometer with two monochromators and two analysators gives the possibility to do "high-resolution" EELS, due to the better energetically homogeneity of the electron beam before and after the scattering.

The electrons are emitted from a tungsten hair-pin filament (Fig 3.7 (b), Fil) and are primarily directed to the lenses with the so called "repeller" (Fig. 3.7 (b), R). The lenses A_1, A_2, A_3 are focusing the electron beam into the premonochromator (Fig. 3.7 (b), A & MP). The electrons are selected (monochromaised) over a range of energy, the energy distribution will be narrowed in other words and even more in the up coming mainmonochromator

(Fig. 3.6 (b), MM). Before the electrons reach the scattering chamber (Fig. 3.7, SC), they are refocused by the lenses S_1 and S_2. The potential of the sample in the scattering chamber sets the electrons finally to the primary Energy E_{in}. During the experiments
"it is important that everything that is in the scattering chamber is on the same potential, namely on 'crystal potential' (which corresponds to the primary energy). This means that the electrical feedthroughs on top of the manipulator should be connected accordingly. Electrical connections to the sample head, copper block and filament (note: the whole manipulator head) *have to be short-cut and put on crystal potential."*
[12, p. 206]

Otherwise the electrons will loose its monochromatic kinetic energy and the resulting loss energies after the scatter process can not be calculated with equation (eq. 3.1).

The scattered electrons are refocused with S_3 and S_4 into the mainanalysator (Fig. 3.7 (b), A_M), where they can be energetically filtered. The second analysator (Fig. 3.7 (b), A_P) erases electrons with high kinetic energy from the energy loss spectrum (these electrons are reflected from the inside of the analysator A_M). At the end the electrons are counted with a channeltron.

Because of the low kinetic energy of the electrons (~5eV), external magnetic and electrical fields can easily deflect them, to prevent this the chamber is equipped with a μ-metal shielding. Apart from that all elements in the spectrometer like lenses, slits and monochromator are covered with graphite in order to equal the work function on all elements and to reduce the generation of secondary electrons.

The analysator part (A_M & A_P) can be rotated around the vertical axis of the scattering chamber from outside the UHV-system. Most measurements are done in specular geometry, the angle of incident ϕ_{in} is equal to the angle ϕ_{out} of the leaving electrons (in general in specular geometry the angle was $\phi_{in} = \phi_{out} = 60°$). But for off-specular measurements ($\phi_{in} \neq \phi_{out}$) the analysator has to be rotated.
During the tuning of the spectrometer no sample is in the scattering chamber and the electrons crossing the scattering chamber in a straight line, emerging from the mainmonochromator and entering the rotated analysator. The tunning has to be done regularly to prevent a bad resolution in the spectrometer. (Michael Sock put in his PhD-thesis a well written instruction about the tunning of the spectrometer, see [12, chapter A3])

A PC program (EELS-Comander31), delivered with the spectrometer, controls all settings of the elements. The computer is linked to the spectrometer via a D/A converter unit. The program on the computer sends the necessary settings for the elements in the spectrometer (lenses and monochromator plates) in digital form to the D/A converter, from there the

commands are “translated” into analog values – voltages – and are applied to the proper element. On the other hand the measured signal at the channeltron goes to the converter, where the current value is transformed into the correct signal for the PC program, so on the screen a spectrum is recorded. The converter builds the interface, the translator, between the analog spectrometer and the (digital) computer program.
The resulting data is intensity as a function of loss energy. If the spectrum contains a peak at a certain energy value ΔE, this indicates that the electrons loose exactly this amount of energy ΔE during the scattering on the surface (a vibration with energy ΔE was excited).

3.2 Sample preparation

The vanadium oxide films are deposited on a Rh(111) crystal, which is spot welded to the sample plate with two tantalum wires (Fig. 3.2).

To clean the substrate surface sputter and annealing cycles are done: The sputtering is done with Ar^+ bombardment, therefore a background pressure of $2x10^{-4}$mbar oxygen in the preparation chamber is combined with the ion gun (Fig. 3.3, Sp) set to high voltage of U_{HV}= 1.5kV and an emission current of I_{Em}= 25mA. The sputtering was followed by annealing of the crystal in UHV conditions, it was heated up to 1400K (~1126°C) by using the electron beam heating for 2 minutes (high voltage on the sample plate U_{HV}= 1kV and emission current I_{Em}= 50mA). During cooling down to room temperature a background pressure of $2x10^{-7}$mbar oxygen pressure in the chamber is adjusted.
In this way carbon atoms due to the surface diffusion during the annealing can be eliminated. As last step of the cleaning process a short annealing is performed: back in UHV the sample is heated up to 1170K (~900°C) to desorb the oxygen from the latter step. For the annealing a high voltage of U_{HV}= 1kV and an emission current of I_{Em}= 50mA is used lasting for 1 minute. Fig. 3.9 shows a LEED picture of the clean Rh(111) surface after the preparation

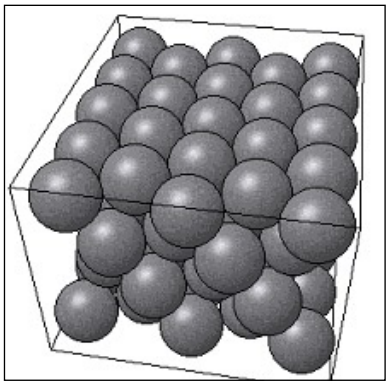

Fig 3.8: Rh(111) crystal, a= 3.8Å

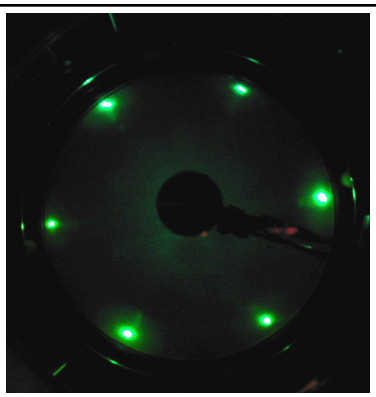

Fig 3.9: LEED pattern of the crystal (E_p= 50eV)

3.3 V_2O_3 (0001) film growth

3.3.1 Vanadyl termination (1x1) V=O

The fabrication of the V_2O_3 film is done in reactive evaporation modus: thus vanadium is evaporated with the electron-beam evaporator onto the crystal surface, while the sample is heated up at 523K (250°C) and the oxygen background pressure of $2x10^{-7}$mbar in the preparation chamber is adjusted.
After the short annealing of the clean Rh(111) crystal the HV is turned off and the sample is heated only by the filament (I_{Fil}= 1.85A). The manipulator head is moved in the way that the sample is facing away from the evaporator. Meanwhile the crystal is brought to the preferred 523K (250°C), the correct settings for the evaporator are found by measuring the rate of the evaporated vanadium with a micro balance.
Vanadium oxide films in the range of 10-15MLE (40-60Å) are produced with an emission current of around I_{Em}= 26mA (I_{Fil}≈1.9A) and a high voltage of U_{HVl}≈ 990V. The proper settings for a stable rate are slightly different every time, because the evaporating amount of V atoms is strongly depending on the position of the vanadium rod in the evaporator. (The rod shrinks during the evaporation and thus has to be moved further in)
1MLE of vanadium on the rhodium (111) surface corresponds to 13.45 digits on the micro balance [12, p. 46], with

$$\left(\frac{\text{time interval}}{\text{digit}}\right) \times \left(\text{X MLE} \times 13.45\right) = \text{evap. time} \qquad \text{(eq. 3.1)}$$

one can calculate the needed time to build a X MLE thick film. The rate is the time interval passing from one digit to the next one (sec/digit) on the micro balance.

When the rate is stable, the micro balance is turned away, the shutter of the evaporator is closed, the sample is moved in front of the evaporator and the oxygen pressure is set to the above mentioned $2x10^{-7}$mbar. The shutter is opened for the calculated evaporation time. After the evaporation the sample is heated 5min. further on and finally cooled down in the oxygen pressure. The latter two steps are necessary firstly to supply enough energy to the film for ordering and secondly to offer enough oxygen to ensure a saturated vanadyl surface.

Studies in our group [12,13] have shown that a final annealing of this surface improves the ordering of the film structure. Changes are visible in HREELS (higher count rate), STM (roughness lower) and LEED (sharper spots).
The annealing to 873K (600°C) is performed in the measurement chamber, with an applied high voltage U_{HV}= 770V and an emission current I_{Em}= 16mA for 1min. 30sec. When

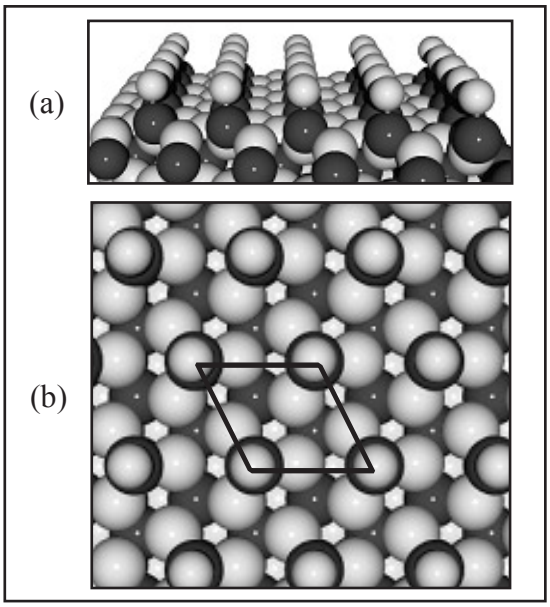

Fig 3.10: Model of the vanadyl terminated surface (V=O(1x1)); (a) sideview , (b) topview bright balls= O; dark balls= V

the sample is back at room temperature it is ready for measurement.

Instead of always preparing a new surface before measurements, the film can also be "reactivated" via reoxidation. In principle it is the same scheme, only the evaporation of vanadium is missing. So the old film is heated up to the necessary 523K (250°C) and then kept at this value for 5min., while oxygen is delivered by background dosing ($2x10^{-7}$mbar O_2). Once again 5 minutes are added at this conditions and then the sample is cooled down in this oxygen ambient. Like before the surface is annealed to 837K(600°C) as a last step.

The vanadium sesquioxide film has the corundum lattice structure, which is known from bulk V_2O_3 crystals. The stacking sequence follows the principle O_3-V-V'-O_3-V-V'-…, where alternating O_3 layers and V_2 layers are the building blocks of the film. However the surface termination is not one of the three possible ideal bulk lattice terminations: O_3 layer, V_2 layer (V-V'), V layer.

These surfaces are thermodynamical unstable under the employed conditions and therefore not favorised, but rather VO groups are formed which sit on a threefold hollow position, above three oxygen atoms (see Fig. 3.10). The oxygen atom in the VO group is double bonded to the vanadium atom and the bond length of the latter is 1.61Å [13], called vanadyl group. (similar behaviour is known from Cr_2O_3, where "chromyls" (Cr=O) are forming on the surface [14])

The vanadyl stretch vibration is detectable in HREEL spectra (Fig. 3.13) at 129meV. It should be mentioned that previous HREELS studies on such surfaces gave the actual evidence for the VO groups on the surface, which were predicted from theory; they are also visible in the atomic resolved STM images (Fig. 3.11). The vanadyl species was also observed by A.C. Dupuis in her PhD thesis in HREELS and IRAS (compare [15] and [16]).

The peak at 47meV in Fig. 3.13 (HREELS) stems from a bulk vibration, like the one at 66meV, which is only visible on cold samples (see Fig. 5.8 in Chapter 5.4.1, p.79). The dominant feature at 80meV is created by the vibration of the VO group to the three oxygen atoms underneath. This peak contains on the high-energy side an almost hidden vibration at 92meV. The detected intensity at 157meV is no vibrational mode, but a double excitation at twice the frequency from the O_3-VO group vibration at 78meV (157~2x78meV).

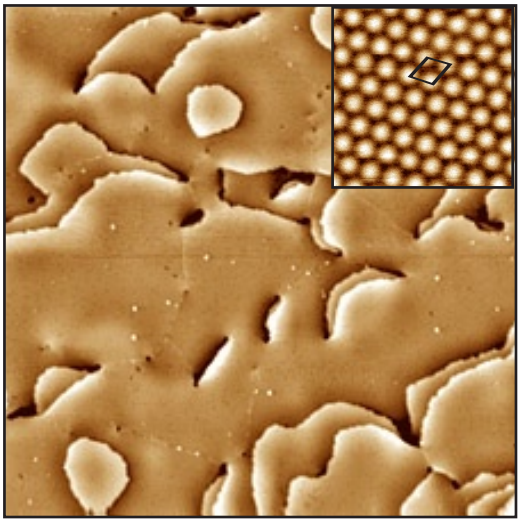

Fig 3.11: Vanadyl surface in STM
The inset shows a high resolution image, visible are the VO groups as bright spots [13]

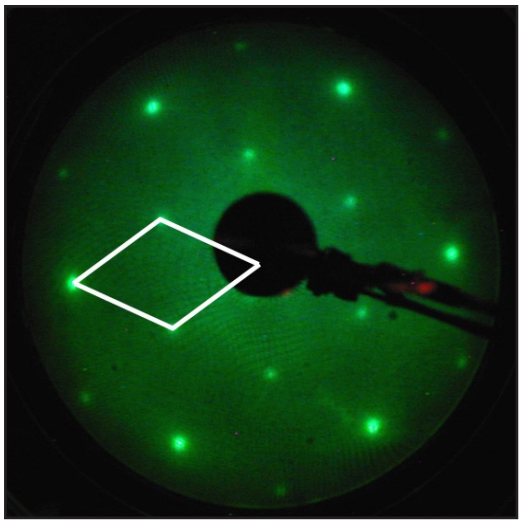

Fig 3.12: In LEED the surface gives a sharp pattern, indicating a highly ordered structure (E_P= 50eV)

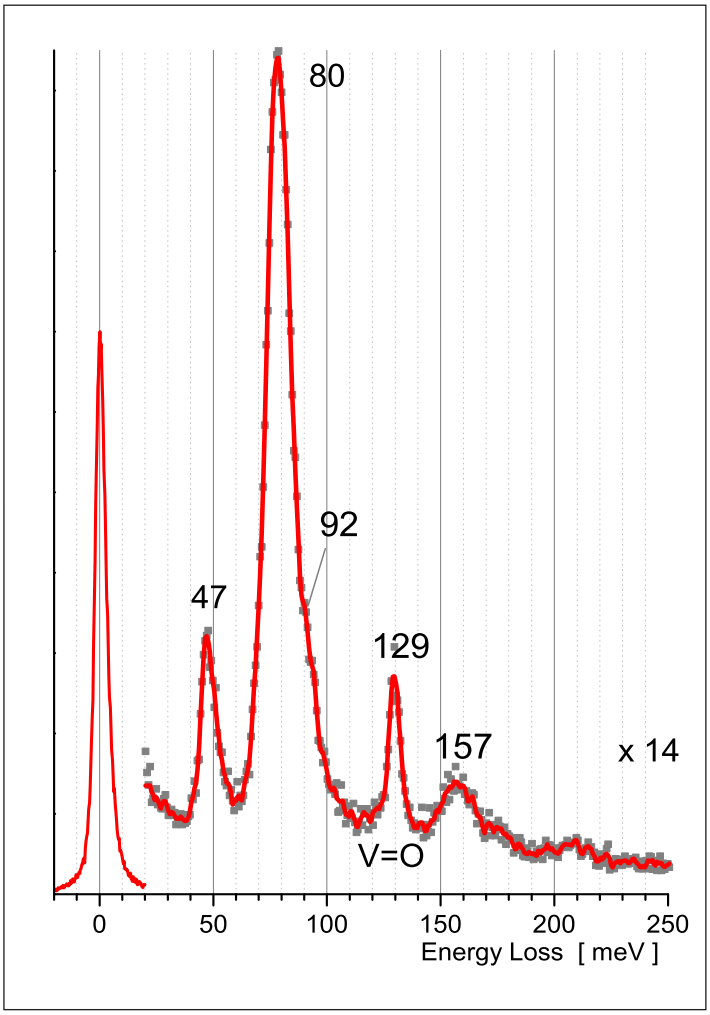

Fig 3.13: Phonon spectrum of the vanadyl terminated V=O(1x1) surface at room temperature after annealing to 600°C

3.3.2 O-rich termination (√3x√3)R30°

Reducing the content of vanadyls on the (1x1) V=O surface involves local changes in the first subsurface layers. The interface gets oxygen richer, because one missing V=O frees three oxygen atoms underneath (the vanadyl sits on a 3-fold hollow site). As mentioned before, the ideal O_3 termination (O_3V_2-O_3V_2-…) is unstable, therefore the lattice structure changes in the way to reduce the surface dipole. Displacement of one vanadium atom from the second V_2 layer to the first one, as it is shown in Fig. 3.14 [17] is the consequence. A surface trilayer is formed followed by a single V-layer, then the stacking sequence is $O_3V_3O_3$-V-O_3V_2-O_3V_2-… .

The O-rich termination is created from a perfect (1x1) V=O surface by annealing the sample in oxygen ambient instead of UHV. The sample temperature is 837K (600°C), the oxygen background pressure is set to $5x10^{-6}$mbar during the annealing. The temperature is reached in two steps: 1) a 30sec flash with U_{HV}= 760V and I_{Em}= 30mA and then 2) a constant heating power with a filament current of I_{Fil}= 2.2A and added high voltage U_{HV}= 240V.
Under these conditions the sample is annealed for 15 minutes. Afterwards the oxygen pressure is kept at this value, till the sample reaches room temperature. The resulting surface contains two unit cells: as one can see from Fig. 3.15, the black unit cell contains two vanadyl groups (1/3 is missing). But there are areas too, where in the unit cell only one vanadyl is left, thus 2/3 of vanadyl groups are gone (Fig. 3.15, gray unit cell).

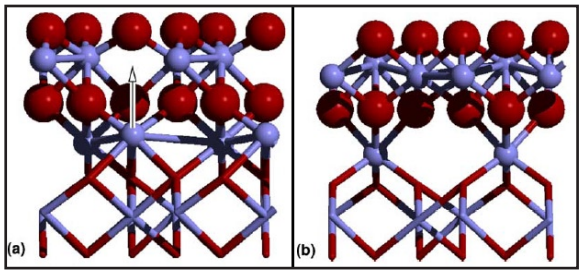

Fig 3.14: Model how the trilayer froms, a vanadium atom from the second metal bilayer moves upwards (a) and generates in (b) a $O_3V_3O_3$ surface layer followed by a V layer; afterwards the stacking deeper into the film is O_3V_2-O_3V_2-... [17]

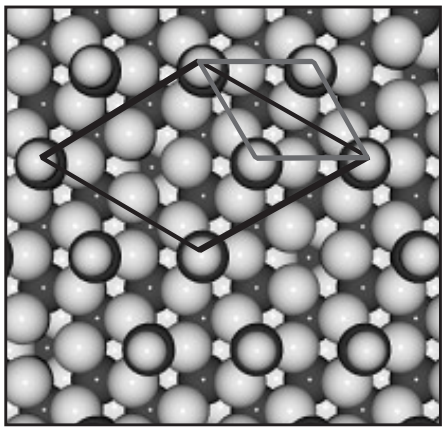

Fig 3.15: The O-rich (√3x√3) structure in a model; the black unit cell may hold one vandyl in the center or none, both cases coexist, the gray unit cell displays the second domain [14]

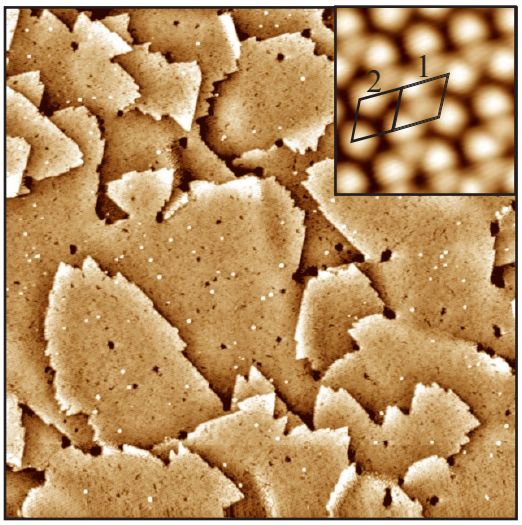

Fig 3.16: The high resolution STM of the O-rich (√3x√3) surface agree with the model, both types of unit cells can be found: (1) one vanadyl inside and (2) with none [13]

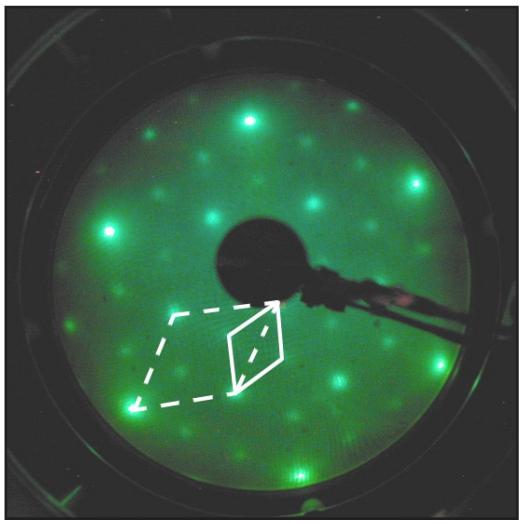

Fig 3.17: The missing vanadyls create a (√3x√3) LEED pattern. The dashed unit cell corresponds with the gray one in the model (Fig. 3.15) (E_p= 55eV)

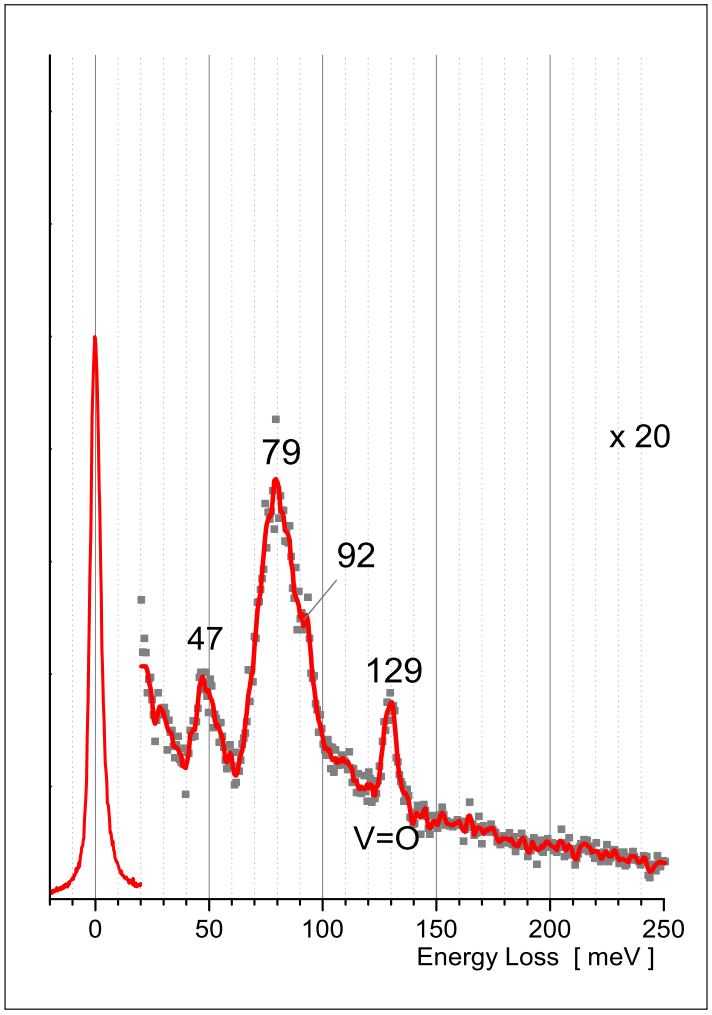

Fig 3.18: HREEL spectrum of the O-rich (√3x√3) termination at room temperature; the lower count rate is visible in the multplication factor and the worser signal-to-noise ratio

In Fig. 3.16 the inset shows the resulting unit cells: the visible area contains bright spots and a dark background (unit cell 2 in Fig. 3.16), but there are also some cells where a weaker spot is seen inside (unit cell 1). It is believed that all visible dots represent vanadyls on the surface. The survey STM image shows a surface with straight boundaries of the terraces.
Comparing this to the model (Fig. 3.15), the weaker spots can be associated as single vanadyls within the unit cell ($(O=V)_{2/3}$-O_3V_2-O_3V-…), whereas areas with only bright spots and black background a unit cell with no vanadyls inside ($(O=V)_{1/3}$-O_3V_2-O_3V-…).

The vibrational spectrum of the (√3x√3)R30° surface at room temperature (Fig 3.18) shows the same losses as the vanadyl (1x1) surface (Fig. 3.12): the two bulk vibrations at 47meV and 92meV, the distinct peak at 79meV coming from the surface oxygen atoms vibrating normal to the interface or, if a vanadyl sits above, in the direction of the bond to the vanadium atom of the VO group. Because there are still V=O dimers on the surface, the stretch vibration at 129meV can also be detected. At 110meV at rather broad and weak feature appears, which is not seen in the vanadyl terminated (1x1) surface.
The count rate in the spectra (Fig. 3.18) is weaker and therefore the signal carries more noise.

In the LEED (Fig. 3.17) a (√3x√3)R30° structure is observable, rotated by 30° in respect to the other unit cell.

3.3.3 V-rich (1x1) termination

A third surface termination can be achieved from the vanadyl terminated surface as a starting point. I evaporated at room temperature vanadium onto the V=O (1x1) surface, in the range of 0.1 - 0.8 MLE thickness. The films with the metal overlayer are "flashed" to ~673K (~400°C), U_{HV}= 760V and I_{Em}= 16mA are the settings on the heating unit, for about 45sec, improving the ordering of the adsorbed metal. From STM studies in our group we know that for low coverage two phases are detectable on the surface (see Fig. 3.22). In the image flat areas coexist with a region containing trimers, it is assumed that the latter are three vanadyls with one vanadium atom in their centre. [12, 13]

With increasing amount of the metallic vanadium, the flat areas are spreading out over the whole surface and no trimers are visible. (0.6MLE of vanadium are enough)
This phase looks like the unstable V_2-layer, but *"we emphasise that these surface are fundamentally different from the ideal V-terminated V_2O_3 (0001) (single or double) layer."* [13, p.. 115]

The STM images (Fig. 3.23) suggest a slightly buckled surface layer of vanadium atoms on a V_2-layer, so the stacking sequence will be V_3-O_3-V_2-O_3-V_2-… .The vanadium atoms are sitting above three oxygen atoms (3-fold hollow sites). High resolution STM images show a surface reconstruction, which can be explained by a surface buckling from two inequivalent vanadium atoms in the top layer; the V atoms with vanadium atoms of the

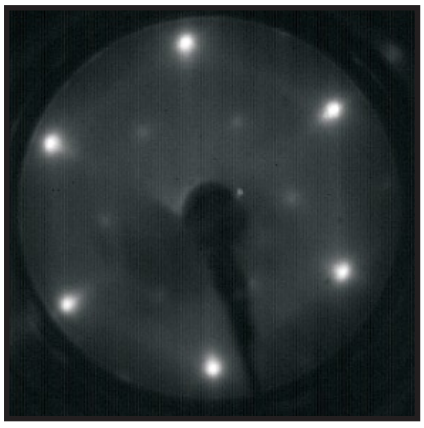

Fig 3.19: The LEED pattern of a 0.6MLE thick vanadium metal layer

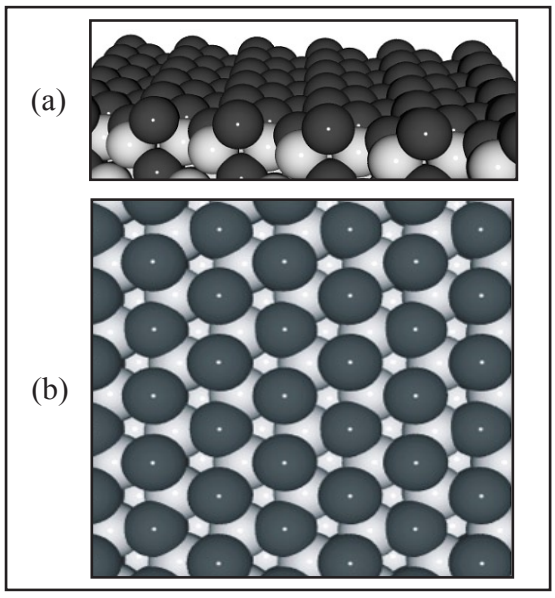

Fig 3.20: Model of the V-rich (1x1) termination. (a) sideview , (b) topview bright balls= O; dark balls= V

next V_2 layer below are 0.1Å higher than the surface V atoms with no vanadium atom underneath.
The resulting LEED picture (Fig. 3.19) shows a (1/√3x1/√3) pattern, rotated by 30° to the pattern of the V=O(1x1) structure. The inner spots are weaker in intensity than the outer ones, maybe originating from the slight buckling of the top V_3 layer. The unit cell can be found in high resolution STM images, too, as one can see in Fig. 3.23.

In HREELS the new surface reconstruction is primary visible by the loss of the vanadyl stretch vibration at 129meV. It is still detectable for vanadium coverages of 0.1-0.15 MLE, but attenuated. The vibration vanishes for depositions above 0.3MLE of metallic vanadium (see Fig. 3.21). The other vibrations 47meV and 76meV are always visible in the spectrum, nevertheless their intensity is decreasing with increasing amount of evaporated vanadium.

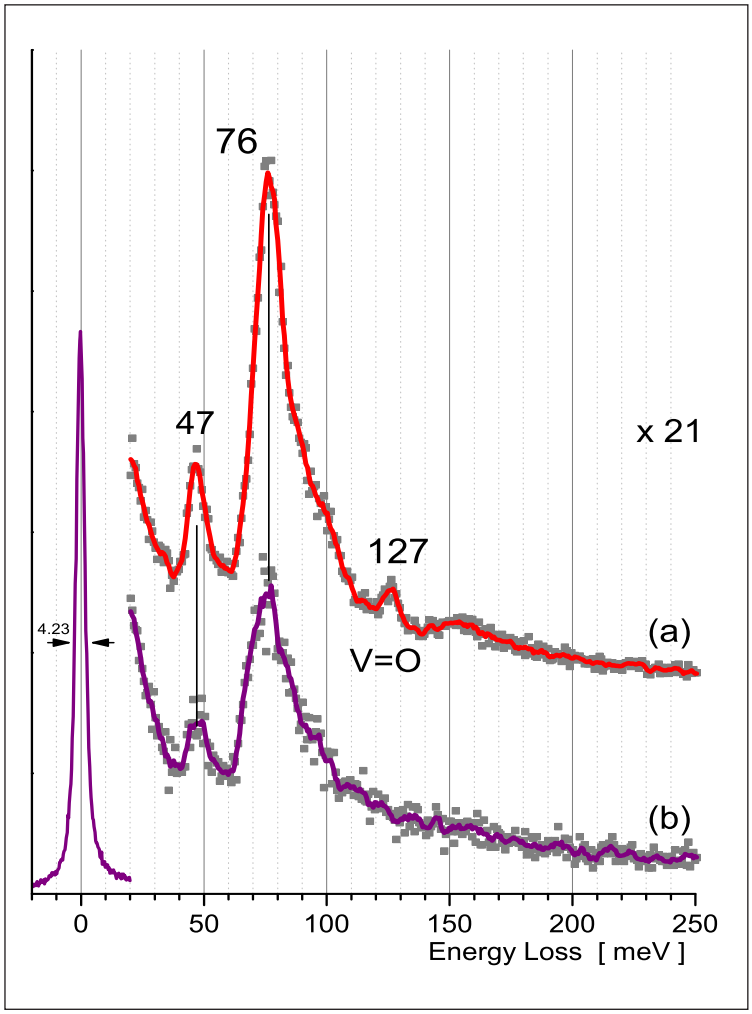

Fig 3.21: Two different coverages of metallic vanadium on the V=O(1x1) surface: (a) 0.15MLE and (b) 0.3MLE; with increasing amount of V atoms the spectrum gets more and more attenuated and the vanadyl stretch vibration gets lost (pure vanadyl terminated surface Fig.3.13, p. 25)

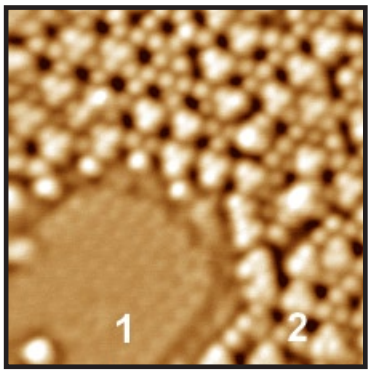

Fig 3.22: In the beginning the V-rich surface shows two phases: one looks like a flat surface (1) and the other one is dominated by "trimers" (2)

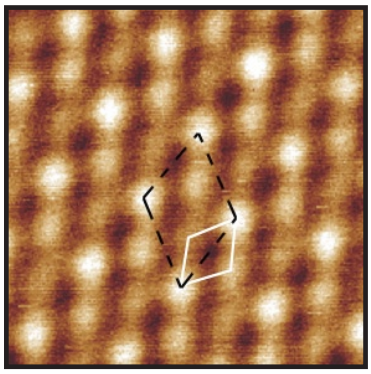

Fig 3.23: High resolution STM image of the flat phase, containing two unit cells, fitting to the model of buckled V-atoms

3.4 Dosing of H_2O

3.4.1 Preparation

Gas Line

The water used in this study is highly pure. It is filled into a glass cuvette, which was cleaned before with acetone and ethanol. The cuvette itself is connected to the gas handing line of the system.

The water is further purified by several "freeze-pump-thaw" cycles: The liquid water is frozen by cooling the cuvette with a mixture of ethanol and liquid nitrogen. When the water gets solid the cuvette is pumped, in this way the remaining gas above the ice is brought away. Before every dosing series all involved gas lines are pumped for several minutes to free them from unwanted rest gas. In the next step the lines are filled with H_2O vapour till the pirani manometer in the GHL displayed atmosphere pressure. The latter step is to saturate the walls of the gas lines with H_2O molecules, so that during the dosing no chemical reactions are taking place, producing unwanted molecules due to dissociation or recombination with the H_2O molecules. This amount of H_2O is then pumped away and the actual filling for the measurements is done.

The working pressure throughout all measurements in the gas line is $6x10^{-2}$mbar, measured by the pirani manometer in the gas handing line.

Sample position

The sample on the manipulator is rotated to the retractable pin-hole doser and is brought into position. The doser is moved into the UHV chamber till the distance to the crystal is ~ 10 mm. By opening the front valve of the doser, the H_2O is dosed on the surface for a certain amount of time. After dosing, the valve is closed and immediately the sample is moved away from the doser (in z-direction) to prevent that further water can adsorb on the surface. To stop leaking water molecules into the chamber, the second valve on the pin-hole doser is opened to pump the volume of the doser nozzle via the turbo pump.

3.4.2 Doser calibration

If one is using a pin-hole doser the time of dosing cannot be compared with dosing from the background pressure, because the former method depends on how close the sample is and how high the pressure in the gas line is; all of this define the rate of dosing. Thus a calibration is essential.

In the following HREEL spectra will be compared between a dosing series done with the pin-hole doser and a dosing series done via background pressure. In this way the dosing amount as a function of time for the pin-hole doser can be set into relation to a certain amount of Langmuir.

As reference feature in the spectrum the frustrated rotation of H_2O at 100meV has been taken (see Chapter 4.2, p. 42), this sharp vibrational mode is visible from the very first dosing steps. The water exposure is done on clean Rh(111) crystal at a sample temperature of 100K (the manipulator is cooled with liquid nitrogen). Two dosing series of water are done, one with the pin-hole doser and one via background pressure with a high precision valve. Afterwards the peak height of the chosen vibration (100meV) is measured in every spectrum, giving a development of the peak height as a function of time (pin-hole doser) and of dosing amount in Langmuir. At least in the beginning of the dosing series the increase in intensity of the peak should be linear, thus the two series are comparable. In Fig. 3.24 both series are presented in one diagram. Comparing the values of the dosing time (seconds) with the dosing amount (L) for the same peak height leads to a value for the pin-hole doser: 92 seconds of dosing with the pin-hole doser are 0.6L with background dosing. The settings for the pin-hole doser are kept always the same for the whole measurements: The H_2O pressure in the gas line to the doser is $6x10^{-2}$mbar and the doser tip is brought to the sample within a spacing of ~10mm. Before every dosing series with water the gas line is pumped out and filled with H_2O vapour one time to saturate the gas line walls, this “test” filling is pumped away and then the filling for the dosing series is done.

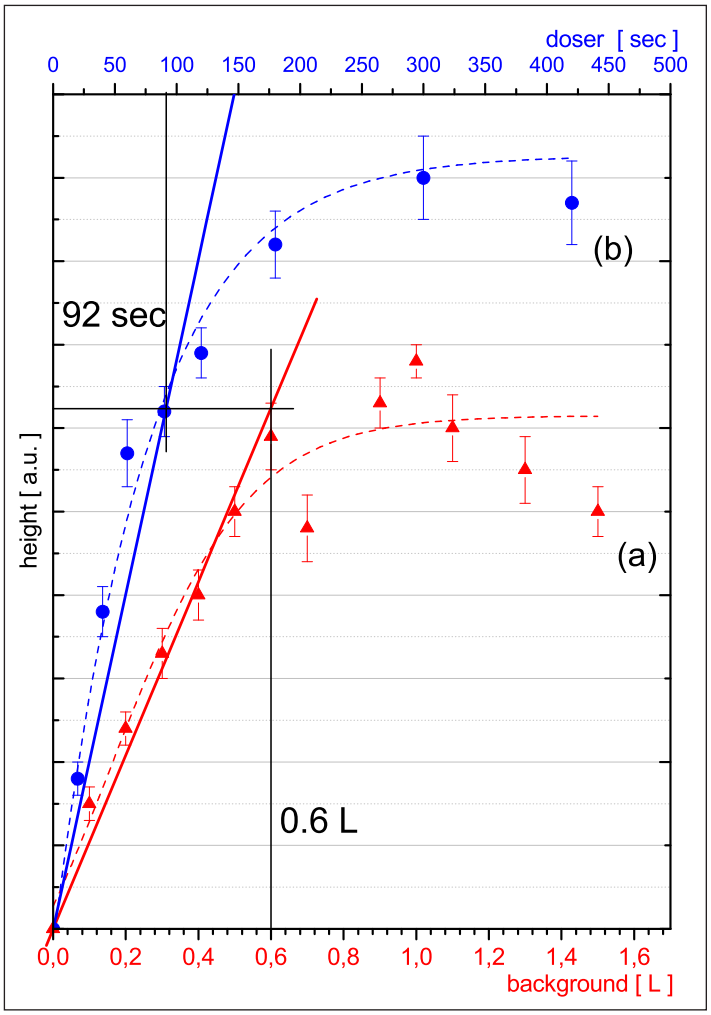

Fig 3.24:The calibration of the pin-hole doser, showing the peak height development for the background pressure dosing series (a) and from the pin-hole doser (b). The two linear fits give a relation between the two dosing series. Result: 92 seconds correspond to 0.6L H_2O.

4. Water adsorption on Rh(111) and V_2O_3 films

4.1 The H_2O molecule

4.1.1 Properties of the molecule

The water molecule is composed by an oxygen atom and two hydrogen atoms. The oxygen atom has a filled K-shell and 6 valence electrons in the L-shell (O: $2s^2 2p^4$), two electrons are missing for a completion of the latter shell. The electron affinity of two can be satisfied by the covalent bond of two hydrogen atoms, each contributes one electron (H:$1s^1$) to the oxygen. In the H_2O molecule the intramolecular bonding leaves the H atoms relatively bare, because their shared electrons are moved towards the oxygen atoms. The repulsion of the remaining "H^+ ions" increases and the angle between the two O-H bonds changes from 90° to 104°. The two dipole moments of the O-H bonds are pointing to the O atom, resulting in a permanent electronic dipole moment of the H_2O molecule.

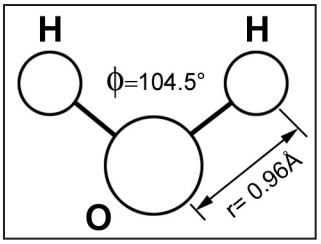

Fig. 4.1: Model of the H_2O molecule, the bond angle is 104.5° and the O-H distance is 0.96Å [18]

The shape of the water molecule generates three degrees of freedom by 3 normal modes of vibration, namely the symmetric stretch (ν_{sym}(OH)), the asymmetric stretch (ν_{asym}(OH)) and the scissors or bending mode (δ(HOH)). Moreover 3 translational and 3 rotational de-

grees of freedom exist, making altogether 9 degrees of freedom for a free, isolated H_2O molecule.
The three rotations are: about the axis perpendicular to the plane of the molecule, the rotation about the O-H line and the rotation about the H-H line

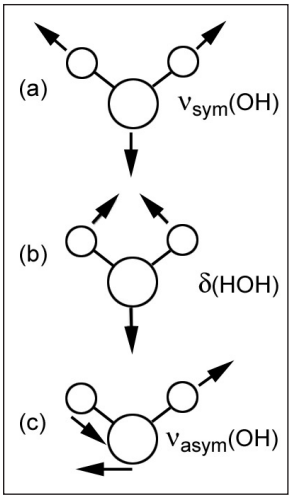

Fig. 4.2: The 3 normal modes of a single H_2O molecule. [18]
(a) symmetric stretch (453meV)
(b) scissors mode (198meV)
(c) asymmetric stretch (465meV)

A single H_2O molecule can bind to another one through a weak electrostatic force - the Van der Waals force. The water molecule possesses a small negative charge concentration at the oxygen atom, on the opposite side of the O-H bond. If the hydrogen atom of a water molecule comes close to another water molecule, it feels a small electrostatic attraction which is sufficient to build a bond, the so called "hydrogen bond". This type of bond is weak and cannot be stable for long molecule chains like in liquid water, the bonds are breaking and reforming constantly.

The H_2O molecule contains 4 valence electrons, which are associated only with the oxygen atom. These electrons, in literature called the two "lone pairs", enable the oxygen atom to adsorb on a surface or coordinate to other molecules by acting as an electron donor.
In terms of a simple Lewis acid-base interaction, the H_2O molecule is the Lewis base, the electron donor, whereas the substrate is the electron acceptor or Lewis acid.
Even the hydrogen bond can be interpreted in this way: the OH part of one molecule is the acidic group, which form a covalent bond to the oxygen lone pair of the other molecule, representing the basic group.
When isolated H_2O molecules form ice and build up a solid structure, the former rotational and translational degrees of freedom are frustrated by the locking of the molecule to a specific location and change into vibration modes. In addition a distinction between the symmetric and asymmetric OH stretch vibration can not be made due to the intermolecular coupling.
The naturally occurring structure of ice has a hexagonal unit cell, with the acronym I_H. A second structure of ice with a cubic unit cell develops, if the temperature is 140K during the growth of the ice layer.

The arrangement of the water molecules in ice can be described by the "Bernal-Fowler-Pauling" (BFP) rules [18, p. 227]:

"(1) Each oxygen atom has two hydrogen atoms attached at 0.96Å with an H-O-H bond angle of about 105°.
(2) Each oxygen atom is tetrahedrally bonded to four other O atoms by hydrogen atoms which are on the O-O axes.
(3) There is only one hydrogen atom on each O-O axis.
(4) non-adjacent molecules do not interact sufficiently to stabilize any structural configurations."

This leads to a hexagonal structure as suggested the first time 1933 by J. Bernal and R. Fowler [19]. In the side view (Fig. 4.4) is shown that the ice forms a bilayer configuration, which comes from the tetrahedral arrangement of the oxygen atoms. In the bilayer the height from the lower layer to the upper one is 0.93Å and the bilayers themselves are separated by 2.76Å

Vibration name	Abbreviation	Energy loss range
OH stretch	ν(OH)	372 – 446 meV
scissors mode	δ(HOH)	205 meV
frustrated rotation	FR	65 – 129 meV
frustrated translation	FT	27 – 30 meV

Tab. 4.1: List of the vibration modes in ice, with their common abbreviation and their loss energies [18, p. 228]

4.1.2 Adsorption of H_2O

When a water molecule approaches a surface it can bind either with one of the lone-pair orbitals from the oxygen atom or with one or both hydrogen atoms to the surface. With the Lewis acid-base model in mind, one expects water attaches via the oxygen atom to electron-poor cationic sites and via the hydrogen atom to electronic-rich anionic sites. Most commonly water adsorbs with the oxygen end to the surface and one or both O-H bonds are oriented away from the surface (hydrogen bonds to the substrate are rare). The bonding is accompanied by a net charge transfer to the surface, the H_2O molecule acts as a Lewis base in this way. The interaction with the surface influences the internal H-O-H bond angle and the O-H bond length. The slight change of the molecule structure is detectable in the values of the vibrational modes. Analogous to the above mentioned bulk ice, the adsorption give rise to additional vibration modes: the hindered or frustrated rota-

tions (FR) also called librations and the frustrated translations (FT) perpendicular to the surface (the stretch vibration of the whole H_2O molecule to the substrate surface). In bulk ice the latter vibration mode is seen between individual H_2O molecules. Besides of that the from gas-phase known modes, the O-H stretch mode ν(OH) and the bending mode δ(HOH) are still active, but due to the interaction with the adsorption sites their frequencies shift to lower values. In general the frequency ranges are fairly similar to the ones in ice (Table 4.1).

The scissors mode is a good indicator for chemisorbed water on the substrate surface. If this vibration can be detected in the spectrum, it indicates that water molecules are adsorbed and further on that they are not dissociated, because all three atoms are involved for this mode. Moreover the frequency value reflects the relative strength of the substrate-H_2O bond. M. Henderson gives as a reference for this vibration the following energy range: 185 – 205 meV [19].

At high coverages of H_2O, when an ice-like phase of water is present, the FT mode is most intense and hydrogen bonding like in bulk ice appears. The frequencies of the OH stretch ν(OH) and the bending mode δ(HOH) are perturbed in that case, too. The potential energy function near the minimum broadens and thus the vibrational energy levels move closer together, all vibration modes where a hydrogen atom is involved are moving to lower frequencies. Additionally the FWHM of the ν(OH) mode increases.

The hydrogen bonding is also a fingerprint for clustering of water molecules on the surface, which leads to the next set of questions in adsorption: What are the parameters for clustering of ad-atoms?

> *"From the energetic perspective, this interplay can be divided into three general categories:*
>
> *1.) where water-water interactions are of comparable or greater strength than those of water-surface interactions (water-water ≥ water-surface);*
> *2.) where water-water interactions are of comparable or weaker strength than those of water-surface interactions (water-water ≦ water-surface);*
> *3.) where water-water interactions are considerably weaker than water-surface interactions (water-water « water-surface);"* [20, p. 60]

The first case (1) together with rapid surface diffusion supports clustering of the adsorbed water molecules. In the second case (2) the stronger interaction between the substrate and the adsorbed material introduces registered molecular water in a monolayer, monomeric water is present; the hydrogen bonding is missing but still possible, their formation is less probable due to the weaker water-water interaction. Because the two interactions are comparable in strength for some substrates (e.g. metals) the system can be brought to a

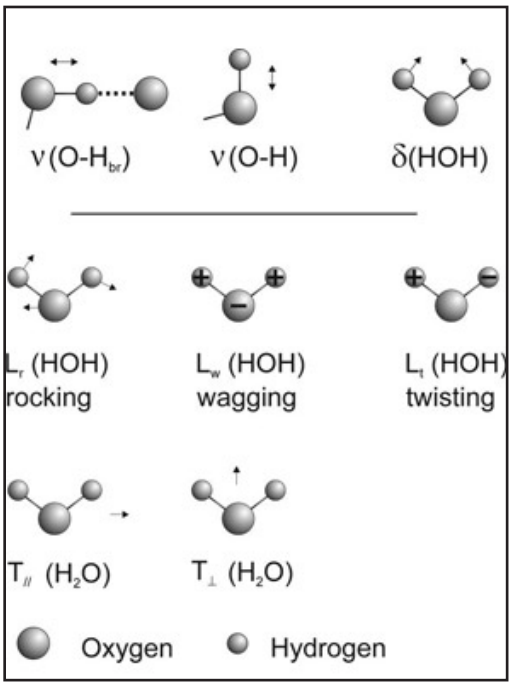

Fig 4.3: Vibrations of the H_2O molecule occurring in ice [21]
The two O-H stretch vibrations ν(O-H_{Br}), ν(O-H) and the bending mode δ(HOH) are dipole-allowed transitions; whereas the three librations L and the two translations T are dipole-forbidden

metastable state by rising the temperature of the sample, diffusion increases and water-water interaction becomes more favourable and clustering appears. On the other hand by lowering the temperature the diffusion becomes slow and clustering unlikely, only high coverages of water bring back the known hydrogen bonds, when neighbouring water molecules are close. Finally if the surface-water interaction is much stronger than the intramolecular interaction of the water molecules, water dissociation takes place.

4.2 Water adsorption on rhodium

4.2.1 Adsorption of H_2O on metals: an overview

The adsorption of water on noble metal surfaces forms primarily clusters. Monomeric water species can only be obtained at temperatures well below 50K [22, 23], at higher temperatures 50-100 K the larger surface diffusion allows the molecule to cluster. In general, for water clusters an important factor is the water coverage and the temperature of the sample: For small doses of water isolated molecules form on the surface, which can then form small clusters depending on the surface diffusion. With increasing coverage the clusters are getting larger and finally a multilayered ice film forms on the surface with long-range order and a network of hydrogen bonds. For the water adsorption on metals the Bernal-Fowler-Pauling rules have to be expanded [20]:

- water adsorbs via the oxygen lone-pair orbital to the metal surface
- tetrahedral bonding configuration is maintained for the water bonds to the surface, even for 2D clusters or incomplete layers
- each H_2O molecule is bound to the system by a minimum of two bonds (either hydrogen bonds to other water molecules and/or with the O lone-pair orbital to the surface)

It is believed that water grows in a bilayer configuration, where the first layer uses one of the oxygen lone-pairs to bind directly to the surface and the second one, perpendicular to the surface, forms hydrogen bonds with other H_2O molecules. [18, 24, 25] The second layer molecules are held only by two hydrogen bonds to the first layer. Only the first bilayer feels the template effect of the substrate, the subsequent layers mainly feel the forces which are present in ice. This explains why multilayered ice on a metal does not differ from bulk ice.

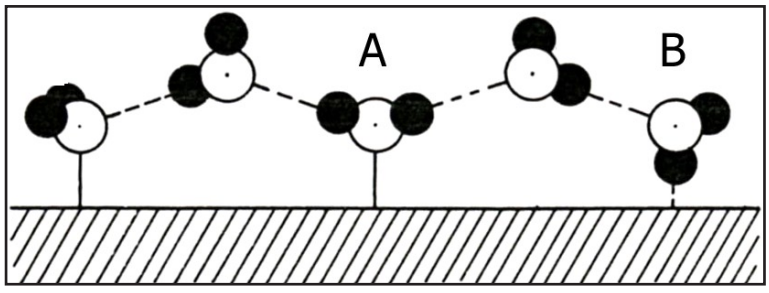

Fig 4.4: Model for the arrangement of the water molecules adsorbed on a surface and building a bilayer structure [18 , p. 235]; H_2O molecule builds a bond to the substrate surface via the oxygen atom (A) and second possibility the water molecule use the hydrogen atom to coordinate to the surface (B)

4.2.2 H_2O adsorption on Rh(111)

On the cold (100K) Rh(111) crystal H_2O forms a (√3x√3)R30° diffraction pattern in LEED, as it is shown in Fig. 4.5. This long-range order is supported by the close match of the lattice constants, for Rh(111) $a_{Rh(111)}$= 4.66Å and for hexagonal ice a_{Ih}= 4.50Å. The here presented LEED pattern agrees with measurements of multi layered ice presented by Gibson et al. [26], Doering and Madey [27], Meng et al. [28] and Thiel et al. [18]. The hexagonal arrangement of the water molecules in shown in Fig. 4.6, the inserted unit cell contains one water molecule from the lower and one from the upper layer.
It should be mentioned that LEED reflects only the positions of the O atoms, which generate the (√3x√3)R30° pattern. The hydrogen atoms do not have a simple superstructure and the scattering is too weak to contribute significantly to the pattern. Because of this , it is still under discussion whether the first layer binds via the oxygen atom to the metal surface [24, 28, 29, 30, 31] or via one hydrogen atom [28, 32]. Both cases have nearly the same oxygen arrangement, thus as soon as the measurement is not sensitive to the positions of the hydrogen atoms, which is true for LEED, the two types of bilayer are indistinguishable.

The HREEL spectrum of water adsorbed on Rh(111) at 100K show four main energy loss features, when a multilayer of ice is dosed (~2L exposure) onto the crystal surface (see Fig. 4.7 (d), 4.8 (d)):

- at the loss energy of 425meV one finds the O-H stretch vibration of the H_2O molecule
- at ~200meV the energy loss feature of the scissors mode δ(HOH)
- in the range of 50 – 100 meV are the hindered rotation modes
- and finally at 30meV a sharp peak marks the vibration of the hindered translation

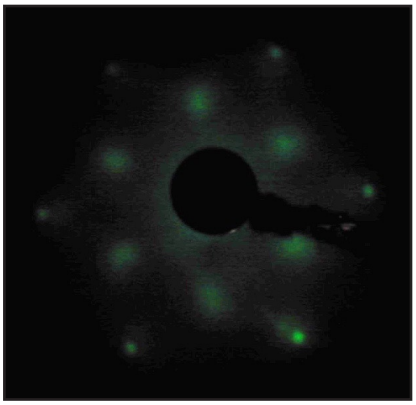

Fig 4.5: LEED pattern of 2.7L of water on Rh(111) at 100K, the inner spots represent the (√3x√3)R30° structure of the ice-like water layer

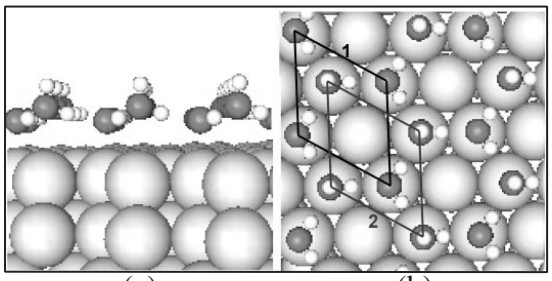

(a) (b)

Fig 4.6: The "H-up" bilayer structure of H_2O molecules on a metal. In the top-view (b) two different domains are found, each unit cell contains one water molecule from the other layer [28, p. 6]

The broad shape of the ν(OH) peak at 425meV comes from the hydrogen bonding in the multilayer of ice. Even at the first appearance (Fig 4.8 (b)) at 0.60L of water the OH stretch mode is not distinct, this indicates the before mentioned clustering of the water molecules on metal surfaces. The molecules build hydrogen bonds with their neighbouring water molecules, even when the coverage is low, and this leads to a broad shape of the OH stretching vibration.

The scissors mode at 200meV can be detected from the very first dosing step (0.15L) in Fig. 4.7 (a). All three atoms of the H_2O molecule are included in this vibration, its detection indicates, that water adsorbs without dissociation. With higher water coverages the scissors mode moves to higher loss energy. This upward shift results from building up an ice-like structure, which becomes more and more independent from the Rh(111) substrate influence. For low coverages (Fig 4.7 (a)-(c)) a peak can be found at 194meV, which is lower than the gas phase value ($\delta(HOH)_{gas}$ = 198meV). The down-shift is due to

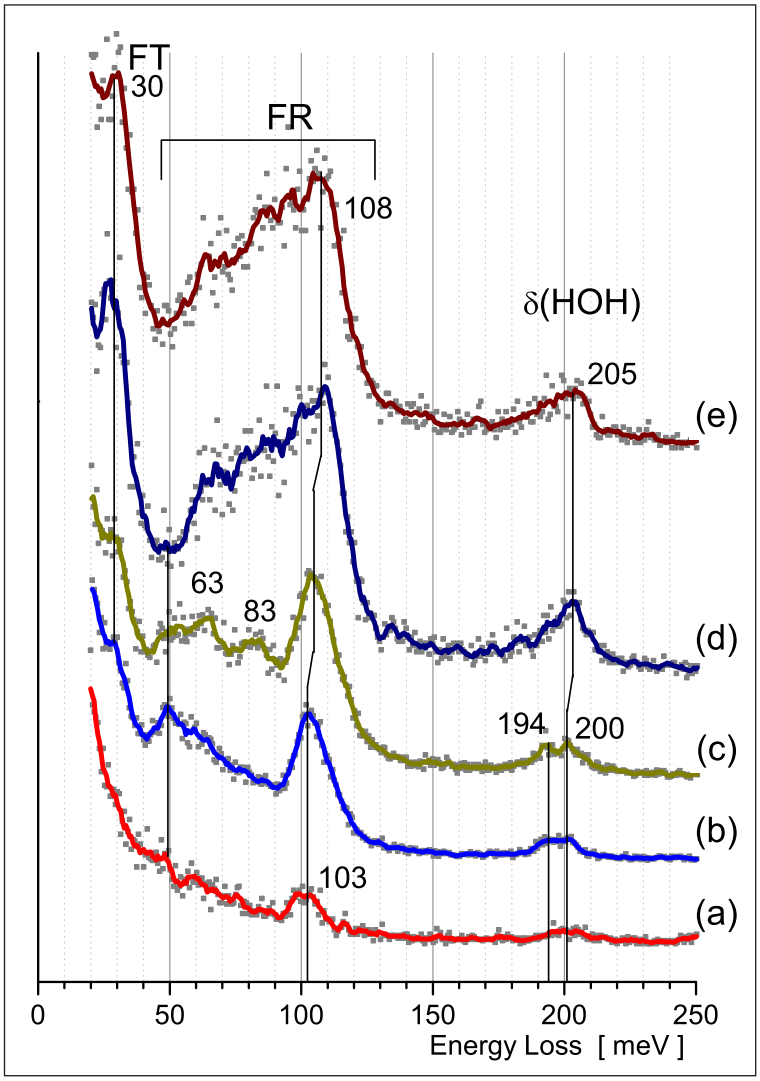

Fig 4.7: HREEL spectra of the H_2O dosing series on Rh(111) at 100K. Dosing steps: (a) 0.15L; (b) 0.60L, (c) 1.20L, (d) 2.00L, (e) 2.70L

the bonding of the water molecule to the metal surface. During the water dosing series *"a change occurs from a strongly bound H_2O molecule with relatively little hydrogen bonding at low coverage to an increasing network of hydrogen bonding at higher coverage"* [29, p. 31]

After the first dosing step (Fig. 4.7 (a)) a small but broad peak develops at 190-200meV, which underlines that the water clusters on Rh(111): the bending mode δ(HOH) influenced by the metal-water bonding is detectable as well as the δ(HOH) mode perturbed by the first hydrogen bonds.

In the energy loss range of 50 – 100 meV the libration modes can be found, containing the three (not-well resolved) hindered rotations, namely the rocking, wagging and twisting (Fig. 4.3). They are best seen at 1.20L (in Fig 4.7 (c)) corresponding to the values/modes seen by Wagner and Moylan [33]: the mode at 105meV is dominating and visible for all dosing steps, like the scissors mode. The second libration is at 83meV and the third peak is at 63meV. The shift of the libration mode at 105meV to 110meV for higher coverage (Fig. 4.7 (d,e)) "*may be explained by the formation of a increased number of hydrogen bonds*" [21, p. 13]. Due to the strong coupling of the vibrational modes no sharp, well-

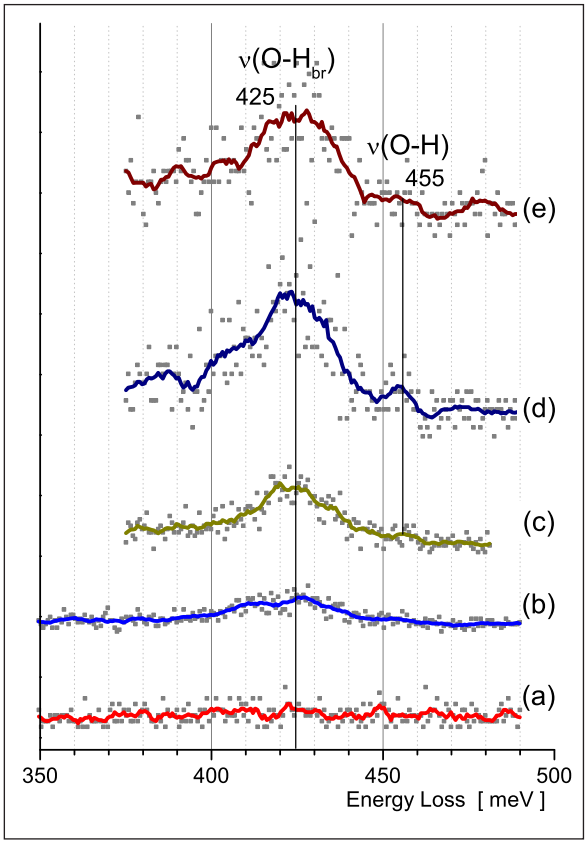

Fig 4.8: HREEL spectra of the H_2O dosing series on Rh(111) at 100K, in the energy range of the ν(OH) vibration.
Dosing steps: (a) 0.15L; (b) 0.60L, (c) 1.20L, (d) 2.00L, (e) 2.74L

defined peaks can be seen. Moreover this coupling allows to excite modes which are normally not dipole active. (see Fig. 4.3) The dipole active vibrations are the symmetric O-H stretch, the substrate-OH_2 stretch and the scissors vibration, whereas the others are not. These three librations are getting dipole active through the hydrogen bonds. Okuyama et al. [34, p. L503] explain their appearance by the less effective screening of the dipole in ice, "*because of its low dielectric constant compared to the metal*".

On the outermost water layer free hydrogen atoms of the H_2O molecules exist, these are not hydrogen bonded to other water molecules. Their OH stretch vibration ν(OH) is 455meV, which is different from the hydrogen bonded $\nu(OH_{Br})$ one at 425meV. Both features can be seen in Fig. 4.8 (d). The hydrogen bond between two H_2O molecules weakens the strength of the intramolecular OH bond, therefore the OH stretch vibration shifts to lower loss energy in the spectrum. The intramolecular O-H distances are elongated, the force of this bond is weaker and thus the frequency is lower. For low coverages of adsorbed water clustering could bring up non-hydrogen-bonded OH stretch vibrations, too. On the edges of the clusters free hydrogen atoms of the water molecule are available.

The peak of the $\nu(O–H_{Br})$ vibration shows a shoulder on the lower loss energy side containing one other not resolved mode. Wagner and Moylan [33, p. 140] explain this for a Pt(111) surface in the way that a more complex water layer form, than it is indicated by the (√3x√3)R30° LEED pattern: *"Instead of a homogenous stretched but not distorted ice layer, this suggests water in two environments, one ice-like and one similar to water on Pt(111)."* They mention that the oxygen atom distances are not uniform in the adsorbed water, causing changes in the vibrational modes.

4.3 Water adsorption on V_2O_3 films

4.3.1 In brief: Adsorption of H_2O on metal oxides

In contrast to metal surfaces, the water molecule can form strong chemisorption bonds to an oxide substrate [20, 35, 36]. One hydrogen proton of the molecule interacts with the surface oxygen, there it can dissociate during the adsorption. Nevertheless, possibly occurring hydroxyl groups on the surface may recombine afterwards. In case of a dissociation the resulting OH groups are not equivalent: one OH group contains the oxygen and one hydrogen atom of the former H_2O molecule, whereas the second H atom forms a hydroxyl by proton transfer to a surface oxygen anion site (see Fig. 4.9). Due to this a bilayer structure of the adsorbed water is not typically seen on metal oxides, because a suitable template for the formation of a ice-like overlayer is missing.

On the surface the recombination of different types of OH can take place and build new water molecules. The clustering and formation of hydrogen bonds is less probably on oxides for low coverage of water than on the metals, because the formed bond to the substrate is much stronger and hinders diffusion.

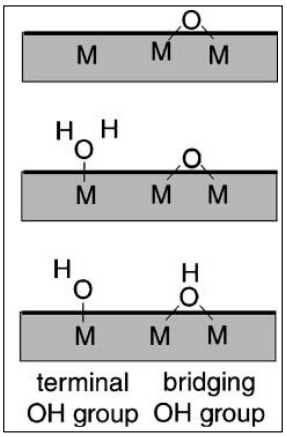

Fig 4.9: On a metal oxide the adsorbing H_2O molecule can find a metal site or an oxygen site. After adsorption the molecule breaks and two hydroxyl groups are created sitting on different sites. Via proton transfer one H moves to the oxygen, the other one stays [20, p. 52]

4.3.2 Vanadyl termination (1x1) V=O

HREELS of the vanadyl terminated (1x1) V=O surface

The vanadyl terminated surface at room temperature shows in HREELS three well-defined peaks (Fig. 4.10 (a)): one at 47meV originating from a bulk vibration, one at 78meV coming from the V=O groups vibrating to the interface oxygen atoms and at 129meV the internal stretch oscillation of the V=O group. The dominant feature at 78meV possesses at the right shoulder of the peak a bulk vibration at 92meV. The HREEL spectrum changes when the sample is cooled to 100K for the following dosing series of water (Fig. 4.10 , (b)). This change of the phonon spectrum is due to the fact that the V_2O_3 film undergoes

a metal-to-insulator phase transition at ~160K. (in "5. Metal-to-Insulator phase transition in V_2O_3 films", p. 78 this is discussed in detail).

The vibration mode at 78meV splits into two, a smaller one at 66meV and a dominant peak at 83meV, which has increased in intensity by a factor of 2.3 to the room temperature peak at 78meV. The bulk vibration at 47meV and the vanadyl stretch vibration at 129meV are not shifting.

The mode at 166meV comes from the double excitation of the intense vibration at 83meV (2x83 ~ 166meV). Like the peak at 213meV, this is a sum excitation of the vanadyl stretch vibration with the V=O-to-substrate vibration (83+129meV ~ 213meV).

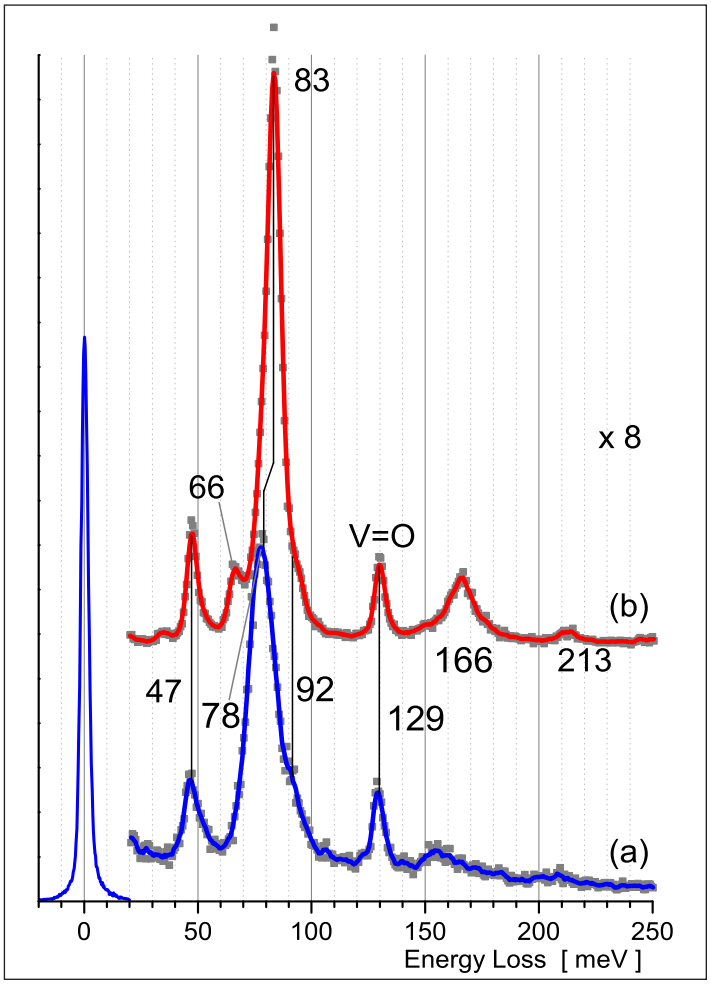

Fig 4.10: By cooling the vanadyl terminated (1x1) surface to 100K the phonon spectrum in HREELS changes. The V_2O_3 film undergoes a metal-to-insulator transition.
(a) room temperature 300K, (b) 100K

Dosing of H_2O at 100K

In Fig. 4.11 (a) the exposure of 0.30L of H_2O induces a shift of the vanadyl peak to lower loss energies by 6meV and the peak height is reduced by more than one half (see Fig. 4.13). Moreover the main peak at 83meV decreases in height, but does not shift. One can see in Fig. 4.13 that for smaller dosing amounts the V=O peak shift is rather small and then at 0.30L increases strongly suggesting that the water molecules are attaching to the vanadyl groups. The shift of the vanadyl peak due to the adsorption of water has been reported by Ranea et al. [38].
Because of the vanadyl peak shift, the feature at 213meV moves to lower loss energies, too. In Fig. 4.11 (b) its position is 204meV, which corresponds to the 6meV shift. In the region of the OH stretch vibration ν(OH) (Fig. 4.12 (b)) no vibrational mode can be detected.

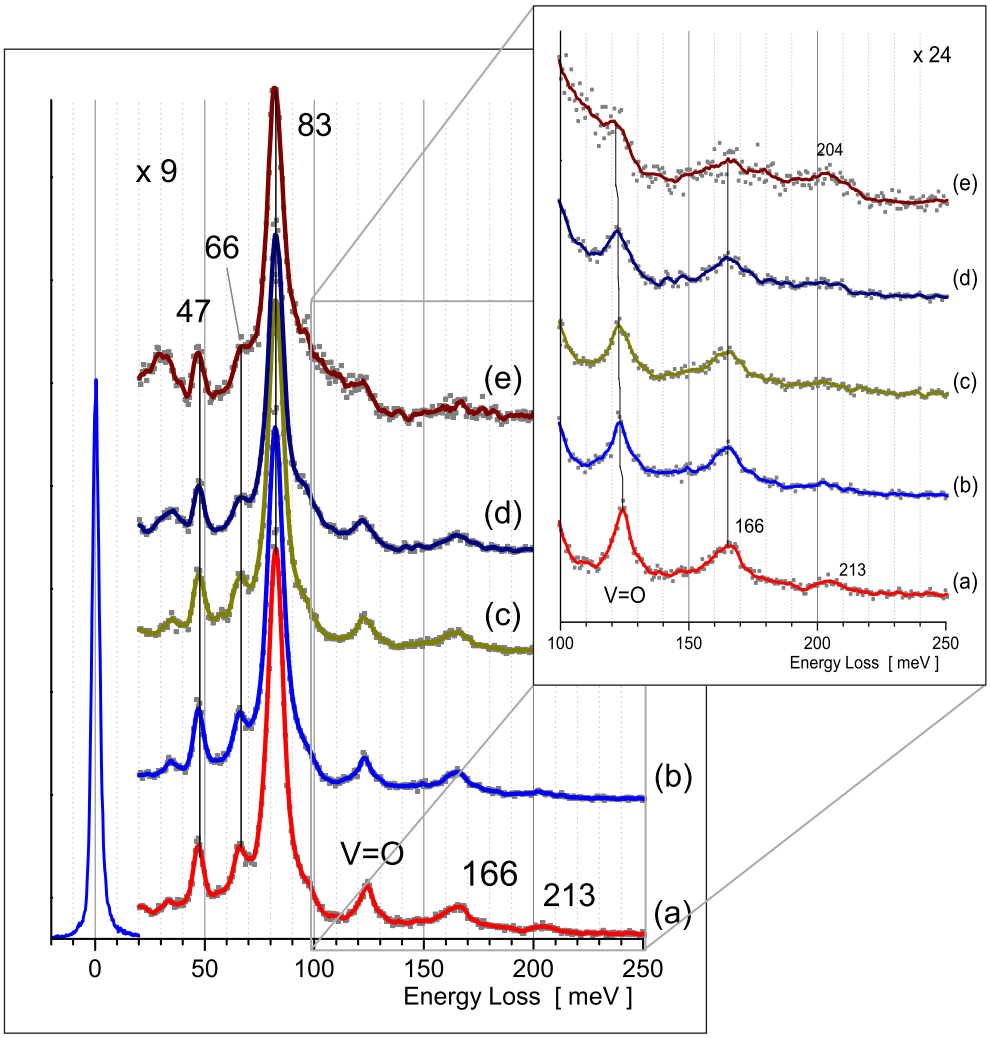

Fig 4.11: The vanadyl terminated (1x1) V=O surface at 100K investigated with HREELS during a series of H_2O dosing. The inset shows all spectra in higher magnification for the region 100 - 250 meV.
(a) 0.30L, (b) 0.40L, (c) 0.80L, (d) 1.20L , (e) 2.00L

At 0.40L of water two weak ν(OH) features can be recognised at 424meV and 455meV in Fig. 4.12 (c). The first, at 424meV, represents the ν(OH_{Br}) stretch vibration, due to hydrogen bonds, and the second at 455meV stands for dangling O-H groups on the surface. A similar result has been shown in the PhD-thesis of A.C. Dupuis [16] for the same surface termination. A possible weak loss feature at 204meV for the bending mode δ(HOH) of molecularly adsorbed water is hidden below the sum excitation loss, which has been shifted to this loss energy. Therefore, at this dosing amount it is not clear where the feature at 204meV comes from. The libration modes can not be seen, they are placed in the region where the intense oxide phonon peaks are located (50 – 100 meV).
Fig. 4.13 indicates that ~0.4L are enough to saturate the (1x1) V=O terminated surface with H_2O. The peak height of the V=O stretch vibration and the mode at 83meV are not decreasing strongly with further amounts of water.

An interesting point to mention is that for 0.80L and 1.20L of water exposure in Fig. 4.12 (c,d) the position of the ν(OH_{Br}) peak shifts to 432meV (Δ=8meV to the spectrum in (c)). In Fig 4.12 (d) the position of the ν(OH) stretch vibration at 455meV stays at the same

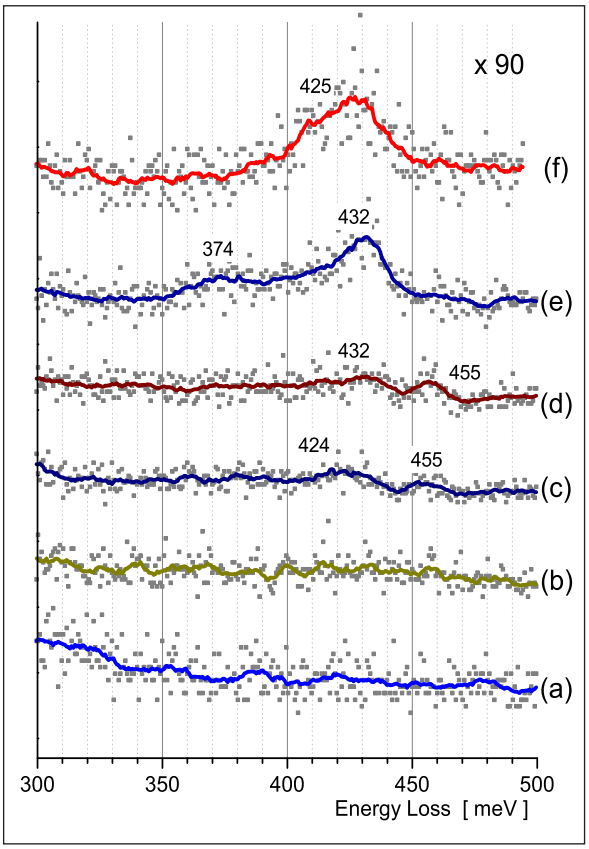

Fig 4.12: HREEL spectra of the H_2O dosing series on the vanadyl termination at 100K, in the energy range of the ν(OH) vibration. Dosing steps: (a) 0.15L; (b) 0.30L, (c) 0.40L, (d) 0.80L, (e) 1.20L, (f) 2.00L

loss energy but disappears in the next spectrum (Fig. 4.12 (e)). At 1.20L a new vibration mode appears at 374meV! This suggests the population of additional high coordinated adsorption sites, an OH group vibration at lower loss energies is possible. In the survey spectra (Fig. 4.11 (d)) the frustrated translation mode at 30meV is visible for the first time and it seems that the bending mode δ(HOH) can be detected at 204meV, because the peak intensity is higher than before at this loss energy

Further dosing (2.00L) increases the peak height of the $\nu(OH_{Br})$ mode and shifts it back to a loss energy of 425meV, leading to the conclusion that an ice-like water layer has been formed. (The OH stretch vibration is perturbed by the hydrogen bondings and not sensitive to the substrate.) In Fig. 4.11 (e) the scissor mode at 204meV is clearly visible, beside the frustrated translation feature at 30meV. This is another strong evidence that multilayers of water are on the V_2O_3 film. Nevertheless, the two oxide vibrations at 47meV and 83meV are still visible.

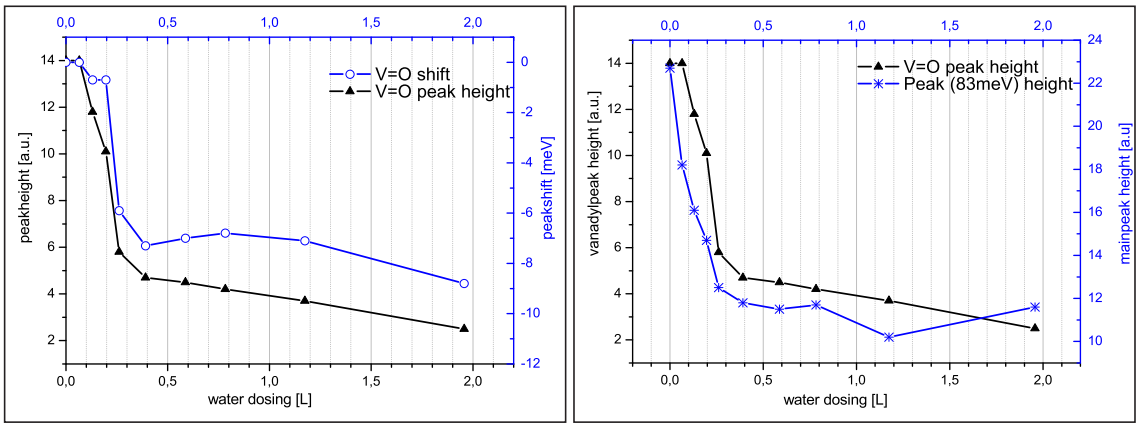

(a) (b)

Fig 4.13: Vanadyl peak shift and height as a function of water exposure (a) and the comparison between the vanadyl peak height and the peak height of the bulk vibration (83meV) with increasing water exposure.
(the minus for the vanadyl peak shift indicates, that the shift is towards lower loss energy)

4.3.3 O-rich termination (√3x√3)R30°

HREELS of the O-rich (√3x√3)R30° surface

As described in Chapter 3.3.2, p. 26, the O-rich termination can be created by annealing a perfect (1x1) V=O surface with an oxygen background pressure. This reduces the quantity of vanadyl groups on the V_2O_3 surface by 1/3. A missing vanadyl frees three surface oxygen atoms and induce subsurface rearrangements. The remaining V=O groups build two domains, which form a (√3x√3)R30° diffraction pattern in LEED.
The HREEL spectrum of the so produced surface comprises, like the (1x1) V=O terminated surface, the two intrinsic phonons at 47meV and 79meV at 300K (Fig. 4.14 (a)). The latter one is now less intense and therefore the vibrational mode at 92meV is better visible. Beside that the V=O groups on the surface generate the loss feature at 129meV,

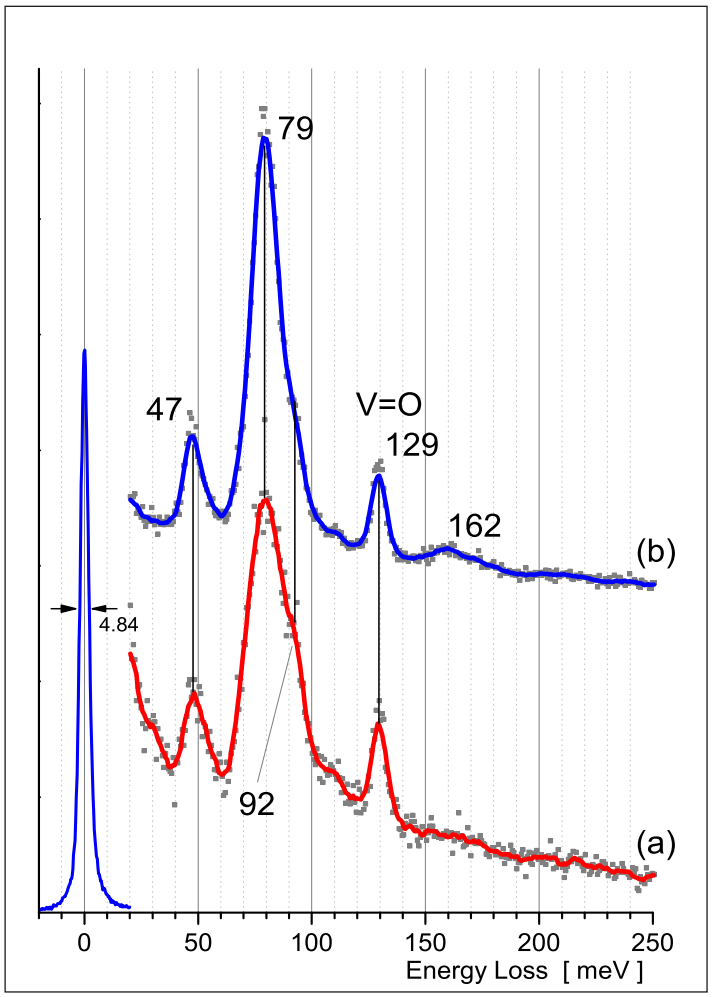

Fig 4.14: HREELS spectrum of the O-rich termination (√3x√3)R30° at room temperature (a) and at 100K (b). No dramatic increase in intensity for the vibration mode at 79meV can be seen when the sample is cooled, as it was for the vanadyl termination

the internal vanadyl stretch vibration. This surface termination is unique in the sense that it does not show the characteristic metal-to-insulator transition, when the sample is brought to 100K (Fig. 4.14 (b)). But a tiny amount of adsorbed water (~0.1L) is enough to bring back the phase transition. (see Chapter 5.4.2, p. 81)

Dosing of H_2O at 100K

If the sample is cooled down to 100K, no change in the peak intensities is measurable, but with the first dose of water (0.1L) the peak height of the phonon at 79meV doubles and the vanadyl peak at 129meV decreases (Fig. 4.15 (a)). The feature at 163meV originates from the double frequency excitation of the peak at 79meV. The main peak at 79meV decreases with further adsorbed water, shown in Fig. 4.17 (b). The vanadyl peak shifts during the dosing step to 0.40L (Fig. 4.15 (c)); the position moves

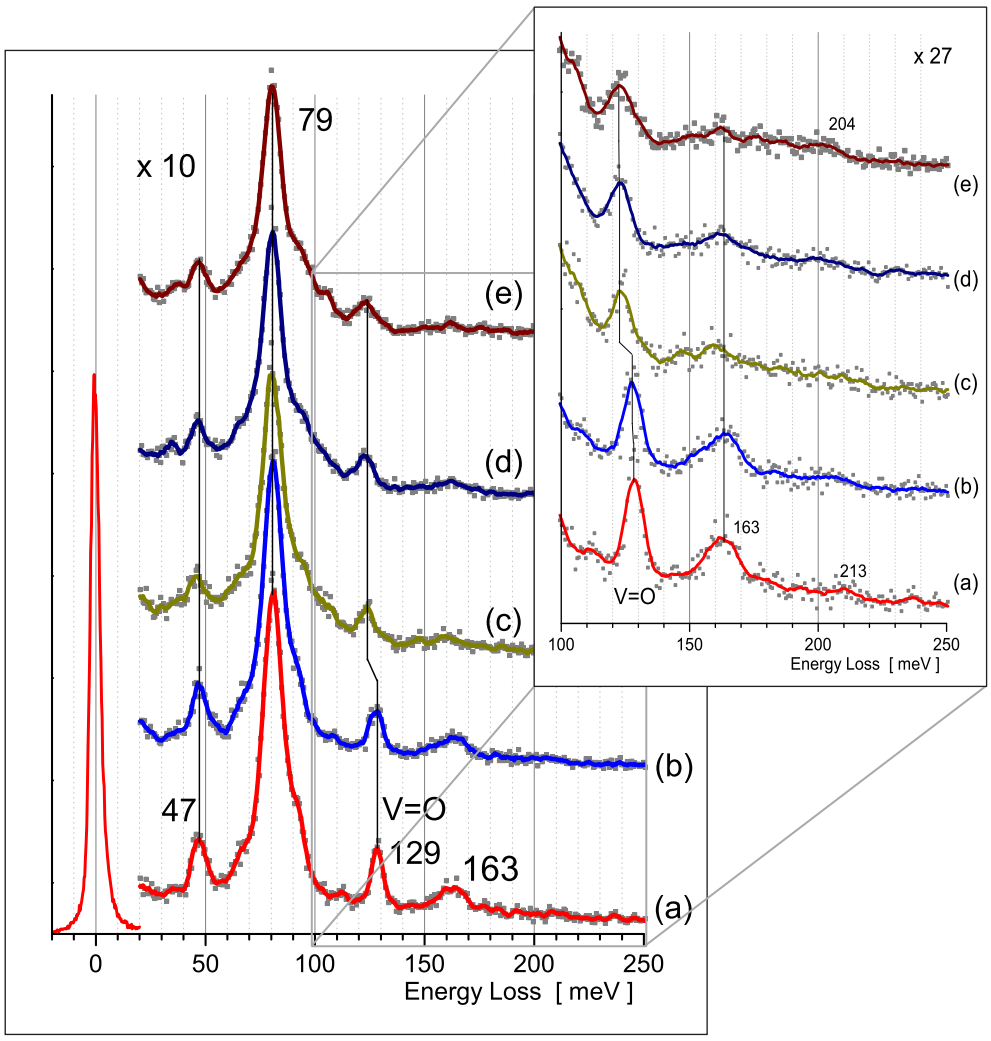

Fig 4.15: HREELS spectra for several H_2O exposures on a surface with O-rich termination ($\sqrt{3}x\sqrt{3}$)R30°; the additional diagram shows the indicated area with higher magnification
(a) 0.10L, (b) 0.20L, (c) 0.40L, (d) 1.20L , (e) 2.00L

Δ=-4meV to lower loss energies (the minus marks the direction of the shift towards lower energies). At the vanadyl terminated (1x1) surface the major shift of the V=O feature happens earlier, at the dosing step from 0.20L to 0.30L (see Fig. 4.13 (a)). Here the vanadyls seem to be saturated at 0.60L. Probably the H_2O molecules are decorating not only the vanadyl groups but also the sites of the former, during the preparation of this termination removed vanadyls.
Further it seems interesting that the height of the vanadyl peak decreases rapidly during the first two steps (0.10L and 0.15L) - by a factor of 2.3 - and then increases again. The maximum forms at 0.30L, afterwards the peak decreases again as seen in Fig. 4.17 (a).

The scissors mode δ(HOH) of water at 204meV appears at 0.60L (not shown); in addition, in the spectrum at 1.20L (Fig.4.15 (d)) the hindered translation appears at ~30meV. With 2.00L of water the spectrum contains beside the vibrational losses of the V_2O_3 film also clearly visible vibrations of the adsorbed H_2O molecules: the hindered translation mode at ~30meV, but less strong than for the V=O (1x1) termination (compare Fig. 4.11 (e)). The libration modes can be seen on the right shoulder of the peak at 79meV, the bending mode at 204meV and finally a broad feature in the range of 350 – 450 meV representing

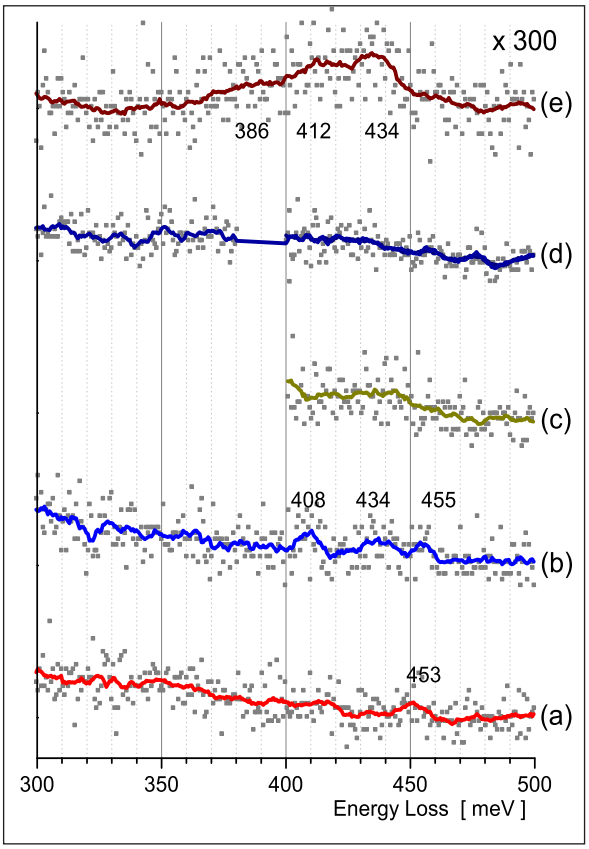

Fig 4.16: The loss energy region for the OH stretch vibration strongly magnified, because of the weak loss intensity
(a) 0.10L, (b) 0.20L, (c) 0.40L, (d) 1.20L , (e) 2.00L

the O-H stretch mode ν(OH) in general (Fig. 4.16 (e)).
The latter can not be resolved very well for lower exposures, due to the higher noise level as compared the vanadyl terminated surface.

In Fig. 4.16 (b) three broad losses are visible at 408meV, 434meV and 455meV. The spectrum (d) for 1.20L of water shows a weak, broad loss energy in the range of 370 – 450 meV. This extremely broad feature can be an indicator for a very complex network of hydrogen bonded OH groups or molecularly adsorbed H_2O molecules.
For 2.00L one dominating ν(OH) vibration can be seen at 434meV (Fig. 4.16 (e)) with a broad shoulder to lower loss energies. In the direction to lower energies one vibration is at 412meV and one hidden in the shoulder of this peak at 386meV.
It is yet not clear what happens at the dosing steps of 0.40L and 1.20L (Fig. 4.16 (c) and (d)), where the ν(OH) mode is very weak in intensity

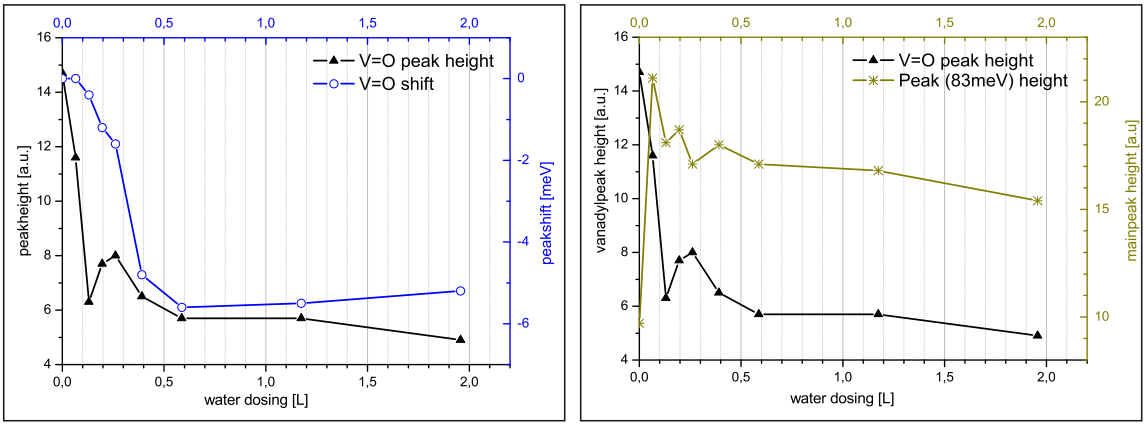

(a) (b)

Fig 4.17: Diagram of the vanadyl shift during the dosing series combined with the change of the vanadyl peak height (a), peak intensities of the vanadyl in comparison with the peak height of the bulk vibration at 79meV (b).
(the minus for the vanadyl peak shift indicates, that the shift is towards lower loss energy)

4.3.4 V-rich (1x1) termination

HREELS of the V-rich (1x1) surface

To create this termination a vanadyl terminated (1x1) surface is covered with V atoms (at room temperature and under UHV conditions, see Chapter 3.3.3 p.29). The here presented metallic vanadium overlayers are evaporated in three different thicknesses: 0.15MLE, 0.3MLE and 0.8MLE. After the evaporation the sample is heated to ~673K (~400°C) for 45 seconds to order the deposited metal atoms.
For the 0.15MLE V-rich termination in HREELS known vibrational losses all from the perfect vanadyl terminated (1x1) surface can be identified. The spectrum at 300K shows losses at 47meV, 76meV and an attenuated V=O peak at 127meV. The other two

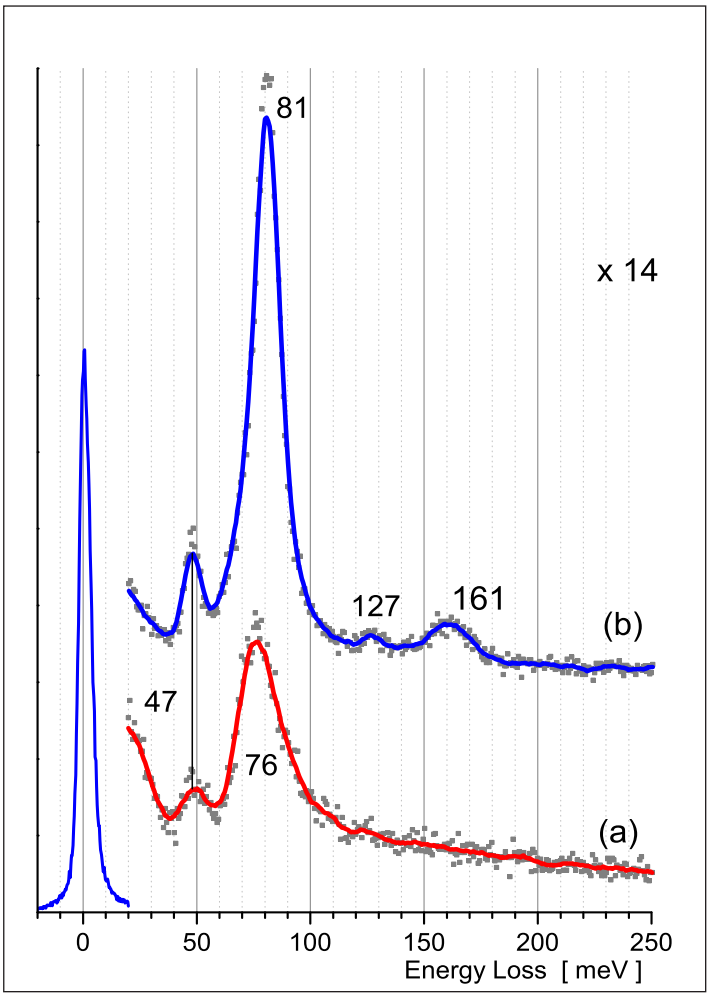

Fig 4.18: 0.8MLE thick V-rich terminated (1x1) surface at room temperature (a) and at 100K (b). The spectra do not show vanadyl stretch vibrations at 123meV (a) and 127meV (b), but this is the sum frequency excitation from both bulk vibrations 47meV and 78meV (300K), 47meV and 81meV (100K).

V-coverages, 0.3MLE and 0.8MLE, do not show the vanadyl stretch vibration any more and only the two vibrations modes at 47meV and 76meV remain.
But in all three cases a cooling to 100K with liquid nitrogen shifts the peak of the O_3-VO vibration to 81meV and the intensity increases. This change in the vibrational spectrum reflects the metal-to-insulator transition of the vanadium oxide film. (see "5. Metal-to-Insulator phase transition in V_2O_3 films"). Only for the 0.15MLE V-rich (1x1) termination the vibration mode at 66meV comes up in Fig. 4.19 (a), compare Fig. 4.18 (b) and 4.19 (a).
The measurable vibration at 126meV in Fig. 4.18 (b) does not come from the V=O stretch vibration. But rather is the frequency sum excitation: in the room temperature spectrum (Fig. 4.18 (a)) the weak peak at 123meV fits to a frequency sum excitation of 47meV and 76meV (47+76 ≈ 123). Due to the shift of the 76meV peak to 81meV also the frequency

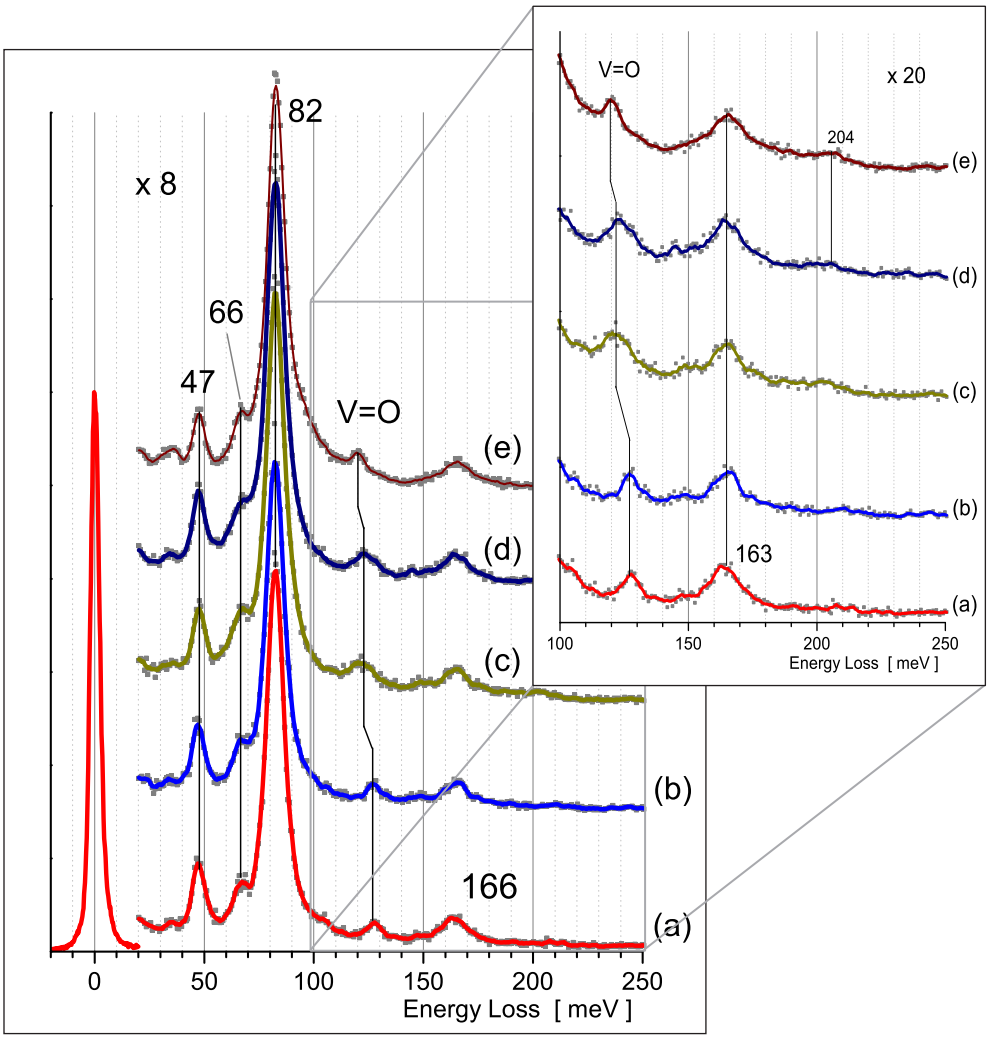

Fig 4.19: Series of HREELS spectra taken for increasing amounts of adsorbed H_2O on a 0.15MLE V-rich terminated (1x1) surface. The inset presents these spectra enlarged in the energy range of 100 - 250meV
(a) 0.15L, (b) 0.30L, (c) 0.40L, (d) 0.60L, (d) 1.20L

sum excitation shifts to higher loss energies resulting in a feature at 126meV (47+76 ~ 126). Moreover the rather sharp feature at 161meV does not mark a vibration in the system, but is the double excitation frequency of the sharp and intense stretch vibration of the VO group to the substrate (2x81 ~ 161).

Dosing H_2O on a 0.15MLE V-rich (1x1) terminated surface

Dosing water to this surface leads to a decrease in height of the vanadyl peak (127meV) and the O_3-VO vibration peak (81meV) and the V=O peak shifts to lower energy. But in Fig. 4.21 (b) one can see that for a water dosing of 0.40L the intensity increases again for both loss features, with a shift of the V=O peak in Fig. 4.21 (a).
This indicates that the water molecules for lower coverages (Fig. 4.19 (a),(b)) prefer the V-atoms on the surface as adsorption site, but with higher coverage (Fig. 4.19 (c)) they attache also to the vanadyls, causing this shift to lower loss energies.
At 0.60L (Fig. 4.19 (d)) a small feature is formed at 204meV, which is typically the scissor

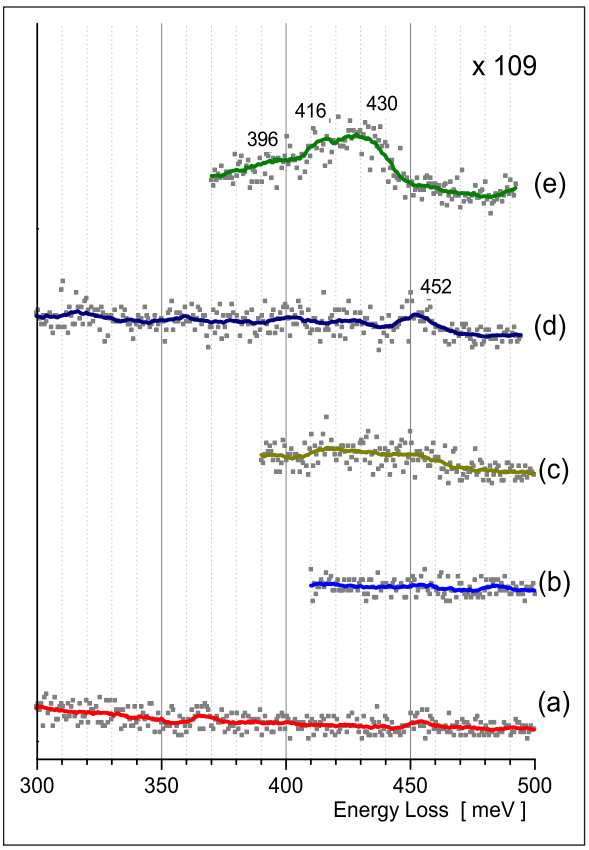

Fig 4.20: A closer look to the region of the ν(OH) stretch modes, for the 0.15MLE V-rich terminated surface covered with an increasing amount of water
(a) 0.15L, (b) 0.30L, (c) 0.40L, (d) 0.60L, (d) 1.20L

mode δ(HOH) of water, when it adsorbs with the oxygen to the surface. Moreover, a peak can be found at 452meV (Fig. 4.20 (d)), which comes from a ν(OH) stretch vibration. The loss energy suggests that the water adsorbs without forming hydrogen bonds. This changes with the exposure of 1.20L of H_2O (Fig. 4.20 (e)), the OH peak has its maximum at 430meV and shows two more not well-separated features at 416meV and 396meV. The broad peak leads to the conclusion that hydrogen bonding appears.
Supported by the additional appearance of the hindered translation mode at 35meV in Fig. 4.19 (e) supports that an ice-like structure forms on the V-rich terminated (1x1) surface for a water dose of (1.20L).

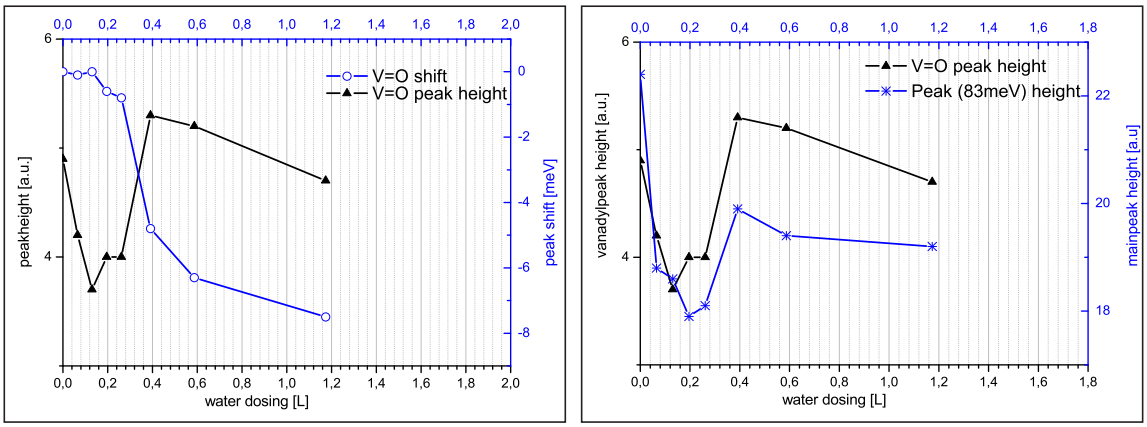

(a) (b)

Fig 4.21: The shift of the vanadyl peak and the change of the intensity for the vanadyl peak and the feature at 82meV summarised in two diagrams containing all dosing steps for the 0.15MLE V-rich (1x1) terminated surface.
(the minus for the vanadyl peak shift indicates, that the shift is towards lower loss energy)

H_2O dosing on 0.3MLE and 0.8MLE V-rich (1x1) termination

At room temperature a vanadium metal overlayer with a coverage of 0.3MLE and 0.8MLE produces a surface, which shows in HREELS the two intrinsic vibrations at 47meV and 76meV, like in Fig. 4.18 (a) for 0.8MLE. When the sample is cooled to 100K the whole spectrum shows a less intense background and the two vibrations get better resolved. In addition the metal-to-insulator transition changes the phonon spectrum (Fig. 4.18 (b)): the peak at 76meV shifts to 81meV when the sample is cooled from 300K to 100K. The features at 126meV is a frequency sum and the one at 163meV is a double frequency excitation (p. 53).
By dosing water on the cold 0.8MLE V-rich terminated sample a narrow ν(OH) vibration can be detected at 453meV (Fig. 4.24 II (a-c)). The position and the shape of the peak leads to the conclusion, that the water dissociates when it comes to the vanadium-rich

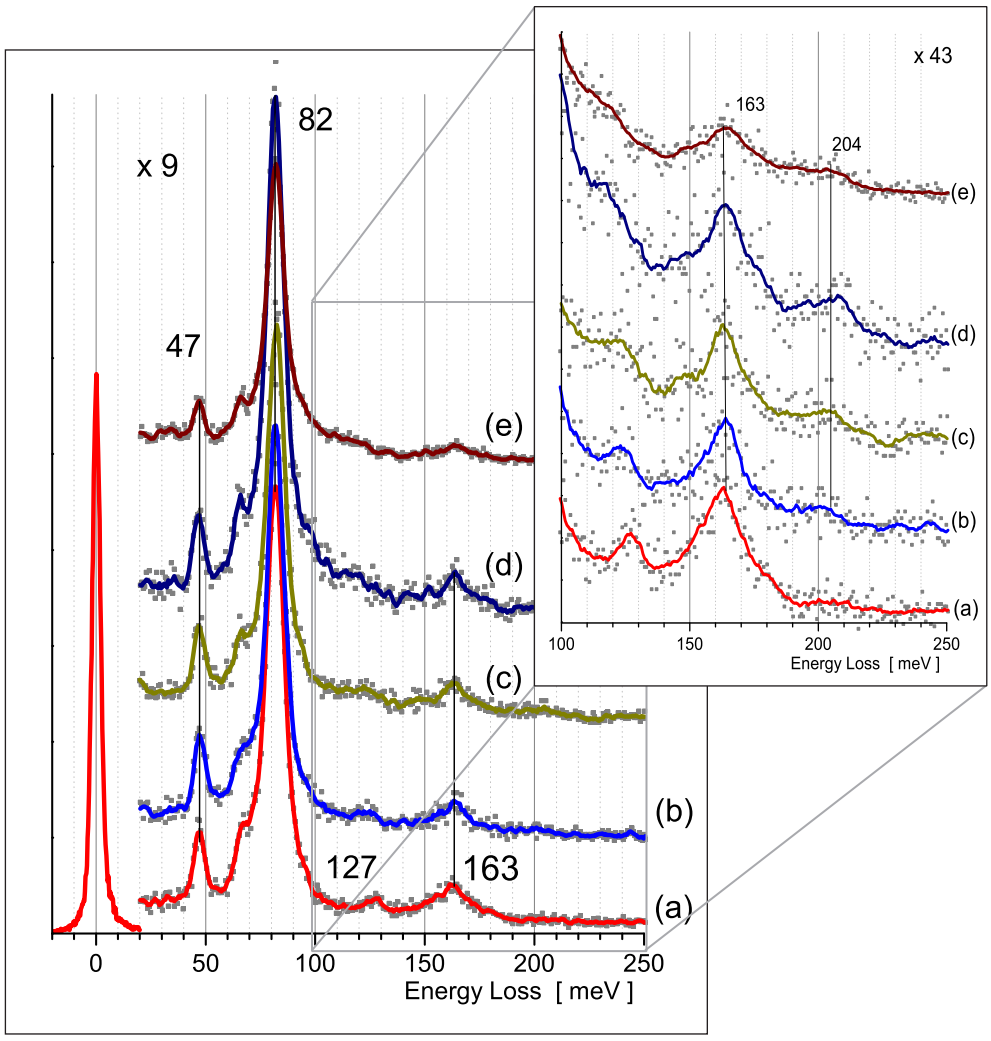

Fig 4.22: 0.3MLE thick V-rich terminated (1x1) surface exposured to different amounts of water and investigated by HREELS at 100K. The inset presents these spectra enlarged in the energy range of 100 - 250meV
(a) 0.15L, (b) 0.20L, (c) 0.40L, (d) 0.60L, (d) 2.00L

surface till a exposure of 0.40L. It is not clear whether the δ(HOH) mode builds up with further dosing steps or if it is hidden in the noise (Fig. 4.24 (a-c)).
At the dosing of 0.60L of water the OH stretch vibration (Fig. 4.24 II (d)) is changing fundamentally and broaden, without building a distinct feature. Hydrogen bonds can be detected in HREELS with the dosing of 2.00L of water in Fig. 4.24 II (e), a very broad feature reaching from 380 - 450 meV is visible. Beside that in Fig. 4.23 (e) the scissors mode at 204meV exists, which indicates that molecularly water is adsorbed and an ice-like structure grows on the surface. On the other hand the 0.3MLE V-rich termination in Fig. 4.24 I (a,b) shows that the OH stretch vibration ν(OH) comes up at 0.20L of water. Like on the 0.8MLE V-rich termination the ν(OH) mode broadens at 0.60L of water in Fig. 4.24 I (d) without forming a well-defined peak. At 2.00L of water the adsorbed molecules connecting together with hydrogen bonds, shown in Fig. 4.24 I (e) as an energetically wide loss feature.

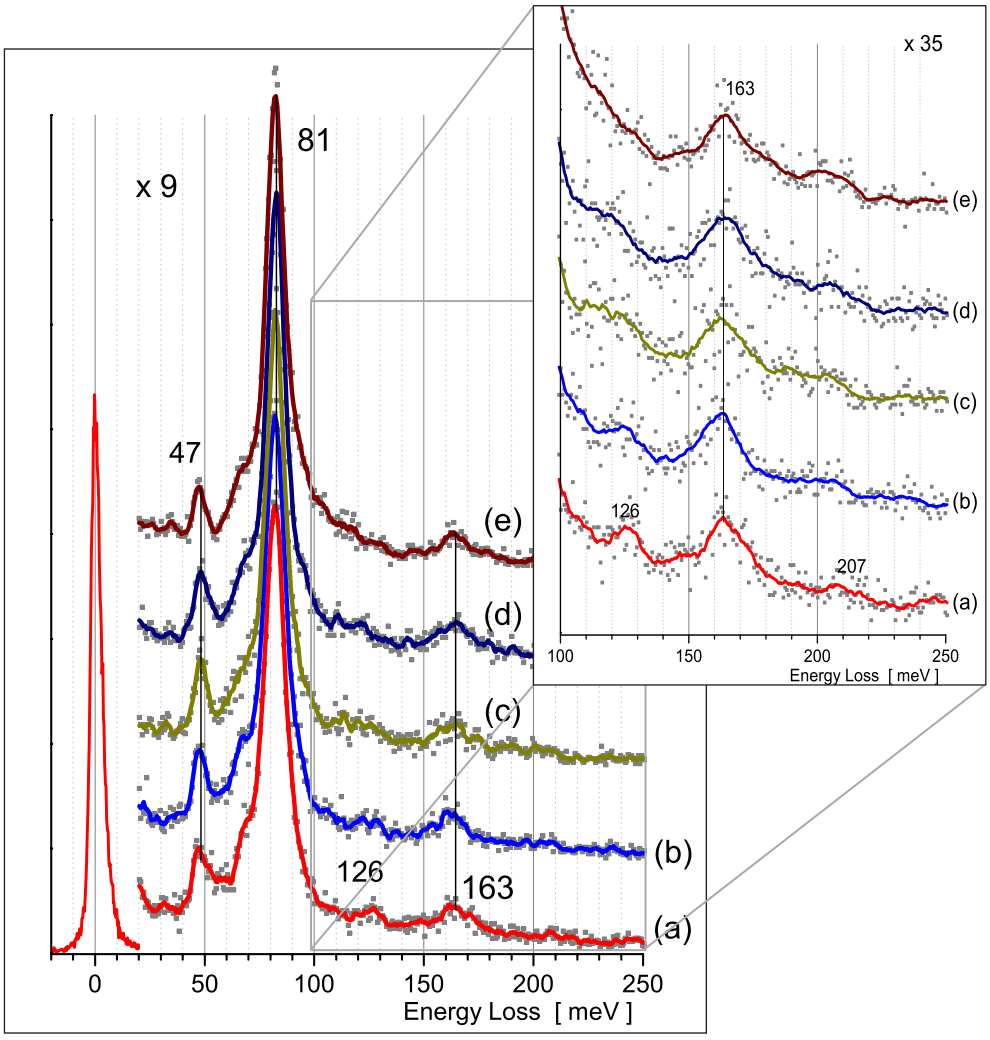

Fig 4.23:0.8MLE thick V-rich terminated (1x1) surface exposured to different amounts of water and investigated by HREELS. The inset presents these spectra enlarged in the energy range of 100 - 250meV
(a) 0.15L, (b) 0.20L, (c) 0.40L, (d) 0.60L, (e) 2.00L

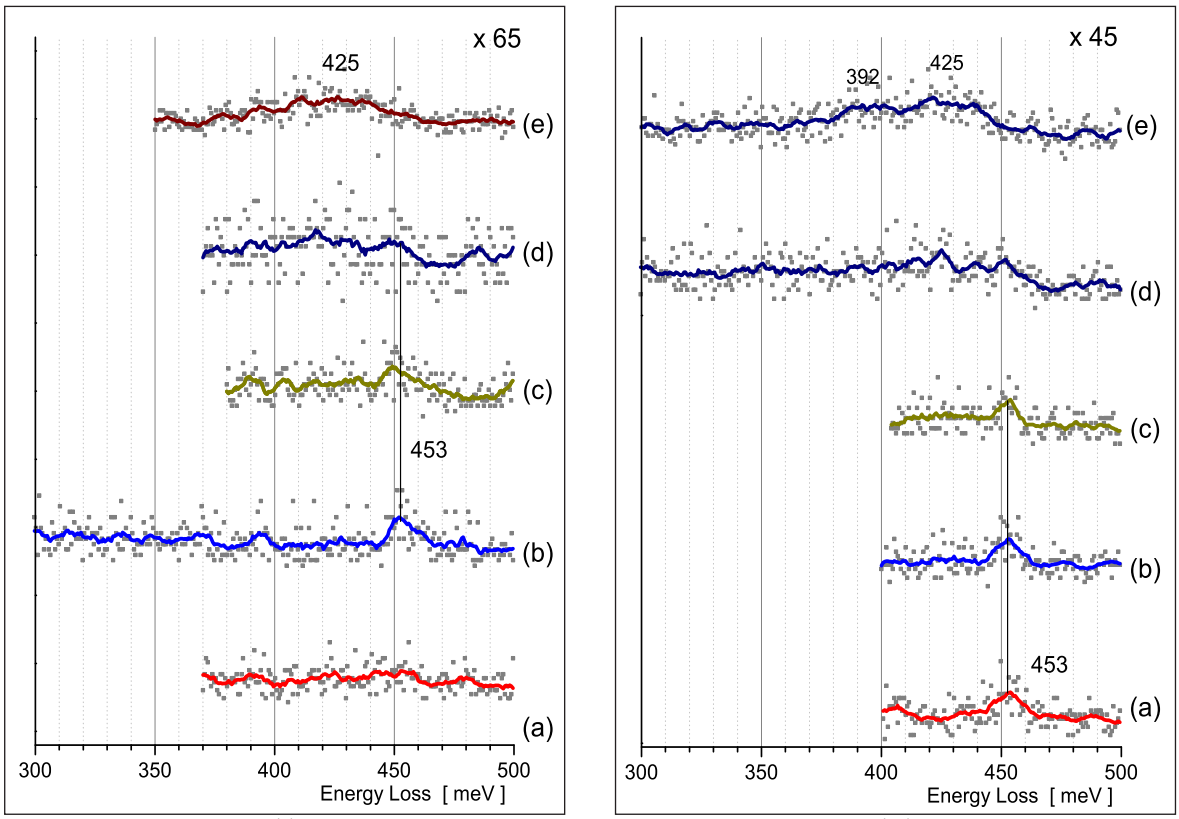

Fig 4.24: The region of the ν(OH) stretch modes, for the 0.3MLE V-rich terminated surface (I) and for the 0.8MLE V-rich termination (II) with different water dosing steps (a) 0.15L, (b) 0.20L, (c) 0.40L, (d) 0.60L, (d) 2.00L

Simultaneously in Fig. 4.22 (e) the vibrational feature for the hindered translation of H_2O molecules shows up at 35meV.

In contrast to the 0.8MLE V-rich terminated surface the binding mode appears on the 0.3MLE V-rich termination at 0.20L (Fig. 4.22 (b)) and stays visible for higher exposures.

Thermal desorption of H_2O on a 0.8MLE V-rich (1x1) termination

The 0.8MLE V-rich (1x1) terminated surface has been cooled down to 100K and 1.1L of molecular water has been dosed onto the cold sample. This ice-like layer on the surface is heated to 150K, 200K, 250K, 300K and 400K and investigated with HREELS after every heating step.

Heating up to 150K does not change the shape of the spectrum. The ν(OH) stretch mode (Fig. 4.25 (b)) is broad and presents no separated vibrations. In the energy range between 30 - 250 meV no change can be seen in Fig. 4.26 (b). Heating up the sample to 200K changes the adsorbed water structure:

The broad ν(OH) peak has disappeared and a new, narrow vibrational mode can be seen (Fig. 4.25 (c)) at 450meV. This suggests that no hydrogen bonds are present on the surface, the water molecules have partly desorbed from the surface. A further heating to 250K brings back the vanadyl stretch vibration at 126meV. M. Sock reports in his PhD-thesis, that heating up a V-rich (1x1) terminated surface to ~800K (~525°C) restores the vanadyl V=O (1x1) termination [12, Chapter 8.2.3]. The hydroxyl groups on the here

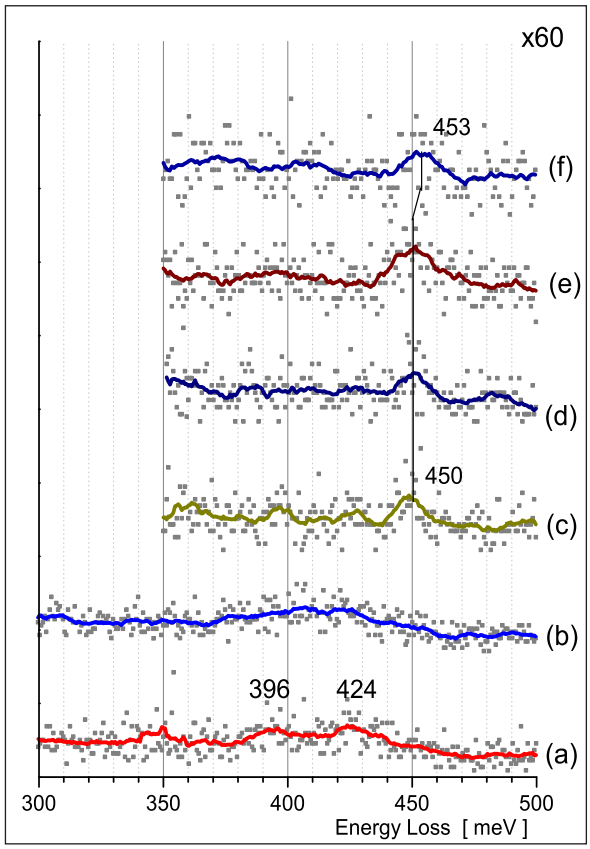

Fig 4.25: 0.8MLE V-rich terminated surface covered with 1.1L water (a) and then heated stepwise to analyse the water desorption in the region of the ν(OH) stretch vibration heating steps: (b) 150K, (c) 200K, (d) 250K, (d) 300K, (e) 400K

presented surface may be used to form vanadyls, explaining why the restoration process takes place at a much lower temperature (200K compared to ~800K). As it is shown in Fig. 4.26 (e,f) heating the sample to higher temperatures, 300K and 400K respectively, does not increase the height of the vanadyl peak any more nor does it desorb the hydroxyl groups, the ν(OH) mode is still visible at 450meV. Note that in the last heating step to 400K the OH stretch vibration shifted to higher loss energies (to 453meV), see Fig. 4.25 (f).

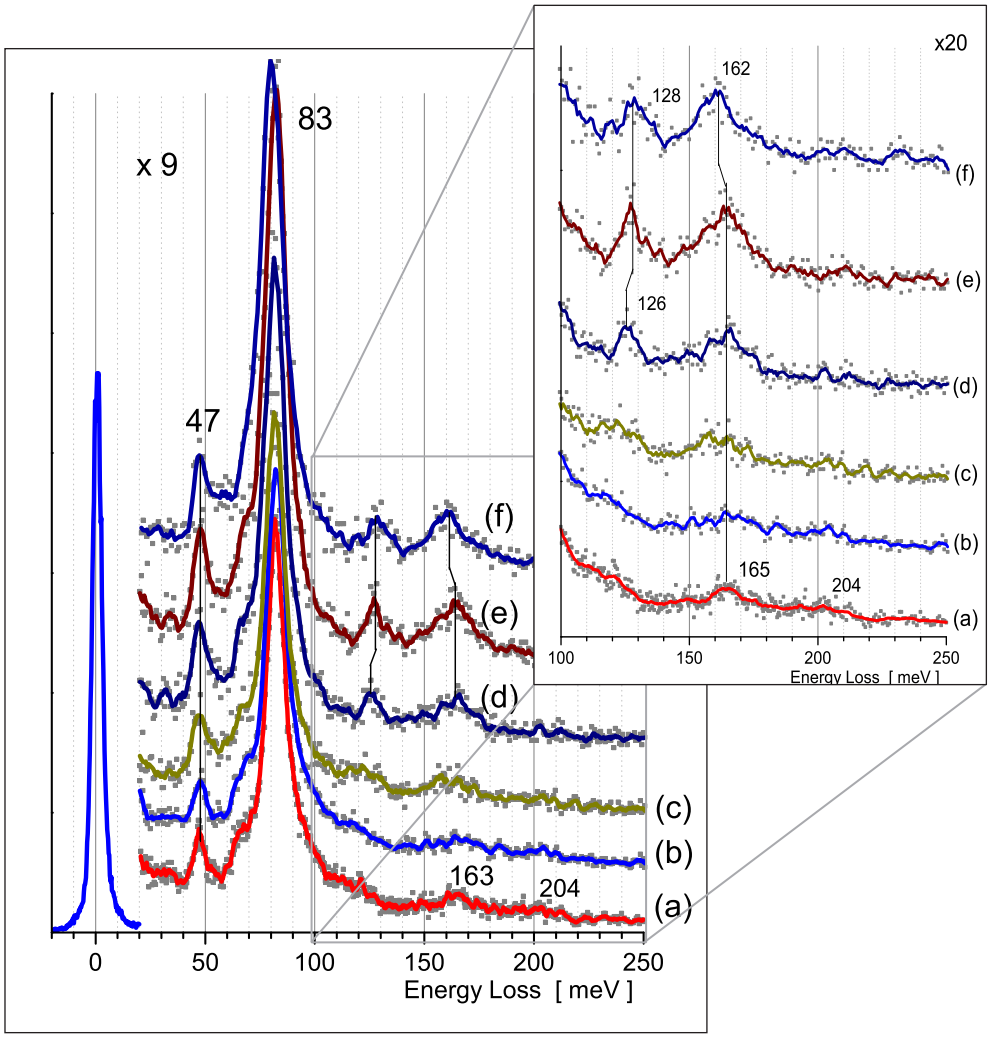

Fig 4.26: 0.8MLE thick V-rich terminated (1x1) surface dosed with 1.1L water (a), and afterwards heated stepwise to 400K.
heating steps: (b) 150K, (c) 200K, (d) 250K, (d) 300K, (e) 400K

4.4 Summary

The adsorption of H_2O on clean Rh(111) and on thin V_2O_3 films is the main topic in this chapter. The HREELS study tried to find differences in the adsorption mechanism, whether the H_2O molecule adsorbs molecularly or dissociates on the surface. For this purpose the attention is focused to the intramolecular O-H stretch vibration of the water molecule, which comprises a lot of information how the molecules are arranged on the surface. Moreover this vibrational feature is detected in an energy region, where no other vibrations are seen. This reveals whether the molecules form clusters or stay at the adsorption site as a monomeric molecule. The strength of the interaction between the adsorbed molecules with the substrate compared to the strength of the interaction between the molecules themselves plays a crucial role for the formation of clusters on the surface. It is known that water on metals reacts substantially different than on oxides, due to the differences in the bond strength to the substrate.

The results from this chapter can be summarised in the following way:

Water on Rh(111)

- At 100K sample temperature the water molecules adsorb molecularly on the crystal surface. The bending mode δ(HOH) is visible from the first dosing steps on. This is evidence that the molecules do not break up during the adsorption.
- Even for small amounts of water the ν(OH) stretch vibration forms broad peaks, indicating that hydrogen bonds are formed between the H_2O molecules. This underlines the model that water clusters on metals.
- Higher exposures of water leading to an ice-like structure on the crystal surface. The bending mode δ(HOH) shifts towards the value known for ice layers. Furthermore, the vibrational modes of the frustrated translations are detectable in HREELS, representing the intermolecular vibrations (H_2O-H_2O) in ice.
- LEED shows a ($\sqrt{3}$x$\sqrt{3}$)R30° structure, suggesting that for high coverage the water molecules build a long-range order.

Water on V_2O_3: vanadyl termination V=O (1x1)

- Adsorbed water shifts the vanadyl peak to lower loss energies. This suggests that the V=O groups are involved in the adsorption process of the water molecules.
- In the region of around 350 - 450 meV the HREELS spectra contain more than one loss feature. It seems that for low coverage water adsorbs both molecularly (ν_1(OH)= 424meV) and dissociates (ν_2(OH)= 455meV). At high coverage a ice-like structure is build; the OH stretch vibration is found at 425meV with a broad shape, due to hydrogen bonding. The vibration mode for frustrated translations can also be identified.

Water on V_2O_3: O-rich termination ($\sqrt{3}x\sqrt{3}$)R30°

- On the "vanadyl defective" surface it is hard to identify vibrational modes originating from water due to the weaker signal intensities in HREELS.
- For small water amounts (0.10L) it seems that hydroxyl groups form on the surface, a single weak vibrational feature can be seen at 453meV. Increasing the water coverage (0.20L) three modes are formed, which are not seen for higher doses. A broad vibrational mode can be seen for 0.40L, suggesting that the OH groups form a network of hydrogen bonds.
- At exposures of 2.00L two not distinct ν(OH) peaks can be seen at 412meV and 434meV. Moreover at 204meV the bending mode and the hindered translations at ~35meV are visible, which give reason to the assumption that an ice-like structure exists on the surface.

Water on V_2O_3: V-rich (1x1) termination

- The 0.15MLE vanadium metal overlayer surface does not show any distinct vibrations for low dosing amounts. The vanadyl peak shift is very small for the dosing steps till 0.30L. Then for 0.40L the peak position moves abruptly over 5meV to lower loss energies. After this dosing step the height of the vanadyl peak and the vibration at 82meV increases again. For coverages above 0.60L the vanadyl peak shifts further on and the intensity is decreasing. This leads to the conclusion that the H_2O firstly adsorbes at the V-layer and then attaches to the remaining V=O groups.
- For 0.3MLE and 0.8MLE V-rich terminated surfaces the adsorbed water forms even at the beginning of the dosing series the ν(OH) mode at 453meV with a narrow shape. It seems the water dissociates on this surface and does not form hydrogen bonds. 2.00L of water on the surface finally forms a broad ν(OH) peak at 425meV, together with the appearance of the hindered translation mode at 35meV.
- Heating up a 0.8MLE V-rich terminated surface, which has been exposed to ~1L of water to 200K, leads to a dissociation of the water molecules. The former broad ν(OH) peak centred around 424meV disappears after the heating and a narrow one at 450meV comes up. The latter feature is generated by the O-H stretch vibration of hydroxyl groups. The OH groups stay on the surface up to ~400K. Heating this surface also induces the restoration of the vanadyl V=O groups on the V-rich termination. At the temperature of 250K the typically loss feature for the V=O stretch vibration appears at 126meV and moves to 128meV by heating the sample to 300K, indicating the oxidation of the vanadium atoms by the adsorbed H_2O.

5. Metal-Insulator phase transition in V_2O_3(0001) films

5.1 Introduction

The vanadium sesquioxide (V_2O_3) undergoes several phase transitions as a function of temperature, dopant concentration and pressure. The material can change the properties from: (1) metal to antiferomagnetic insulator
(2) insulator to antiferomagnetic insulator and
(3) metal to insulator
Hence, the phase diagram (Fig. 5.1) consists of three different regimes. In 1946 Foëx experimentally observed in V_2O_3 a transition by cooling the sample to a temperature below 160K [39]. The vanadium oxide changes from metallic to antiferomagnetic insulating at the latter mentioned temperature.

By the improving Mott theory in the following years, the phase transition became a very active research field from 1970 on. The most reliable theory in the case of V_2O_3 is the Mott-Hubbard model, which will be explained later on. One could say vanadium sesquioxide is the prototype for this transition.
Metal-to-insulator transitions are a subject of great interest, because they are depending strongly on the detailed properties of the electronic and geometrical structure.

In this study I will look at the before mentioned (see Chapter 3.3, p. 23) three different surface terminations of V_2O_3 films and how the phase transition is seen in HREELS. Moreover, it will be shown that the surface structure and the adsorption of molecular water can change the transition behaviour.

5.2 Theoretical Background

5.2.1 The phase transition in general

V_2O_3 can switch it's electrical properties from insulating to metallic. By definition an insulator is a material with vanishing electrical conductivity, whereas a metal contains electrons, which are able to move and thus a transport of electrical charge in the solid state can take place.
The distinction between "metal" and "insulator" is strictly limited to zero temperature, because even insulating materials display a finite conductivity, since thermal excitations can bring electrons in states above the energy gap into the conduction band.
Nevertheless for technical purposes the classification "metal" and "insulator" can be employed, because the absolute values of the conductivity for various materials differ by many orders of magnitude.

The possible charge transport in bulk crystals is influenced by the surroundings:

(1) the itinerating electrons interact with the potentials of the ions in the lattice sites,
(2) one electron interacts with another electron (Coulomb repulsion is an example for this)
(3) and finally, external applied fields (***E***, ***B*** fields of electrical and/or magnetic nature, respectively) can cause different behaviour in the conductivity.

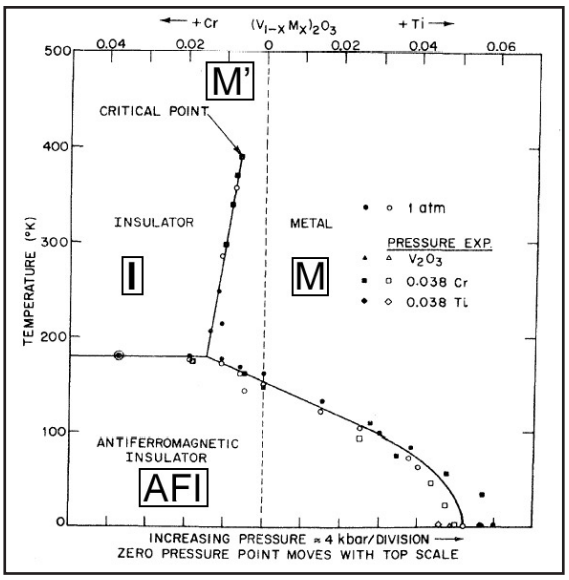

Fig 5.1: Phase diagram from McWhan et al., it shows the four phases of bulk V_2O_3 [46]. (M) is the regime of the paramagnetic metallic phase, (I) represents the paramagnetic insulating and (AFI) the antiferomagnetic insulating phase; at elevated temperatures another metal phase exists (M')

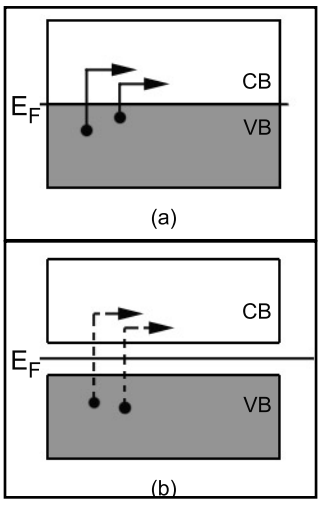

Fig. 5.2: Band model, comparing metal (a) to insulator (b), where a energy gap is developed and no electrons are in the conduction band (CB)

In the first case (1) three different insulator classes can be distinguished due to the interaction of the electrons with the ions. In the classes one could apply with "single-electron theory".

Band Insulator: The "Bloch-Wilson" or "Band Insulator" is the simplest case: the lattice of the sample is ideal (has no defects); the electron-electron interaction is neglected; the problem is reduced to single electrons in a periodic potential.
"The interaction between the electron and the periodic ion potential gives rise to an energy gap between the lowest conduction band and the highest valence band. Consequently, there are no free carriers available for the transport of charge." [40, p. 15]

Peierls Insulator: In this approach the "static" ion potential responds to the moving electrons, which was not taken into account in the "Band Insulator". The periodic array of the lattice deforms due to the ion-electron interaction, in turn the new periodic potential influences the electron transport, too. This can give rise to a metal-to-insulator transition, as a consequence of the symmetry breaking of the original lattice.
It should be mentioned that also the electrostatic (crystal) fields possibly induce lattice deformations, in this way the states are shifted up the electrical field of the surrounding atoms (crystal field effect).

Anderson Insulator: Disorder or lattice defects interact with free, independent electrons inducing localization. A disorder driven metal-to-insulator transition may appear in materials with a strong structural disorder or with a strong impurity scattering.
The picture of single electrons in a crystal is very simplified, the electron-electron interaction has to play a role in the conductivity behaviour of a material. The Coulomb force/potential is strong and long-ranging and therefore it seems to be a drastic assumption, if one does not put this into the model. The point of view changes from a single electron problem to a many-body problem.
It brings us to point (2) of the above mentioned list of influences and the next step is the concept of a Mott insulator.

5.2.2 Mott insulator

Mott observed during studies on NiO that it is insulating, although it should be metallic on the basis of the Bloch-Wilson band theory. He solved the problem by adding a strong Coulomb repulsion term of the electrons, which causes a ground state wave function of NiO that is localized (also called "Heitler-London-form") and leads to an insulating state [41]. A transition from the insulating to the metallic phase should be possible by the application of high pressure. The material changes abrupt from a localized insulator to a band metal. This electronic transition, with no change in the basic lattice structure (only lattice site distances are changing) is called a Mott-transition.

The Coulomb repulsion tends to keep electrons apart from each other; the kinetic energy E_{kin} on the other hand tries to spread out the electrons over the whole crystal.

$$g_{\sigma,\sigma'}(\vec{r},\vec{r}') = <\hat{\psi}^{+}_{\sigma}(\vec{r})\hat{\psi}^{+}_{\sigma'}(\vec{r}')\hat{\psi}_{\sigma'}(\vec{r}')\hat{\psi}_{\sigma}(\vec{r})> - <\hat{n}_{\sigma}(\vec{r})><\hat{n}_{\sigma'}(\vec{r}')> \qquad \text{(eq. 5.1)}$$

The left term in the formula (eq. 5.1) represents the probability to find an electron σ' at $\vec{r}'$, when an electron σ sits at $\vec{r}$. The last part is the product of two-fermion expectation values, where $\hat{n}_{\sigma}(\vec{r}')$ and $\hat{n}_{\sigma'}(\vec{r}')$, respectively, are particle density operators.
The pair correlation function, the measurement of the electron-electron interaction, contains the effect of the particle statistic for electrons (for fermions the Pauli exclusion principle forbids electrons with the same spin on the same orbital) and moreover the "true" electron correlation from the direct interaction itself.
The Pauli principle reduces the probability to find two electrons with the same spin close together – these electrons are kept apart – and reduces in this way their Coulomb interaction. The pair correlation function for equal spins is not vanishing and there is an "exchange" of electrons. If the pair correlation function is vanishing for non interacting electrons of different spin, the electrons are not correlated. If they are correlated this means $g_{\sigma,\sigma'}(\vec{r})$ has a value different from zero. When the size of the pair correlation function of both parts is comparable, the electron system is called "strongly correlated". The resulting correlation strength $g_{\sigma,\sigma'}(\vec{r})$ of the electron-electron interaction can create local moments to minimize the Coulomb repulsion in the system.
"Mott himself describes a Mott insulator as a material that would be metal, if no moments were found." [40, p. 34]
The gap in the excitation spectrum can originate from long-range order of the pre-formed moments (what is called a Mott-Heisenberg insulator) or as reviewed in this section by a quantum phase transition driven by charge and/or spin correlations (Mott-Hubbard insulator).

5.2.3 Mott-Hubbard insulator

In the Mott-model "hydrogen atoms" with Bohr radius a_B were arranged on a cubic lattice with a lattice constant a. On each lattice site sits an atom with one electron, there are single occupied sites so to say and with a half-filled band. Further on, in the model one assumes, that the effective electron-electron interaction will be local, short-range Coulomb repulsion. This can be expressed by the so called "Hubbard U", which represents the intraatomic energy:

$$U = E(H \rightarrow H^+) - |E(H \rightarrow H^-)| = E(H^-) + E(H^+) - 2E(H) \qquad \text{(eq. 5.2)}$$

containing the ionisation energy ($E(H \rightarrow H^+)$) and the electron affinity ($E(H \rightarrow H^-)$). The electrons may tunnel between neighbouring atoms ("tight binding" approximation for independent electrons) leading to a second parameter the bandwidth W,

$$W = 2Zt \qquad \text{(eq. 5.3)}$$

where Z is the number of nearest neighbours and t is the tunnel amplitude, depending on the ratio of a/a_B.
The Hamiltonian consists of two terms,

$$H = \sum_{i,j,\sigma} t_{ij} c^+_{i\sigma} c_{j\sigma} + U \sum_i n_{i\uparrow} n_{i\downarrow} \qquad \text{(eq. 5.4)}$$

where the first sum represents a tunnelling probability for an electron of spin σ at the lattice site i and t_{ij} describes the transfer of the electron from i to site j. The sum is related to the intraatomic energy or bandwidth W. The second term is the Coulomb repulsion term, when two electrons with different spin are sitting on the same site.

If the distances between the "hydrogen atoms" are getting smaller, the overlap of the atomic wave functions will increase more and more. This leads to an enhancement of screening and the electrons tend to move away from their lattice site (delocalise).

From the tight binding approximation it is known, that when single atoms are kept far apart the electrons are localised on the atoms. Well separated energy states exist for each atom. By reducing the distances of the atoms the states are splitting into bands of states, e.g. for transition metals the d-bands are well-defined, narrow bands. A further decrease of the interatomic distances results in an increasing bandwidth, the bands may broaden so much that they finally intersect.

The lower and the upper Hubbard band mark actually the situation, where two bands are coming very close but are still separated by an energy gap. An additional approaching of

the atoms carries out that the bandwidth of the two Hubbard bands is increasing and finally the insulating gap disappears because of the overlap of the bands. This happens roughly when the lattice sites distance "a" equals the Bohr radius a_B of the "hydrogen atom".
In terms of energy the metal-insulator transition starts at U≈W, where the bandwidth W gets in the range of the intraatomic energy scale U, the critical inner energy U_c is reached.
In the case of W<<U , the overlap is barely existent, the material has insulating character. The repulsive energy does not allow the creation of a conduction band. In the other way round, W>>U, the system is metallic.

In a Mott-Hubbard insulator the electron-electron interaction, the heart of the transition, opens a gap (E_g= U-W) in the spectrum of charge excitations with growing U/W ratio into lower and upper Hubbard band (Fig 5.3). At large U/W ratio finally the electrons are localised on each site and the system will be in the insulating state. The end is reached with the "atomic limit" t=0 (→W=0 and therefore U/W= ∞), here the atoms in the lattice act like single atoms.
Varying the U/W ratio has the effect that the sample undergoes a phase transition, switching between insulator and metal. The long-range ordering of magnetic moments is not taken into account at this point of view.

If the preformed local moments are included in the model, they could long-range order and spin excitations well separated from charge excitation occur. The Mott-Hubbard insulator changes to a Mott-Heisenberg insulator. This long-range ordering of the magnetic moments may happen below the Néel temperature of the material. Additionally a thermo-

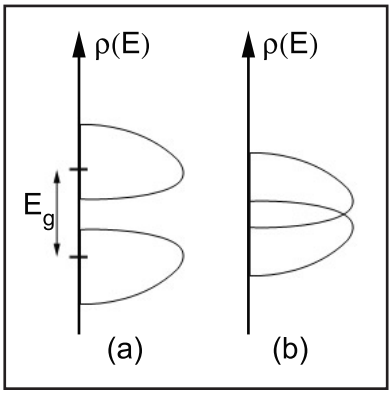

Fig 5.3: Hubbard bands: the original two bands (a) merge to one (b); the system gains free charge carriers and becomes metallic, the lower and upper Hubbard band are separated by a gap E_g= U-W

dynamic phase transition will transfer the paramagnetic behaviour to antiferomagnetic. Above the Néel temperature the material is a paramagnetic metal or Mott-Hubbard insulator. Below this temperature antiferomagnetism appears, the Mott-Hubbard (quantum phase) transition is hidden behind the Mott-Heisenberg (thermodynamic phase) transition.

In "reality" the model of the phase transition forced by the s-electrons is way to simple! The correlations of the d-electrons are more important if one is dealing with transition metals (V, Fe, Ni,…) and the d-bandwidth is smaller compared for example to the s-band of alkali metals. In the model of Mott for calculating E_g (eq. 5.2, 5.3), electrons were taken from the s-band to infinity or added from infinity to the band. However, in transition metals the electron moves from a 3d-level to an energetically close 4s-level. This fact reduces the value of the intraatomic energy U. Moreover, in a solid state a possible charge disproportion is screened by surrounding electrons of the neighbour atoms. Thus the bandwidth W is smaller in a transition metal and the Coulomb interaction, which gives rise to an insulating ground state is reduced, too, compared to the s-band model.

In the case of metal oxides a hybridisation of the oxygen 2p-levels with the 3d-levels (and also 4s-levels) of the transition metal atoms take place. Mostly the oxygen-like bonding bands lie below the Fermi energy and are occupied, whereas unoccupied antibonding bands (3d-, 4s-levels) are shifted above the Fermi energy.

This causes normally a less strong screening of the repulsive Coulomb interaction of the 3d electron and the insulating phase is more likely. The V_2O_3 is at the boundary between metallic and insulating behaviour, the 4s band almost crosses the 3d band and indeed there is a transition from metal to insulator at T≈ 160K (see Fig. 5.1), combined with changes in the volume and lattice structure.
Because of the oxygen in the lattice structure the energy for an excitation is no longer determined only by the energy difference of the two Hubbard bands but by the "charge-transfer" energy Δ.
The electron changes orbital and moves from a metal d-level to an oxygen p-level.

transition-metal: $U = E(d^{n+1}) + E(d^{n-1}) - 2E(d^n)$ (eq. 5.5)

plus oxygen: $\Delta = E(d^{n-1}) - E(d^n) + E(p^{n'+1}) - E(p^{n'})$ (eq. 5.6)

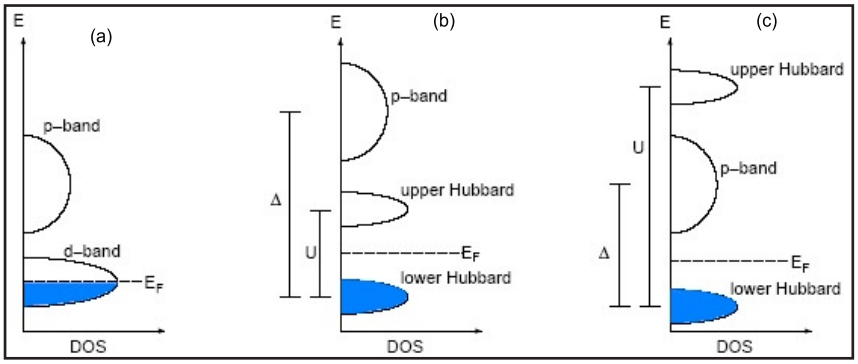

Fig 5.4: The three possible band adjustments in a multi-band Mott-Hubbard insulator:
(a) displays the case of the metallic phase, the d-band is not split;
(b) U>0 and U<Δ, this sketches the Mott-Hubbard insulator;
(c) U>0 and U>Δ, here the electron goes from the lower Hubbard band to a p-band, it is the charge-transfer insulator; [42, p. 378]

Generally spoken: if Δ < U (p-orbital lies between the two Hubbard bands) the energy gap for a charge excitation is depended on the charge–transfer energy Δ and will form a "charge-transfer" insulator. When the upper Hubbard band is located below the p-band (this means Δ>U), the on-site interaction U is dominating the excitation process, therefore U will drive the possible metal-to-insulator transition. (see Fig. 5.4)

Since the fact that a Mott (-Hubbard) transition is only exactly defined at 0K, because there the two phases – metallic and insulating – are well separated in sense of conductivity, a theoretical concept for nonzero temperatures is the introduction of the quasiparticle picture.
Coming from the metal phase the almost localised electrons and their interaction at the phase transition to the insulating state can be reformulated in quasiparticle terms. A quasiparticle peak largely separated from the lower and upper Hubbard band and the p-band as well is found. The width of this peak vanishes in the limit of the metal-to-insulator point. (see [42, 43, 44, 45])

5.3 Phase transitions in V_2O_3

As mentioned in the introduction to this chapter, it was published the first time 1946 that V_2O_3 undergoes a phase transition as temperature is lowered to ~160K [1]. McWhan et al. [46] figured out three different phases in bulk V_2O_3, which can be obtained by varying the temperature, the doping rate of impurities (e.g. Cr, Ti) or by applying pressure.
As one can see from the phase diagram (Fig. 5.1) there are three main regions: in the upper left area a paramagnetic insulating phase (I), on the right hand side a paramagnetic metallic phase (M) and in the lower part of the diagram an antiferomagnetic insulating phase (AFI) occur. A defined phase boundary is not found at temperatures above 380K, the material changes continuously from the insulating phase to the metallic (M') phase.

Whereas the lattice structure of the antiferomagnetic phase (AFI) is monoclinic, the three other phases have all the rombohedreal corundum structure, known from similar oxides like Al_2O_3, Fe_2O_3 or Cr_2O_3. However, it seems that V_2O_3 is in some way special, because it reacts sensitively on small changes in the lattice distances of the vanadium atoms.

5.3.1 Pure V_2O_3

A vanadium sesquioxide crystal at room temperature is isostructural with a α-Al_3O_2 crystal, it possesses a corundum lattice structure. Starting at room temperature (300K) and following the dashed line upwards, which represents pure V_2O_3, in Fig. 5.1 to higher temperatures the material undergoes at ~550K [54] a transition to another metallic phase (M'). This M' phase is visible in resistivity measurements, but there is no structural change in the lattice.
Instead of heating up one could also cool down the sample and this would be equivalent in going down the dashed line in the phase diagram (Fig. 5.1). At ~160K a first-order phase transition takes place, the structure changes from rombohedreal to monoclinic and additional a long-range antiferomagnetic order is established (this is the one which Foëx saw in 1946).
The c-axis contracts (~5%), but the a-axis expands: often the ratio c/a is used as a parameter for the transition, because it reflects the change of the V-V distance. This distortion, sketched in Fig. 5.5, of the trigonal structure to monoclinic can be visualised by a rotation of the V_a-V_b pair in the c-a plane counter clockwise by 1.8°, implying an increase in the distance of the V_a-V_c pair by 0.11Å [47]. The vanadium-vanadium distance of the adjacent c-a planes however, stays almost the same, like the V-O distances. The interatomic distances between oxygen atoms vary in such a way that they arrange to the movement of the V-V pairs and they become skewed.

During the phase transition from the metallic to the insulating phase at ~160K the volume of the unit cell enlarges by 3.5%, which can even cause cracks in bulk crystals.
The fact that the metal atoms are moving further apart and an insulating phase can be established, underlines the basic concept of the Mott transition. The before delocalised conducting electrons are getting more localised, due to the decreasing overlap of the 3d-bands in the V atoms. The additional advent of the antiferomagnetism in the cold sample comes from the ordering of the localised spins (the Néel temperature for V_2O_3 is T_N= 180K) (further reading [48, 49, 50]).
The V-V distance regulates the ratio between the Coulomb repulsion of the electrons (U) and the bandwidth (W). This indicates that the phase transition is driven by the Mott-Hubbard mechanism. (see Chapter 5.2.3, p. 69) Because of the additional ordering of the spins and therefore the presence of the antiferomagnetic insulating phase it would be more precise to say V_2O_3 experiences a Mott-Heisenberg transition, which hides the Mott-Hubbard quantum phase transition.

Due to the crystal-field splitting there are four 3d states per vanadium pair around the Fermi energy: two degenerated bands of e_g and two other ones of a_g symmetry.
Goodenough [51] predicts vanadium 3d bands in three symmetries:

- the e^{π}_g orbitals lying between the V pairs in the basal
- the a_{1g} orbitals between V pairs along the c-axis
- and finally the e^{σ} orbitals with components both perpendicular and parallel to c

In the metallic phase of V_2O_3 the bands e^{π}_g and a_{1g} are overlapping and cross the Fermi level E_F, therefore they are partially filled. The empty bands $e^{\pi}_g{}^*$ and $a_{1g}{}^*$ have their lower band edge 0.8eV and 1.6eV, respectively, above the Fermi edge. (Fig. 5.7)
The oxygen 2p-band is around 6eV wide and the upper band edge lies 3.7eV below the E_F, the double degenerated e^{σ} sits 2.6eV above the Fermi level (values taken from [52]).

If the vanadium sesquioxide sample is brought to 160K by cooling, the metal-metal distances are increasing as mentioned above. The overlap of e^{π}_g and a_{1g} no longer exists; on the one hand a_{1g} and $a_{1g}{}^*$ move closer together and on the other e^{π}_g and $e^{\pi}_g{}^*$ separate more. A gap develops: e^{π}_g stays below E_F and becomes a full band and a_{1g} lies above the Fermi edge as an empty band.

In this model a Hubbard on-site repulsion can be taken into account and the split a_{1g}-band builds the lower and upper Hubbard band. (The V 3d - O 2p hybridisation was not present in the model of Goodenough, which plays a role in the appearance of the phase transition).

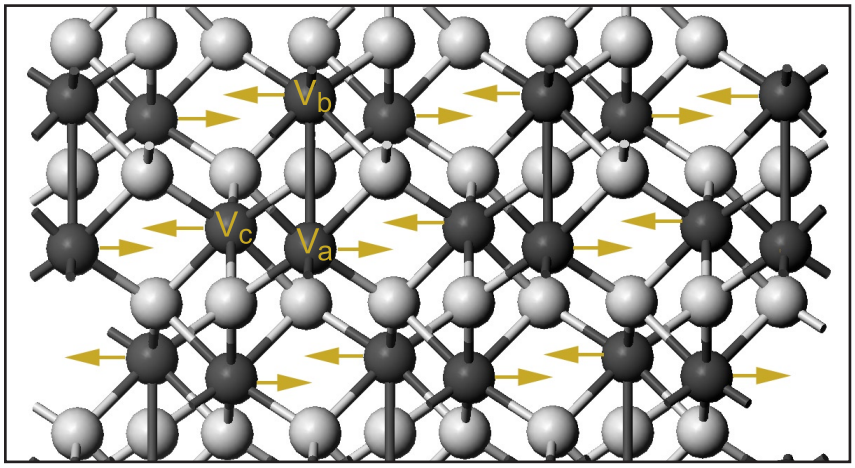

Fig 5.5: Changes in a V_2O_3 crystal: the in vanadium atoms V_a and V_c are moving apart in the V layer, whereas the oxygen atoms almost stay at the same position (dark balls= V; bright balls= O) [47, 53]

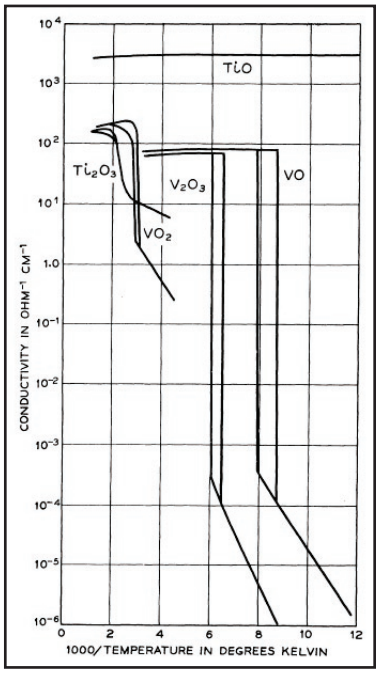

Fig 5.6: Example for a resistivity measurement of V_2O_3 (and other metal oxides), visible is the significant drop in conductivity at around 155K [54]

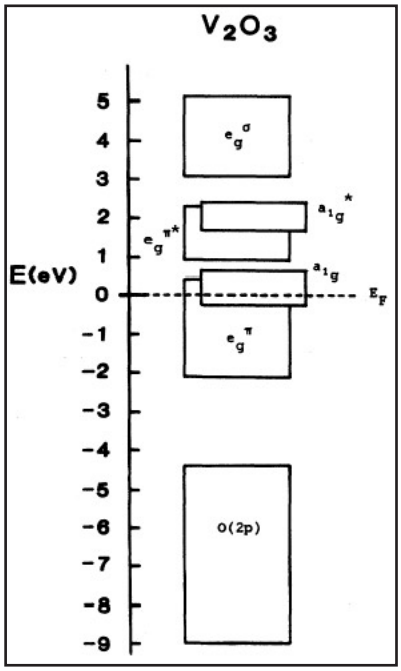

Fig 5.7: Band alignment in V_2O_3 crystals at room temperature (300K) showing the metallic phase [55]

5.3.2 Pressure, Doping and Nonstoichiometric V_2O_3

Pressure

By applying external hydrostatic pressure on the V_2O_3 crystal the temperature induced phase transition M-AFI from the phase diagram (Fig. 5.1) can be totally suppressed. This time in the phase diagram of McWhan the vertical dashed line is the starting point of Zero applied pressure. The phase transition from the metallic (M) to the insulating (AFI) phase is set at 160K. But with increasing pressure, one would move from the dashed line to the right side of the diagram, the temperature of the phase transition drops. The transition can be completely suppressed with pressures above 25kbar.
It is believed that the external pressure changes the c/a ratio of the lattice in the way that the 3d electrons of the V-V pairs can still interact even at low temperature.

Doping

V_2O_3 is close to an instability and therefore a small change in the lattice positions of the metal atoms is enough to change the conducting properties by several orders of magnitude. Instead of "manually" changing the lattice by using external pressure one could introduce impurities into the lattice and force small changes in the site distances. Most studies were done with Cr or Ti, both have different influence on the crystal lattice.
Chromium brings the V_2O_3 sample even at room temperature to an insulating phase. This can be easily seen in the phase diagram (Fig. 5.1), beginning with pure V_2O_3 at the dashed line and increasing the chromium concentration by going to the left hand side of the phase diagram. First of all the phase transition from the metallic state to the antiferomagnetic state takes place at higher temperatures, later a paramagnetic insulating phase (I) occurs with further Cr-doping (the structure stays rombohedreal). It seems that chromium puts a negative chemical pressure on the lattice, the c/a ratio is decreasing which implies a larger distance of the V-V pairs (the bandwidth is reduced, the insulating state is stabilised). Rather small amounts of these impurity atoms are sufficient to drive the vanadium oxide system to the insulating phase. [47, 54, 56, 57, 58]

4% are enough - $(V_{1-0.96}Cr_{0.04})_2O_3$ – to reach the insulating phase (I) at room temperature. The volume is ≈1% larger than in pure V_2O_3, all V-pair distances are expanded at room temperature, but as said before the corundum structure is preserved, which in return gives a volume change at the transition from corundum to the monoclinic phase of only –0.1%; this is substantially smaller than in pure V_2O_3 (1.4%). In other words, with 4% of Cr-doping, the elongated V-V distances increases a little bit more at 180K, the new transition temperature, and the insulating phase (I) becomes antiferomagnetic because of the spin ordering. [56]

Ti atoms produce the contrary effect of Cr in the lattice of vanadium sesquioxide. Here the chemical pressure reduces the distances of the V atoms. Titanium doped samples act like pure V_2O_3 under external pressure. The phase transition temperature from metal to insulator moves to lower values and even can be totally suppressed at Ti concentrations above x= 0.05 (≡ 5%, $(V_{1-x}Ti_x)_2O_3$) [54,59]. The substitutional titanium increases the volume of the sample, which means that the c/a ratio increases. Hence, the 3d-orbitals overlap more and the bandwidth increases, the system becomes more metallic. This effect is strong enough to encourage the metallic phase, even if the substituted Ti^{3+} cation contributes only one 3d electron, while a V^{3+} cation has two.

Nonstoichometric V_2O_3

Beside hydrostatic external pressure and doping (chemical pressure) of the V_2O_3 there is a third possibility to produce a similar effect: introducing oxygen-poor or metal-deficient samples of vanadium sesquioxide obtained by a partial occupancy of the metal sites (in the case of the stoichometric lattice the oxygen sites are fully occupied).

The vacancies of V atoms introduce acceptor sites in the material, making it more extrinsic. The Fermi level moves more into the valence band and make the sample more metallic. Moreover, the missing atoms create sites for oxygen reorientations, providing the system extra states at the Fermi edge, which could participate in the transport of electrons. M. Yethiray [54] reports that the quality of the their used V_2O_3 samples could be gauged by the phase transition temperature, because it is so sensitive to the oxygen content in the lattice.

5.4 Metal-to-insulator transition seen in V_2O_3 thin film experiments

During the investigation of different surface terminations of thin films of V_2O_3 (50-60Å) we observed intensity changes in the phonon spectra of epitaxially produced films as a function of temperature. In the following chapter the vibrational structure of the vanadyl terminated V=O (1x1), the vanadyl reduced O-rich ($\sqrt{3}x\sqrt{3}$)R30° surface structure, and the vanadium terminated V-rich (1x1) surface will be compared by HREELS and XPS* data.

It will be shown that the well known phenomena of vanadium sesquioxide crystals is also detectable in bulk-like thin films. The result suggests that the surface termination plays a crucial role in the observation of a MIT below 160K.

5.4.1 Vanadyl termination (1x1)V=O

The V_2O_3 film with the vanadyl terminated (1x1) V=O surface termination is achieved by depositing vanadium on the substrate crystal under the following conditions:

The Rh(111) crystal is heated to 523K (250°C) and in the UHV chamber an oxygen background pressure of $2x10^{-7}$mbar is set. After evaporation the sample is heated 5min further on and then cooled down to room temperature in the oxygen ambient. A final annealing of the film to 873K (600°C) in UHV conditions produce the (1x1) V=O termination with a stacking sequence of O=V-O_3-VV'-O_3-VV'-... . Every vanadyl is bond to three surface oxygen atoms building a (1x1) unit cell, which contains one V=O group. (see also Chapter 3.3.1, p. 23)

300K

Starting from the room temperature, the HREELS spectrum of a 15MLE thick film (≈60Å) contains three prominent peaks. In Fig. 5.8 (a) the first one at 47meV originates from the "bulk" like V_2O_3 structure. The high intensity peak at 78meV with a visible shoulder at 92meV is expected to come from the surface oxygen atoms moving in the direction of their bonding to the vanadyl group (also called "breathing mode") [17]. The feature of 92meV is a bulk vibration. The distinct loss at 129meV represent the stretch vibration of the vanadyl group V=O, at higher loss energies on can see the double excitation of the "breathing mode" (78meV) at 157meV.

* recorded by S. Surnev, J. Schoiswohl, M. Sock during a scientific stay at MAXlab (Lund, Sweden)

100K

Cooling the sample down with liquid nitrogen the spectrum undergoes a dramatic change, visible in Fig 5.8 (b): the former peak at 78meV splits into a minor loss feature at 66meV and a sharp intense one at 83meV. The intensity of the latter is almost doubled compared to the one at room temperature (300K) in this region, whereas the other visible vibrations on the surface are not shifted. The V=O stretch vibration is still at 129meV as the bulk feature at 47meV.

Due to this intensity increase also the double-frequency feature, now at 166meV (2x83meV), is much more distinct, it is shifted from the former 157meV because of the frequency shift from 78meV to 83meV. Moreover, a frequency-sum feature appears at 213meV, formed by the losses at 83meV and 47meV.

There are predictions that a bulk peak should be at 66meV [17, p. 12, §C], which is only visible in the HREEL spectrum of the cold sample (100K). At 300K the loss peak

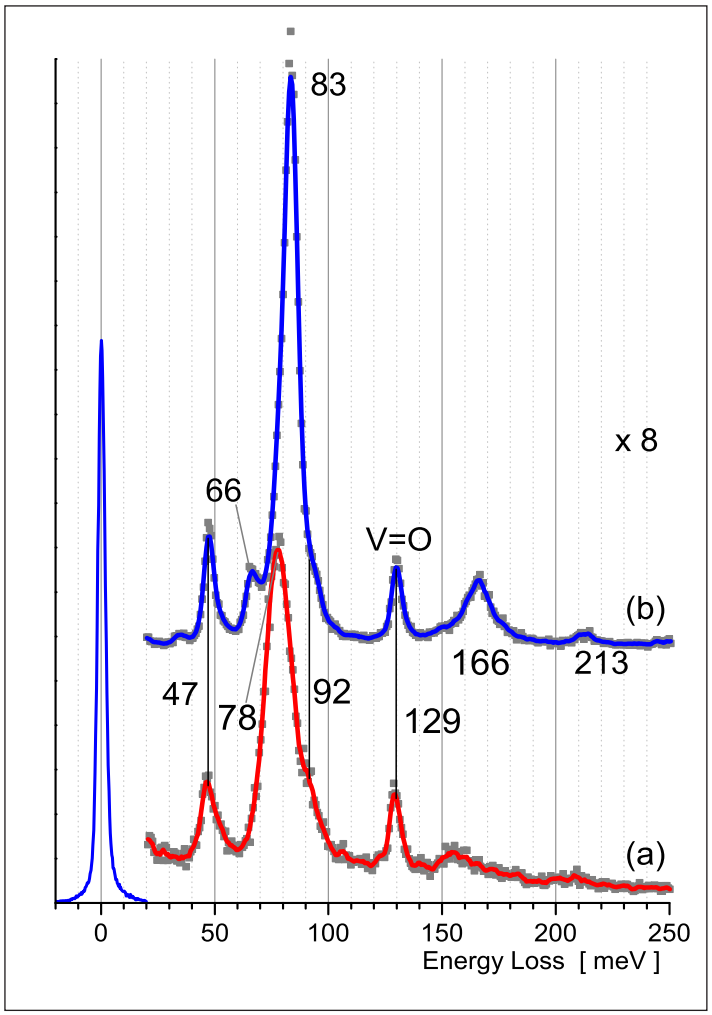

Fig 5.8: Phonon spectrum of the vanadyl terminated (1x1)V=O surface at (a) room temperature (300K) and at 100K (b). The peak at 78meV splits into a minor peak at 66meV and a high intensity peak at 83meV, when the sample is cooled down to 100K.

at 78meV hides this vibration in its left tail. The shift of the vibration coming from the oxygen surface atoms (from 78meV to about 5meV to higher loss energy) could be interpreted in a first guess as the small rearrangement of the oxygen atoms during the metal-to-insulator transition at 160K (to compensate the movement of the V-V pairs as it is known from V_2O_3 crystals (see 5.3.1 "Pure V_2O_3", p. 73])).

In our group valence band measurements were done (Fig. 5.9) on the same surface terminations underlining the present results of the HREEL spectroscopy. A primary energy of hν= 517eV was used. The low energy part of the V 3d peak is moving to higher binding energies at 100K. The density of states closer to the Fermi level is decreasing, indicating that the thin film is getting less metallic. The measurements were done in grazing emission to enhance the surface sensitivity and done with this primary energy to increase the count rate by exciting V 2p electrons to the V 3d states (so called resonant photoemission). Repeated measurements done with different photon energies (21.2eV, 110eV) show a similar behaviour.

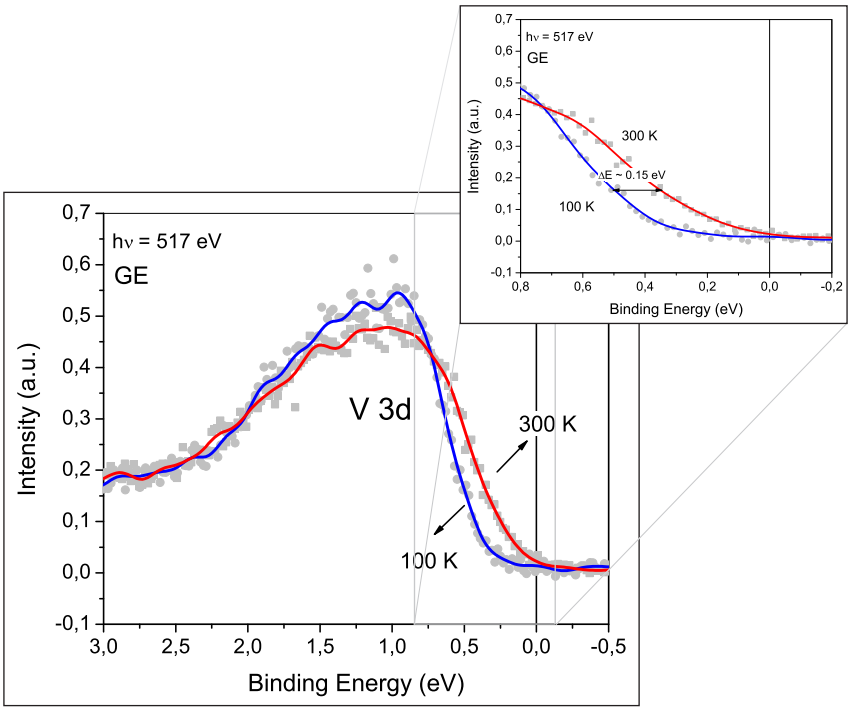

Fig 5.9: Resonant Photoemission (hν= 517eV) of the vanadyl termination for two temperatures 300K and 100K. The density of states close to the Fermi edge decreases, when the surface is cooled down to 100K.

5.4.2 O-rich termination (√3x√3)R30°

By removing 1/3 of the vanadyl groups from the vanadyl terminated surface by annealing the sample in oxygen ambient ($5x10^{-6}$mbar) one can achieve an oxygen richer surface with a (√3x√3)R30° superstructure. (see Chapter 3.3.2, p. 26)
The missing vanadyls force the surface layers to local reconstructions, because the oxygen surface layer from the bulk stacking (O_3VV'-O_3VV'-…) is not a stable configuration. As Kresse et al. [17] have shown, a vanadium atom from the second metal bilayer moves to the first metal layer, which is lying underneath the surface oxygen atoms. In this way the surface dipole vanishes and the surface is relaxed at this location, the stacking sequence is $O_3V_2V'O_3$-V-O_3VV'-O_3VV'-… .

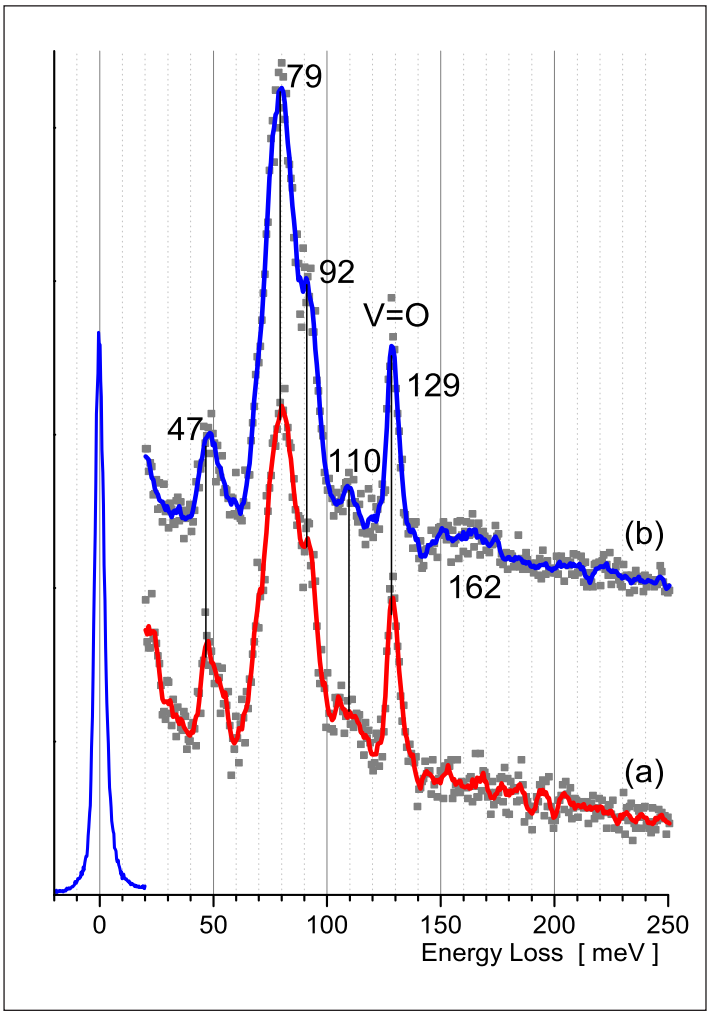

Fig 5.10: The HREEL spectrum of the (vanadyl reduced) O-rich (√3x√3)R30° surface at room temperature (a) and at 100K (b); the two curves are the same at both temperatrues.

300K

The results from HREELS at room temperature differ not very much from the ones for the vanadyl (1x1) termination. At first glance in Fig. 5.10 (a) the three main features 47meV, 79meV and 129meV are also visible at this surface, but a closer look shows some differences compared to the (1x1)V=O surface (Fig. 5.8 (a)): the whole spectrum contains a smaller signal to noise ratio, because all losses are less intense this time (that fact can be seen by the lack of overtones in the spectrum). Furthermore, a new vibration mode can be found at 110meV, whose origin is still under discussion. The main peak in Fig. 5.10 (a) at 79meV, with a more intense shoulder at 92meV, comes this time not only from the three oxygen atoms underneath a V=O group vibrating parallel to their vanadium bond, but also from the relaxed parts of the surface, where no vanadyl group is present above. Here the three topmost oxygen atoms are oscillating normal to the surface plane [17]. The 92meV feature is better separated due to the lower intensity of the loss at 79meV.

100K

Switching now to the cold surface (100K) and to Fig. 5.10 (b), the big difference to before is that there is no big increase in intensity in the 79meV peak (only a slight increase by a factor of 1.2) and no shift to higher loss energies!

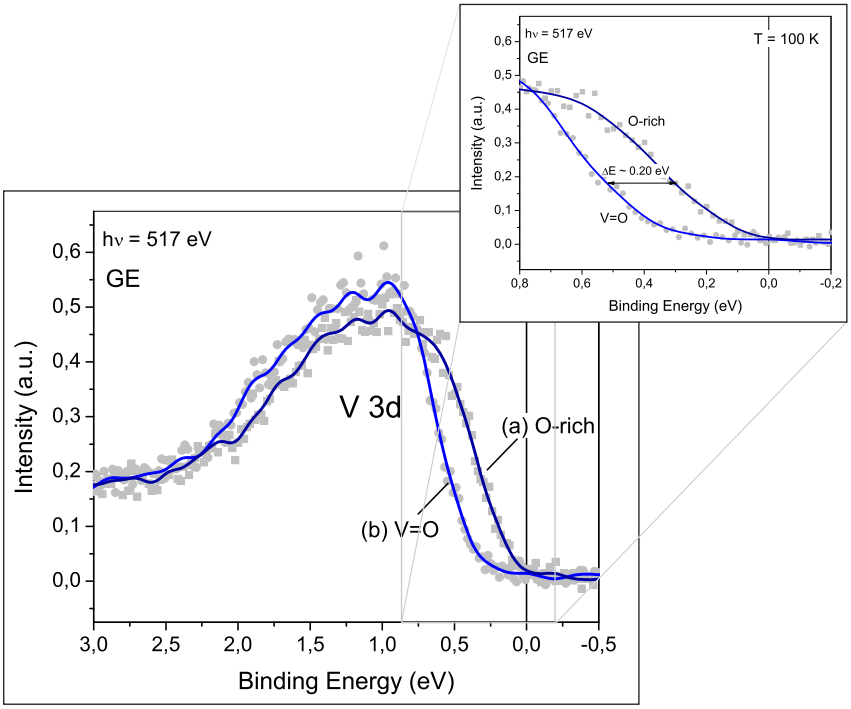

Fig 5.11: Spectrum of the (a) O-rich (√3x√3) and (b) vanadyl (1x1) surface termination at 100K measured with resonant photemission (hν= 517eV). The density of states at the O-rich termination reaches closer to the Fermi edge than the V=O (1x1) surface (see also Fig 5.9)

In addition, the XPS measurements on this particular surface, again done by my colleagues during a stay at MAXlab, show no shift of the V 3d state towards higher binding energies (Fig 5.11). The O-rich (√3x√3) surface spectrum taken at 100K follows closely the one of the (1x1) vanadyl termination at room temperature (300K).

Both techniques, HREELS and XPS, show the same tendency of the vanadyl reduced surface: the cooling to 100K does not bring up the signs for observing a metal-to-insulator phase transitions on this kind of surface termination.

H_2O effect

In a subsequent series of experiments small amounts of molecular water (~0.1L) were dosed onto the (√3x√3)R30° surface at 100K.

Surprisingly, as shown in Fig. 5.12 (b), this induces a large intensity change of the peak

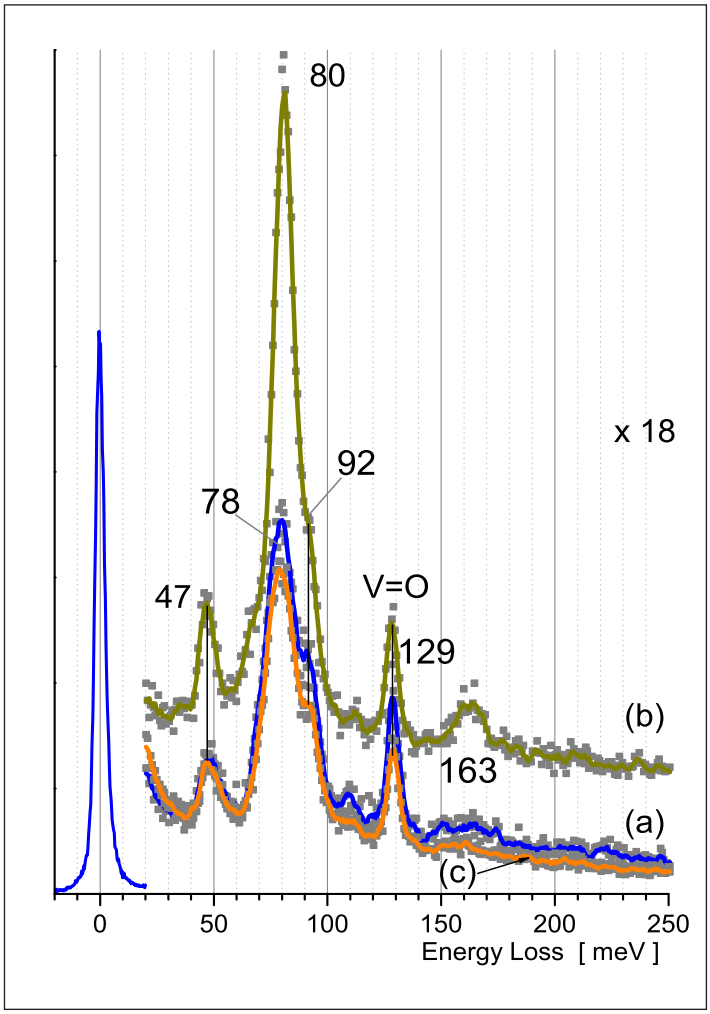

Fig 5.12: Desorption of the molecular water causes a reduction of the high intensity peak at 80meV (c). The system shows the same result as measured before, when the sample was cold and no H_2O was added to the surface (a).

at 79meV! The peak height doubled, but only a small shift is visible; on the leading edge of the peak the bulk feature at 66meV can be suspected, the higher energy side shows still the feature at 92meV, now less distinct because of the increased peak height of the loss at 80meV. The loss feature at 163meV fits to a possible double-frequency excitation of the most prominent peak (80meV)

Desorbing the H_2O molecules causes again a decrease of the main 80meV loss, i.e. the thin film of vanadium oxide does not show the phase transition any more (visualised by the orange graph in Fig. 5.12 (c)). The effect of the water is therefore reversible and can be repeated several times.

5.4.3 V-rich (1x1) termination

Another surface termination is obtained, as introduced in Chapter 3.3.3, by firstly producing a perfect vanadyl terminated (1x1)V=O surface and afterwards depositing small amounts of vanadium onto it at room temperature. In the next step, the thus created surface is flashed to 450°C to order the overlayer, forming a slightly buckled surface and a stacking sequence of V-V_2O_3-V_2O_3-… (shown in Fig. 3.20, p. 29) With increasing amount of additional V atoms the vanadyl peak gets more and more suppressed. 0.3MLE of V metal are enough to cover all the vanadyls groups.

In Fig 5.13 (a) (0.1MLE vanadium metal) one can see that at room temperature three vibrations are detectable at 46meV, 76meV and 129meV. The vanadyl peak has become smaller by 50% compared to the (1x1)V=O surface (not presented in the figure). Looking at the spectrum Fig. 5.13 (b) the former peak at 76meV splits into two, 66meV and

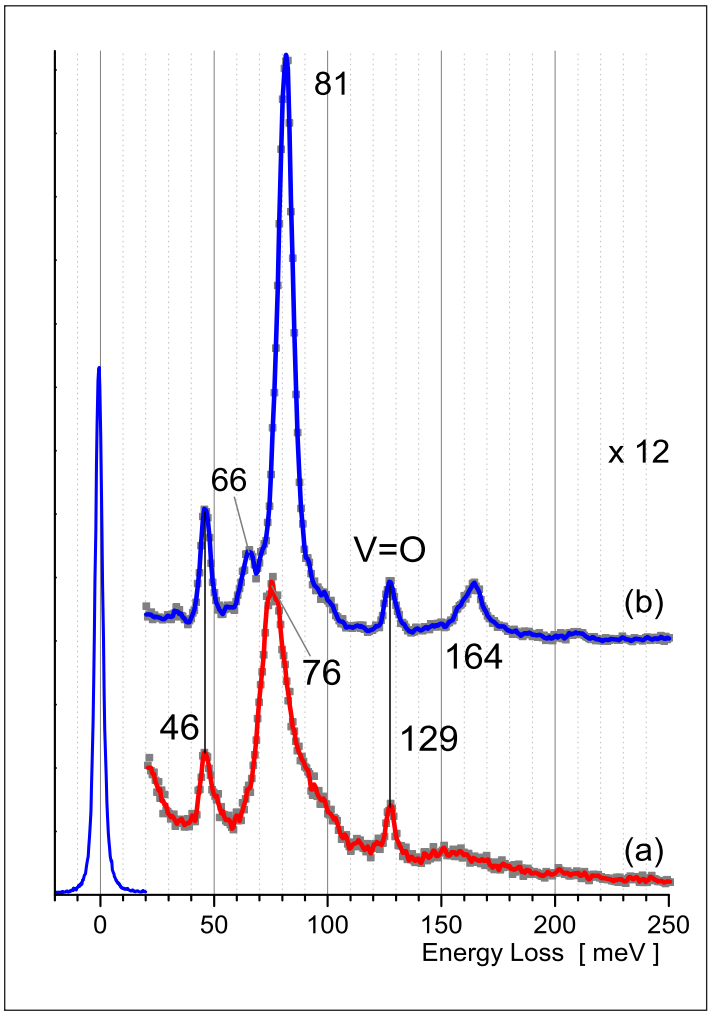

Fig 5.13: The comparison between the spectras at room temperature (a) and at 100K (b) of the vanadium terminated surface. The vanadium metal coverage is 0.1MLE.

81meV, and the intensity is doubled. Once again because of the high intensity of the 81meV feature, the double frequency excitation at 164meV is visible.
This is the behaviour as we know it already from the (1x1) V=O surface (Fig. 5.8).

With further deposition of V on a vanadyl terminated surface the characteristic feature of the V=O stretch vibration gets lost, 0.3MLE and 0.8MLE Vmetal were measured (Fig. 5.14 (a) and 5.15 (a)).
Moreover, at 100K the peak at 66meV can not be clearly separated from the left shoulder of the 82meV vibration as it was with 0.1MLE V metal on top. Note the energy loss at 128meV on the cold sample, which does not come from vanadyl vibrations but it is generated by the frequency sum excitation of 46meV and 82meV. This is always present on the cold surface, but not visible until now, because the much stronger vanadyl stretch vibration coincides with the same energy loss position.

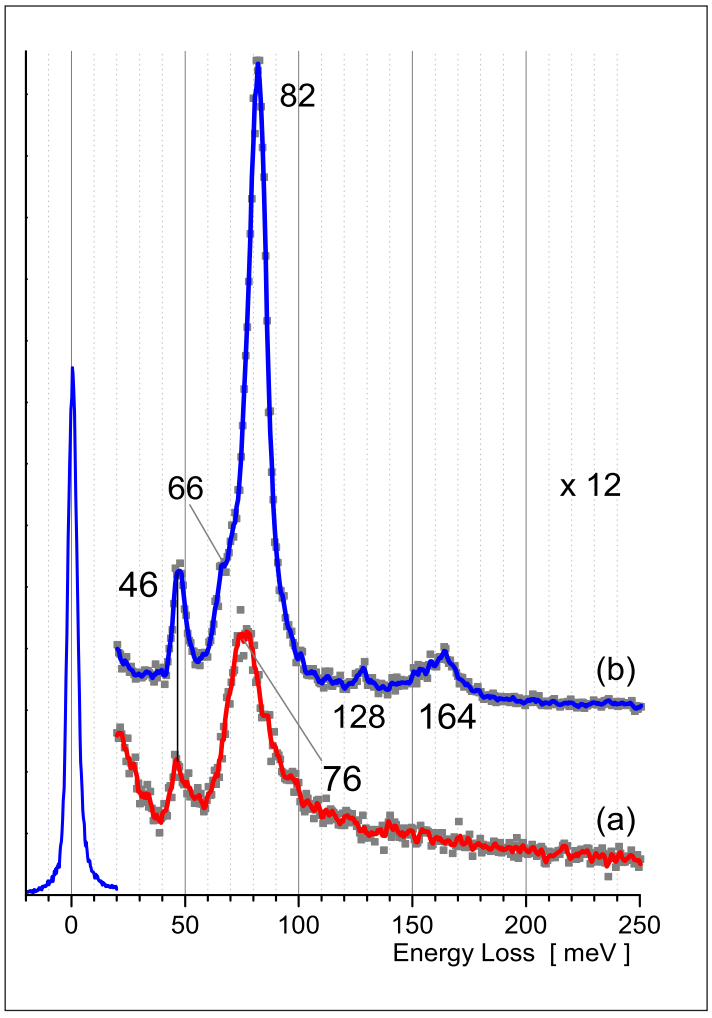

Fig 5.14:HREELS spectra for a 0.3MLE V-rich (1x1) film for two temperatures 300K (a) and 100K (b)

Compared to the O-rich (√3x√3) and (1x1)V=O surface terminations the high energy side of the 81meV feature at all V metal coverages does not show a vibronic component at 92meV. In general it seems that for both temperatures, 100K and 300K, the high energy side of the peak in the area around 80meV (76meV and 81meV) is broaden.

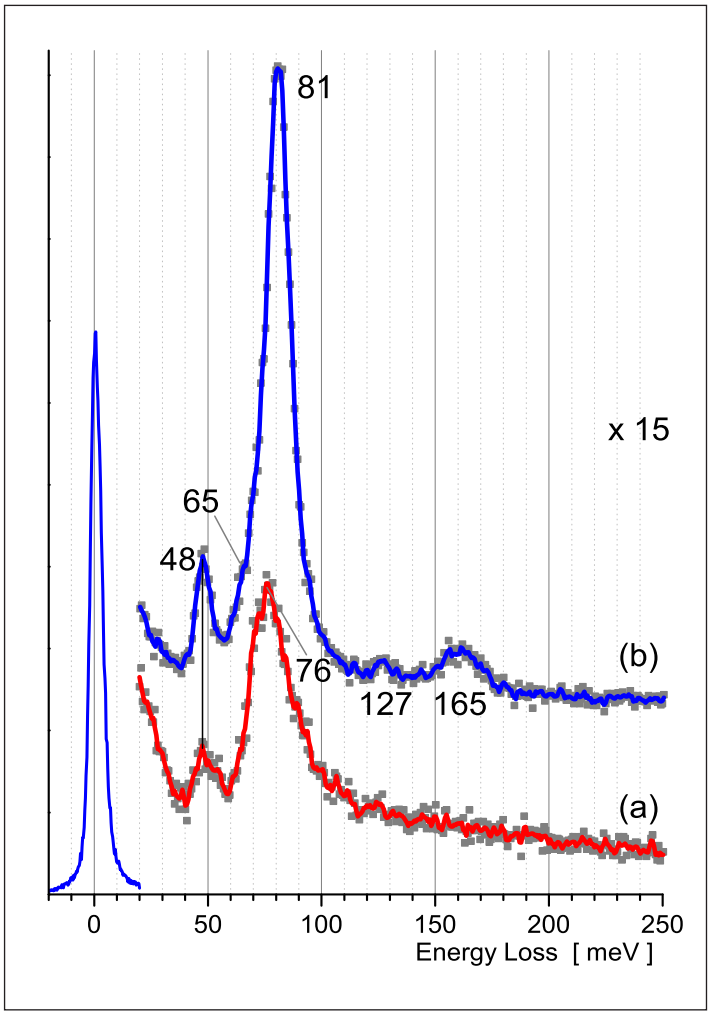

Fig 5.15:0.8MLE V-rich (1x1) film measured for two temperatures 300K (a) and 100K (b) in the HREEL spectroscope

5.5 Summary

Thin films of V_2O_3 undergo a phase transition when cooled down to 100K. However it seems that the surface structure is an important factor and should not be neglected. This is illustrated by the fact that the O-rich (√3x√3)R30° surface has a suppressed phase transition, which can be brought back by adsorbing water on the surface (this could explain why Q. Luo et al. [60] could not see a phase transition on their thin films of V_2O_3). Suggested in the literature that the mismatch between substrate lattice and thin film lattice can cause strain effects and bring the c/a ratio in vanadium sesquioxide structures to values, which drive or disable the known bulk phase transition. V_2O_3 is a metal oxide, in which small changes in the V-V distance can cause different values in conductivity. Therefore four phases are detectable as a function of pressure, dopant concentration, temperature or vacancies in the lattice. In our HREELS study we observed for three different surface terminations, the following results:

Vanadyl termination V=O (1x1) surface

- A change in the vibrational spectrum of the vanadyl terminated V=O(1x1) surface is measured, when the sample is brought down to 100K. The most prominent peak in the HREELS spectrum at 78meV splits into two peaks: a minor one at the loss energy of 66meV and a high intensity one at 83meV (intensity doubled compared to the room temperature loss at 78meV)
  The other loss features in the spectrum (47meV, 92meV, 129meV) remain unchanged. It seems that the electron energy loss spectroscopy reflects the metal-to-insulator transition of the V_2O_3 thin film. Valence band measurement on the same surface terminations underline the HREELS results, the V3d density of states close to the Fermi edge is reduced at 100K indicating that the V_2O_3 film becomes more insulating.

O-rich termination (√3x√3)R30°

- The oxygen rich (√3x√3)R30° termination shows no change in the phonon structure by cooling down to 100K. The spectrum looks very similar to the one at 300K.
- A new loss structure, compared to the V=O(1x1) surface, is detectable at 110meV for this surface structure at both temperatures.
- The XPS V3d data of the cold O-rich (√3x√3)R30° surface follow the room temperature data (sic!) of the vanadyl terminated surface. The surface seems to be still in the metallic phase.
- Traces of molecular adsorbed water however restore the phase transition. The HREEL spectra surprisingly show the intensity change of the peak at 78meV, which shifts to higher loss energy (80meV).

- Desorbing the H_2O molecules brings the spectrum back to the shape of the one without water molecules adsorbed. The high intensity feature at 80meV is gone and shifted back to 78meV, it looks like the phase transition is quenched again.

- The missing vanadyl groups on the (√3x√3)R30° surface force the near interface layers to relax. DFT-theory predicts [17] that a vanadium atom from the second bilayer moves up into the first V bilayer, right underneath the surface oxygen atoms. This local relaxation can introduces strain effects into the lattice, making it more rigid or at the surface more metallic. Moreover as it is known from non-stoichometric V_2O_3 crystals, missing vanadium atoms introduce not fully occupied oxygen sites [54]. It seems that this disorder adds states in the gap and influence the conduction mechanism strongly [59]. The conductivity increases at low temperatures, which hinders the phase transition to insulating behaviour at 100K.
- The adsorbed water molecules on the surface are acting like impurities or dopants and influence the surface in the way that in the HREEL spectrum the vibrational structure of the metallic surface is visible again.

<u>V-rich (1x1) termination</u>

- Depositing vanadium metal atoms on the vanadyl (1x1) surface quenches the vanadyl vibrations but does not change the transition behaviour. In the energy loss spectra for different V-metal (0.3MLE, 0.6MLE, 0.8MLE) the sign of the metal-to-insulator transition is preserved. The intensity increases and the shift to higher energy of the fingerprint vibration at 82meV at 100K is visible. For a surface covered with 0.1MLE vanadium the splitting is still existing , the cold spectrum shows a peak at 66meV and 81meV, as it is seen for the vanadyl terminated surface.

The phase changes in V_2O_3 are far from being completely understood, neither in experimental nor in theoretical sense. But the concept of the Mott-Hubbard insulator/transition seems to be a good approach for a deeper understanding of the phase transition. In the case of our thin films the question is whether the phase transition extends up into the outermost surface layer. This is a very interesting question. The strong influence of very small amounts of adsorbed water molecules would however indicate that the surface layer is involved in the transition.

6. Summary

In this diploma thesis the adsorption of water on thin films of V_2O_3 grown on a Rh(111) crystal was studied by HREEL spectroscopy. Furthermore, the metal-to-insulator phase transition known from bulk V_2O_3 is seen in HREELS for the here used vanadium oxide films. The vanadium sesquioxide films have been prepared in three different surface terminations, which are obtained by reactive evaporation of vanadium onto the rhodium crystal or by depositing an overlayer of metallic vanadium on V_2O_3.

Metal-Insulator phase transition in V_2O_3 films

- The phase transition on the vanadyl termination (1x1) V=O can be seen in HREELS at 100K by the intensity change of the vibration representing the stretch mode of the V=O group to the surface. This peak (at 78meV at 300K) splits into two, a smaller one at 66meV, a bulk vibration, which was covered before by the feature at 78meV, and a second one with twice the intensity at 83meV. The other loss features are not changed. Resonant photoemission spectroscopy of the V3d state underline the HREELS results.
- On the O-rich (√3x√3)R30° termination the shape of the spectrum at 100K is unchanged, which would suggest that the surface does not undergo the MIT phase transition. In XPS also no change in the density of state close to the Fermi edge is seen. The phase transition seems to be quenched at 100K for this surface termination. But traces of water can restore the phase transition, with the characteristic increase of the main feature at ~80meV. Interestingly, desorbing the water brings the system back to the suppressed metal-to-insulator transition.

- Deposition of vanadium metal on a vanadyl terminated (1x1) V=O surface, building the V-rich (1x1) termination, does attenuate the vanadyl peak at 129meV, but the phase transition remains visible in HREELS at 100K.

Water adsorption on Rh(111)

- Even at small amounts of adsorbed water hydrogen bondings are formed, which can be seen in a broadening of the ν(OH) stretch vibration, and the molecule adsorbs molecularly, which can be seen in the detectable δ(HOH) vibration, in which all three atoms of the water molecule are participating. At high coverage water forms an ice-like structure on the metal surface, as identified by the frustrated translation mode and the shift of the bending mode δ(HOH) to the value of ice.

Water on the vanadyl termination V=O (1x1)

- The vanadyl peak is shifted to lower loss energy with increasing amount of water adsorption, which indicates that the H_2O molecules coordinate to the V=O groups. It seems that for low coverage the adsorbed water both dissociates and stays intact, since both vibrational fingerprints in the ν(OH) region can be seen (ν_1(OH)= 425meV, ν_2(OH)= 453meV). For high dosing amounts an ice-like structure forms on the vanadium oxide film.

Water on the O-rich termination (√3x√3)R30°

- Small water amounts form hydroxyl groups on this surface termination, which are forming hydrogen bonds with increasing water coverage. At almost 2L of water an ice-like structure is formed, the bending mode an the frustrated translation mode is visible in the HREEL spectrum.

Water on the V-rich (1x1) termination

- For the surface with the 0.15MLE V-rich (1x1) termination the vanadyl shift is very small till a dosing range of 0.40L, then the peak shifts 5meV towards lower loss energy. The delay in the shift of the V=O peak leads to the conclusion, that the water adsorbes in the beginning at the V-layer and then goes to the vanadyls.
- For 0.3MLE and 0.8MLE vanadium-rich terminated surfaces the water dissociates, indicated by the ν(OH) mode at 453meV, and no hydrogen bonds are formed. In the last dosing step, 2.00L of water, the OH-stretch vibration forms a broad peak together with the appearance of the frustrated translation feature.

- Thermal desorption of the water from a 0.8MLE V-rich (1x1) termination happens at 200K. HREELS shows the formation of hydroxyl groups at this temperature, which stay on the surface even at 400K. These OH groups on the vanadium metal layer bring back the vanadyl groups when the sample is heated to 250K.

Bibliography

[1] J.T. Yates, T.E. Madey, “Vibrational Spectroscopy of Molecules on Surfaces - Methods of surface characterization Vol. 1.
Plenum Press (1987)

[2] Andrew Zangwill, “Physics at surfaces”
Cambridge University Press (1990)

[3] H. Ibach, D.L. Mills, „Energy Electron Loss Spectroscopy and Surface Vibrations”
Academic Press (1982)

[4] M. Henzler, W Göpel, „Oberflächenphysik des Festkörpers“
Teubner (0)

[5] M.W. Urban, “Vibrational Spectroscopy of Molecules and Macromolecules on surface”
Wiley-Interscience (1993)

[6] H. Haken, H.C. Wolf, „Atom- und Quantenphysik - Einführung in die exp. und theor. Grundlagen“
Springer (1996)

[7] R.E. Palmer, P.J. Rous
Reviews of Modern Physics , Vol. 64, Issue 2, p. 383–440 (1992)

[8] M.A. Van Hove, W.H. Weinberg, C.-M. Chan, “Low-Energy Electron Diffraction - Springer Series in Surface Science. 6”
Springer (1986)

[9] Helge Haberkern
„Elektronen-Energieverlust-Spektroskopie großer Moleküle“
Universität zu Köln (2002)

[10] Ingrid Kardinal
Hochauflösende Spektroskopie an adsorbierten Molekülen auf einer Ni(110)-Oberfläche: Schwingungszustände und elektronische Niveaus
K.-F. University Graz (1998)

[11] Renate Duschek, PhD-Thesis
Model Organic-Inorganic Interfaces Studie by Electron Spectroscopy
K.-F. Universtity Graz (2000)

[12] Michael Sock, PhD-Thesis
Growth and Properties of vanadium Oxide Nanolayers on Transition Metal Surfaces: Electron Spectroscopy Studies
K.F.-University Graz (2004)

[13] J. Schoiswohl, M. Sock, S. Surnev, M. G. Ramsey, F. P. Netzer, G. Kresse and J. N. Andersen
Surface Science, Vol. **555**, Issue 2-3, p. 101-117 (2004)

[14] O. Seiferth, K. Wolter, B. Dillmann, G. Klivenyi, H. -J. Freund, D. Scarano and A. Zecchina
Surface Science, Vol. **421**, Issue 1-2, p. 176-190 (1999)

[15] A.-C. Dupuis, M. Abu Haija, B. Richter, H. Kuhlenbeck and H. -J. Freund
Surface Science, Vol. **539**, Issue 1-3, p. 99-112 (2003)

[16] Anna-Claire Dupuis, PhD-Thesis
V_2O_3 (0001)/Au(111) and /W(110): Growth, Electronic Structure and Adsorption Properties
Humboldt-University Berlin (2002)

[17] G. Kresse, S. Surnev, J. Schoiswohl and F. P. Netzer
Surface Science, Vol. **555**, Issue 2-3, p. 118-134 (2004)

[18] P.A. Thiel, T.E. Madey
Surface Science Reports, Vol. **7**, Issue 6-8, p. 211-385 (1987)

[19] J.D. Bernal, R.H. Fowler
Journal of Chemical Physics, Vol. **1**, p. 335 (1933)

[20] Michael A. Henderson
Surface Science Reports, Vol. **46,** Issue 1-8, p. 1-308 (2002)

[21] K. Jacobi, K. Bedürftig, Y. Wang, G. Ertl
Surface Science, Vol. **472**, p. 9-20 (2001)

[22] A.L. Glebov, A.P. Graham, A. Menzel
Surface Science, Vol. 427-428, p. 22 (1999)

[23] H. Ogasawara, J. Yoshinobu, M. Kawai
Journal of Chemical Physics, Vol. **111**, p. 7003 (1999)

[24] J. Kiss, F. Solymosi
Surface Science, Vol. **177**, Issue 1, p. 191-206 (1986)

[25] Robert W. Whitworth, Victor F. Petrenko, "Physics of Ice "
Oxford University Press (1999)

[26] K.D. Gibson, M. Viste, S.J. Sibener
Journal of Chemical Physics, Vol. **112**, Issue 21, p. 9582-9589 (2000)

[27] D.L. Doering and T.E. Madey
Surface Science, Vol. **123**, Issue 2-3, p. 305-337 (1982)

[28] S. Meng, E.G. Wang, S. Gao
Physical Review B, Vol. **69**, Issue 19, p. 195404 (2004)

[29] R. Brosseau, M. R. Brustein and T. H. Ellis
Surface Science, Vol. **280**, Issue 1-2, p. 23-37 (1993)

[30] Yamada, T.; Okuyama, H.; Aruga, T.; Nishijima, M.
Journal of Physical Chemistry, Vol. **107,** Issue 50, p. 13962 (2003)

[31] A. Michaelides, V.A. Ranea, P.L. De Andres, D.A. King
Physical Review Letters, Vol. **90,** Issue 21, p. 2161021 (2003)

[32] R. Ludwig
Angewandte Chemie International Edition, Vol. 42, Issue 30, p. 3458 - 3460 (2003)

[33] F.T. Wagner, T.E. Moylan
Surface Science, Vol. **191**, p. 121-146 (1987)

[34] H. Okuyama, T. Yamada, S. Thachepan, T. Aruga and M. Nishijima
Surface Science, Vol. **515**, Issue 2-3, p. L499-L503 (2002)

[35] G. Tzvetkov, Y. Zubavichus, G. Koller, Th. Schmidt, C. Heske, E. Umbach, M. Grunze, M. G. Ramsey and F. P. Netzer
Surface Science, Vol. **543**, Issue 1-3, p. 131-140 (2003)

[36] J. Ahdjoudj, C. Minot
Surface Science, Vol. **402-404**, p. 104-109 (1998)

[37] M.A. Henderson, S.A. Chambers
Surface Science, Vol. **449,** p. 135-150 (1999)

[38] V.A. Ranea, J.L. Vicente, E.E. Mola, P. Arnal, H. Thomas, L. Gambaro
Surface Science, Vol. **463**, p. 115-124 (2000)

[39] M. Foex,
Comptes rendus de l'Académie des Sciences ,Vol. **223**, p. 1126 (1946)

[40] F. Gebhard, "The Mott Metal-Insulator Transition - Models and Methods",
Springer Tracts in Modern Physics 137 (1997)

[41] N. F. Mott, Review of Modern Physics,
Vol. **40**, Issue 4, p. 677-683 (1968)

[42] Y. Ōno, R. Bulla, A.C. Hewson,
The European Physical Journal B - Condensed Matter, Vol. **19**, p. 375 - 384 (2001)

[43] Jozef Spalek,
Journal of Solid State Chemistry, Vol. **88**, Issue 1, p. 70-93 (1999)

[44] J. Spalek, A. M. Oles, J. M. Honig**,**
Physical Review B, Vol. **28,** Issue 12, p. 6802–6811 (1983)

[45] J. Spalek, A. Datta, J. M. Honig,
Physical Review Letters, Vol. **59**, Issue 6, p. 728–731 (1987)

[46] D. B. McWhan, A. Menth, J. P. Remeika, W. F. Brinkman, and T. M. Rice**,**
Physical Review B, Vol. **7**, Issue 5, p. 1920–1931 (1973)

[47] A. I. Frenkel, E. A. Stern and F. A. Chudnovsky**,**
Solid State Communications, Vol. **102**, Issue 9, p. 637-641 (1997)

[48] R. M. Moon**,**
Journal of Applied Physics, Vol. **41**, Issue 3, p. 883 (1970)

[49] E. D. Jones,
Physical Review, Vol. **137**, Issue 3A, p. A978–A982 (1965)

[50] K. Kosuge**,**
Journal of Physics and Chemistry of Solids , Vol. **28**, Issue 8, p. 1613-1621 (1967)

[51] J.B. Goodenough,
Progress in Solid State Chemistry , Vol. **5**, p. 145-399 (1971)

[52] R.L. Kurtz, V.E. Henrich,
Physical Review B , Vol. **28**, Issue 12, p. 6699–6706 (1983)

[53] P. D. Dernier and M. Marezio,
Physical Review B, Vol. **2**, Issue 9, p. 3771–3776 (1970)

[54] M. Yethiraj,
Journal of Solid State Chemistry, Vol. **88**, Issue 1, p. 53-69 (1999)

[55] V.E. Henrich & P.A. Cox,

Cambridge University Press (1996)

[56] T. M. Rice, D. B. McWhan,
Journal of Research and Development, Vol. **14**, Issue 32, p. 251 (1970)

[57] D. B. McWhan, J. P. Remeika,
Physical Review B, Vol. **2**, Issue 9, p. 3734- 3750 (1970)

[58] S.-K. Mo, J. D. Denlinger, H.-D. Kim, J.-H. Park, J. W. Allen, A. Sekiyama, A. Yamasaki, K. Kadono, S. Suga, Y. Saitoh, T. Muro, P. Metcalf, G. Keller, K. Held, V. Eyert, V. I. Anisimov, and D. Vollhardt,
Physical Review Letters, Vol. **90**, p. 186403 (2003)

[59] S. A. Carter, Yang and T. F. Rosenbaum, J. Spalek, J. M. Honig ,
Physical Review B , Vol. **43**, Issue 1, p. 607-614 (1991)

[60] Q. Luo, Q. Guo, and E. G. Wang,
Applied Physics Letters, Vol. 84, Issue 13, p. 2337-2339 (2004)

List of Figures

Acknowledgements

First of all I have to really thank Prof. Dr. Falko Netzer for his support, he gave me the opportunity to do my diploma thesis in his group and moreover he offered me the possibility to go to the synchrotron in Sweden (MAXlab) for two weeks and to participate at one conference (July 2004 in Venice) and on one workshop (October 2004 Seggau).
Further on I have to thank Prof. Dr. Zarko Surnev for answering my questions about the vanadium oxide films and for the great time here in Graz and in Sweden.
I also want to mention Prof. Mike Ramsey, who invited me for a trip to the synchrotron in Berlin and had always an ear for my problems and concerns during my work.

Of course “mere words could not express my feelings for” Michi Sock, my HREELS teacher, Hannes Schoiswohl, my desk-neighbour and mental refresher when things were not going so well. Not to forget Georg Koller, he always brought light to my empty mind.
Finally I want to send my best regards to Jan, Carla, George, Barbara and Georg P, whom I met at the end of my thesis. It was one of my best times in my life, even when sometimes things were not going so smooth and and a bad pressure was in the chamber.
Best wishes to the surface science group Graz!